Electrospinning for Pharmaceutical Applications

by

Blair Kathryn Brettmann

Submitted to the Department of Chemical Engineering
in partial fulfillment of the requirements for the degree of

Doctor of Philosophy

at the

MASSACHUSETTS INSTITUTE OF TECHNOLOGY

June 2012

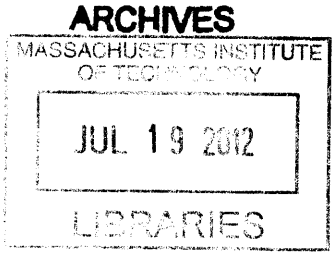

Author .....
Department of Chemical Engineering
May 3, 2012

Certified by .....
Bernhardt L. Trout
Professor of Chemical Engineering
Thesis Supervisor

Accepted by .....
Patrick S. Doyle
Professor of Chemical Engineering
Chair, Committee for Graduate Students

Electrospinning for Pharmaceutical Applications

by

Blair Kathryn Brettmann

Submitted to the Department of Chemical Engineering
on May 3, 2012, in partial fulfillment of the
requirements for the degree of
Doctor of Philosophy

Abstract

The pharmaceutical industry is currently shifting from batch to continuous manufacturing, and for downstream processes, this shift can reduce costs and improve quality provided the new unit operations are chosen properly. Electrospinning, a method of making nanofiber mats from solutions of an active pharmaceutical ingredient (API), polymer and solvent, has shown great promise for producing final solid dosage forms with minimal process steps. In this thesis, we explore the use of electrospinning to produce fiber mats containing either amorphous or crystalline API, aiming to develop the process such that it can be used for a wide variety of final drug products. Key to utilizing electrospinning to make these products is understanding the composition and behavior of the final fiber mats. For fibers containing amorphous API, this means it is essential to understand the level of mixing between API and polymer and the stability of the final product, and for fibers containing crystalline API, the crystal morphology and extent of dispersion within the polymer must be understood.

The mixing level of amorphous API and polymer in fibers was analyzed using solid state nuclear magnetic resonance relaxation times. It was found that, for aliskiren/poly(vinyl pyrrolidone) and indomethacin/poly(vinyl pyrrolidone) formulations, the materials are intimately mixed following electrospinning, with no phase separation down to a 2-10 nm domain size. This was not the case for a 4:1 aliskiren:poly(vinyl pyrrolidone) formulation prepared by hot melt extrusion, an alternative method for co-processing API and excipients, as solid state NMR analysis showed phase separation with domains of 20-80 nm or larger. The same electrospun formulations were shown to be stable as solid solutions for 6 mo. when stored at 40°C in a desiccator, indicating that electrospinning is a viable method to produce physically stable formulations containing amorphous API.

To produce fibers containing crystalline API, two methods were used. In the first, an API/polymer solution was electrospun using the same method as for producing fibers containing amorphous API. It was found that spinning with a crystalline polymer can result in crystalline API in the fibers, but the crystallinity ultimately depends on more than the polymer and API properties. Due to the complexity of using this method, we developed the second method, involving electrospinning a suspension of API crystals in the polymer/solvent solution. We demonstrated the feasibility of spinning particles of up to $10\mu m$ diameter using polystyrene beads and then applied the process to electrospin two different APIs, albendazole and famotidine. The electrospun mats contained crystalline APIs well-dispersed within the fibers and tablets prepared from the mats displayed a higher dissolution rate than fibers prepared from powder blends.

Thesis Supervisor: Bernhardt L. Trout
Title: Professor of Chemical Engineering

Acknowledgments

The completion of my PhD would never have been possible without the support of many people and organizations. I wish to express my sincere thanks to all of you who supported me over the last 5 years.

Special thanks to my thesis adviser Bernhardt Trout for giving me the opportunity to explore all the facets of this project and for support of my non-scientific interests throughout my years at MIT.

All members of my thesis committee, Alan Hatton, Allan Myerson and Gregory Rutledge brought unique perspectives to my work and were instrumental in expanding the scope and improving the quality of the work.

I greatly appreciate the financial support from Novartis, but would also like to thank all of the Novartis employees who participated in the joint meetings at MIT. In particular, Norbert Rasenack and Srinivasan Rajan went above and beyond to help me start my NMR work.

My solid state NMR experiments were performed in the Francis Bitter Magnet Lab at MIT, which is supported by NIH grant EB002026. The director, Robert Griffin, and a former PhD student, Galia Debelouchina were extremely helpful with planning and teaching me to carry out the experiments. I could not have done this work without their support and the generous use of the facility.

I was fortunate to be a member of the Trout, Myerson and Hatton groups throughout my PhD and have enjoyed having so many great colleagues to work with. So many members of these groups have contributed ideas and knowledge to my thesis and I would not have been able to finish without them.

A few particular colleagues went out of their way to help me over the last 5 years:

Keith Chadwick was instrumental in teaching me what a PhD is about and how to come up with a research plan.

Keith Forward, Mao Wang and Eve Revalor made for wonderful colleagues on the electroprocessing team, never ceasing to motivate me to work hard to make this technology appealing to Novartis.

I have had two great UROPs working with me in the last year, Shirley Tsang and Flora Cheng. They have done an amazing job and collected much of the data for the second half of my thesis.

Of course, there are other forms of support than merely technical, and there are many people in my life that helped me through the ups and downs of the PhD program.

My friends Becky Ladewski and Bradley Niesner

Amanda Engler and the rest of the MIT water polo team

The students in MIT German House, where I have the privilege of being a GRT

My parents, Barie and Sue, and brothers, Josh, Luke, and Matthew, who give me freedom and encouragement to pursue the path I feel is best for me

My wonderful boyfriend Björn Benneke, who patiently encouraged me during the hard times and helped me enjoy life during the good times.

Contents

List of Figures

List of Tables

Nomenclature

Acronyms

ABZ Albendazole

API Active Pharmaceutical Ingredient

ATR Attenuated Total Reflectance

BCS Biopharmaceutical Classification System

CBZ Carbamazepine

CP Cross Polarization

DSC Differential Scanning Calorimetry

DMF Dimethyl formamide

EtOH Ethanol

FAM Famotidine

FBML Francis Bitter Magnet Lab

FDA Food and Drug Administration

FTIR Fourier Transform Infrared Spectroscopy

HPMC Hydroxypropyl methylcellulose

IBU Ibuprofen

IBUss Ibuprofen sodium salt

IND Indomethacin

MAS Magic Angle Spinning

MeOH Methanol

$\mathbf{M}_w$ Weight averaged molecular weight

NMR Nuclear Magnetic Resonance

NY Nylon

PAA Poly(acrylic acid)

PAT Process Analytical Technology

PCL Polycaprolactone

PD Proton Decoupling

PEO Poly(ethylene oxide)

PLLA Poly(l-lactic acid)

PMMA Poly(methyl methacrylate)

PS Polystyrene

PVC Poly(vinyl chloride)

PVP Poly(vinyl pyrrolidone)

rf Radio Frequency

RH Relative Humidity

SEM Scanning Electron Microscopy

SPP Aliskiren

Tg Glass Transition Temperature

TGA Thermogravimetric Analysis

THF Tetrahydrofuran

TPPM Two Pulse Phase Modulation

USP United States Pharmacopeia

XRD X-ray Diffraction

Symbols

$\triangle h_{melt,API}$ Enthalpy of melting of the pure API

$\triangle h_{melt,samp}$ Enthalpy of melting of the sample

$\triangle h_{recryst}$ Enthalpy of crystallization of the API

γ Surface tension of the fluid

η Viscosity of the fluid

Ω Rotation rate of the spindle

ρ_1 Density of component 1

ρ_2 Density of component 2

ρ_{fluid} Density of the fluid

ρ_{part} Density of the particle

τ Mixing time

A Surface area

C Concentration in solution

Ca Capillary number

C_{sat} Solubility

D Diffusion coefficient

$\frac{dm}{dt}$ Dissolution rate

F_{drag} Drag force

F_g Force due to gravity

g Acceleration due to gravity

h Diffusional path length

I Intensity

L Domain size

m Magnetization

Q Flow rate

r Space vector

Re Reynold's number

r_p Radius of the particle

r_s Radius of the spindle

r_w Radius of the wire

t Diffusion time

$T_1(^1H)$ Spin lattice relaxation time

$T_{1\rho}(^1H)$ Spin lattice relaxation time in the rotating frame

T_i Relaxation time constant

t_{jet} Lifetime of the jet

V_A Applied voltage

V_{drop} Volume of the drop on the wire

v_{fluid} Velocity of the fluid

v_{part} Velocity of the particle

v_{rel} Relative velocity

v_s Settling velocity

w_1 Weight fraction of component 1

w_2 Weight fraction of component 2

z Thickness of the liquid film entrained on the wire

Chapter 1

Introduction

The process of going from raw ingredients to a formulated drug product is long, complicated and expensive. In current pharmaceutical manufacturing practices, the operations are done batch-wise, an often inefficient method of production. One area that is particularly costly is the lengthy route from purified active pharmaceutical ingredient (API) to final product, as this section often includes time-consuming drying, blending and granulation steps. In developing new continuous manufacturing processes, one approach is to co-process the API and all necessary excipients from a solution to a tablet without any powder handling steps.

Various continuous processes have been proposed to decrease the powder handling steps and provide efficient blending of API and excipients including melt extrusion [1, 2], thin film casting [3] and electrospinning [4–8]. Though a less-traditional technique, electrospinning has distinct advantages over extrusion and thin film casting. Because of the high surface area generated during electrospinning, the evaporation rate of the solvent is incredibly high, allowing for more efficient drying at ambient temperatures than is possible with thin film casting. In addition, no heat is necessary to blend ingredients during electrospinning, as they are already well blended in the liquid solution prior to spinning, making it more applicable for heat-sensitive API than melt extrusion.

In electrospinning, fibers of 20-2000 nm diameter are produced from a solution of a polymer, solvent and any desired additives. This approach, however, has a very

low production rate, on the order of 1 mg solids/min for the materials used in this work. This is insufficient for application to an industrial manufacturing process, and so we use a newer technology for the scale up of electrospinning, referred to as "free surface electrospinning" or "needleless electrospinning." In free surface electrospinning, jetting occurs from a free liquid surface, such as a film on a rotating drum, disk or wire spindle or from the surface of gaseous bubbles [9–18]. This results in the formation of multiple Taylor cones and jets and a high production rate, on the order of 8 mg/min for the materials and equipment used in this work. The free surface electrospinning technique has previously be adapted as a commercial unit and is available through Elmarco (Liberec, Czech Republic).

Though scale-up of electrospinning is possible with such approaches as free surface electrospinning, a further challenge prevents the technique from being applied for pharmaceutical manufacturing. Due to the rapid solvent evaporation during electrospinning, the drug is often present in the resulting fibers in its amorphous form [6–8, 19, 20]. This can be advantageous for a poorly water soluble drug, as the amorphous form often has a higher water solubility than the crystalline form, but it also introduces physical stability issues, with the amorphous API crystallizing over time [21]. For this technique to become generally applicable as a manufacturing process, it must also be able to produce fibers containing crystalline API.

My thesis approaches this challenge in two ways. First, I acknowledge that the amorphous form is potentially useful and aim to develop a better understanding of the molecular behavior of the amorphous drug and polymer mixture. Second, I design and characterize a process for producing crystalline drug in the electrospun fibers, a technique that will allow electrospinning to be used for a much larger fraction of APIs. These are both necessary problems to overcome in order to apply electrospinning to large-scale pharmaceutical applications.

Obtaining API in the amorphous form using electrospinning is an exciting result for researchers studying poorly water soluble drugs, as the combination of high surface area of the fibers and amorphous API aids in increasing solubility. One factor that strongly affects the rate of solid state crystallization, and thus the stability of the

amorphous form is the mobility of the API. Many studies have been done on methods to decrease the mobility of the API by co-processing with polymer excipients, and electrospinning of drug and polymer is one of the leading methods of doing this. Two mechanisms may contribute to the decreased mobility: the antiplasticizing effect of polymer excipients [22, 23] and hydrogen bonding between some API and excipients [23–25]. These effects are strongest in a solid solution, where the contact between the drug and the polymer is maximum.

Some have argued that, following electrospinning, the API is present in the polymer as a solid solution, basing their conclusion on the burst release dissolution profile [20]. The dissolution profile, however, would be similar for a solid solution and a solid dispersion with a small domain size. Another method commonly used in the literature to support the claim of a solid solution is by measuring the glass transition temperature (Tg) of the mixture. According to the Gordon-Taylor equation, for a system with no intermolecular interactions, there will be only one Tg of a homogeneous mixture and it will be an intermediate of the two components [26]. Verreck *et al.* measured the glass transition temperature of electrospun fibers containing itraconazole and PVP and found that there was only one Tg for the mixture, but it was not where predicted by the Gordon-Taylor equation, indicating either phase separation or a solid solution with interaction between components [8]. The Tg, however, has been shown to be a poor indicator of phase separation in many cases [27–30]. Thus, despite the potential electrospinning has shown for producing amorphous formulations, it is still necessary to find conclusive evidence that the end result is a solid solution prior to utilizing this technology to create final solid dosage forms.

For dispersions of amorphous materials, there are few options to quantify domain size of any phase separation when the domain size is likely 2-50 nm. Solid state nuclear magnetic resonance (NMR) has been used to characterize the domain size of solid dispersions containing two amorphous materials [31–35]. The spin lattice relaxation time and the spin lattice relaxation time in the rotating frame ($T_1(^1H)$ and $T_{1\rho}(^1H)$, respectively) are measurable time constants for proton spin diffusion and are related to the diffusion length scale [35]. If the relaxation time measured from the NMR

peaks of one component in a mixture is equal to that measured from the NMR peaks of the other component in a mixture, the sample is intimately mixed on that length scale. If the relaxation time values differ, then the sample has heterogeneities of that length scale or larger.

In this work, solid state NMR is used to measure the spin lattice relaxation times for formulations prepared by electrospinning in order to determine whether the APIs and polymer were well-mixed down to small length scales (Section 4.2.3). As supporting evidence, the Tg of the mixture was determined and compared to that predicted by the Gordon-Taylor equation (Section 4.2.2). To compare electrospinning to other methods of forming solid dispersions, an API and polymer mixture was prepared using hot melt extrusion and also tested using solid state NMR relaxation time analysis.

This study also utilizes the solid state NMR relaxation time analysis to examine the physical stability of amorphous API in electrospun solid solutions (Section 4.3.4). Typical physical stability studies of pharmaceutical formulations involve storage at high temperatures and/or high humidity and analysis via X-ray diffraction (XRD) and differential scanning calorimetry (DSC) to determine crystallinity as a function of time [36]. Here, we apply solid state NMR relaxation time analysis to investigate the homogeneity of solid solutions over time, rather than only examining the crystallization of the API over time. Since physical stability is enhanced in a solid solution, it is desirable that the two components remain intimately mixed over a typical shelf life, preventing an opportunity for crystallization. We also use Fourier transform infrared spectroscopy (FTIR) to probe the interactions between the API and polymer to determine whether interactions contribute to stability (Section 4.3.3).

Even if elctrospinning produces stable amorphous solid solutions, there will be API for which a crystalline form will be preferred. Hence, we focus on electrospinning formulations containing crystalline API in the second half of the thesis (Chapter 5). We explore two approaches to forming fibers containing crystalline API:

1) Electrospin a solution of fully dissolved API/polymer/solvent with parameters chosen such that the API is crystalline following electrospinning.

2) Electrospin a suspension of API crystals in a dissolved polymer solution, with

the solvent chosen such that the API crystals will not dissolve.

A few studies on electrospinning of API have found that the API is partially crystalline immediately after electrospinning using approach (1) [37–39]. All three studies used a polymer that itself crystallizes during electrospinning, either polycaprolactone (PCL) or poly(ethylene oxide) (PEO). Natu *et al.* found that the API was partially crystalline in only one formulation examined, that with greater than 10 wt% API [38], and Ignatious *et al.* determined that, at drug loadings higher than 35.9 wt%, nabumetone exhibits a melting endotherm when analyzed immediately after electrospinning [39]. Section 5.2 presents the results of electrospinning two APIs dissolved in solutions with 9 different polymers. The percent crystallinity and the fiber morphology are analyzed to determine which API or polymer properties, if any, determine whether the API crystallizes during the electrospinning process. Though the three previous studies obtained fibers containing crystalline API by this method, the studies considered only one API/polymer combination each and did not go in depth as to how the API is able to crystallize despite the high evaporation rate.

As an alternative to crystallization during spinning, we present a method of electrospinning suspensions of API crystals in a polymer solution. Examples of particles that have been electrospun along with the polymer are various types of nanoparticles (2-100 nm), including magnetite [40] and TiO_2 [41, 42] with diameters of less than 20 nm, $CaCO_3$ with diameters of 40-100 nm [43, 44], carbon black nanoparticles with diameters of 10-20 nm [45], and metals such as iron and nickel with diameters of 1-20 nm [46, 47]. One active research area is electrospinning of carbon nanotubes, which have small diameters but often have a very high aspect ratio [41, 48, 49].

A few researchers have employed even larger particle sizes, including Salalha *et al.*, who electrospun solutions containing bacteria and viruses, some on the order of 1 μm x 2 μm, [50] and Wang *et al.* who electrospun solutions containing clays as large as 4-5 μm in lateral dimensions [51, 52]. Two groups have electrospun solutions containing silica or polystyrene beads with the aim of producing superhydrophobic surfaces, succeeding in spinning with particles up to a 1 μm diameter [53,54]. None of these papers have addressed the effect of particles, particularly large (micro) particles,

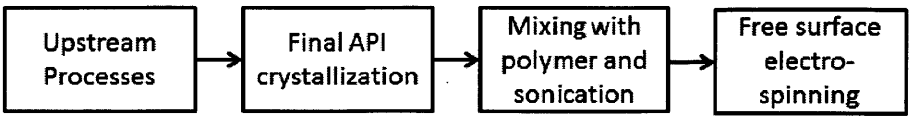

Figure 1-1: Proposed manufacturing process for electrospinning API crystal suspensions to produce fibers containing crystalline API.

on fiber diameter. In addition, all of this work has been done using the single needle electrospinning apparatus, which has a low production rate.

Section 5.3 presents a study of the spinnability of microparticles using free surface electrospinning. Spherical polystyrene beads of 1, 3, 5, and 10 μm diameter were used as model particles in order to determine how particle size affects the spinnability with the free surface approach and the final fiber diameter.

Electrospinning of particles was also applied to API crystals and the results are presented in Section 5.4. For this approach we envision a process such as the one in Figure 1-1. The electrospinning would follow the final API crystallization step, without the need to re-dissolve the API or dry the crystals, and the only added step, mixing with a polymer and sonication, is a simple and quick process.

Once we have demonstrated that producing fiber mats containing crystalline API is feasible, we look deeper into the properties of the resulting mats, particularly the properties affecting bioavailability. The dissolution rate (related to the bioavailability) is effected by the crystal size, the extent of dispersion in the polymer, and the crystalline morphology. It is important to understand these properties and how they compare to the API crystals as received and/or blended mixtures with the same excipient. Though an improved dissolution rate compared to a compressed powder tablet is not the aim in this case, an understanding of any differences in the dissolution rate is essential.

The overall aim of the work in this thesis is to carefully characterize the fibers resulting from electrospinning API and excipients such that we develop sufficient process understanding to apply electrospinning to a continuous industrial pharmaceutical manufacturing line. Specific aims include:

1) Characterize the mixing level of the amorphous API and polymer immediately

following electrospinning.

2) Determine the mixing level of the amorphous API and polymer and crystallinity of the API as a function of time over a 6 mo. period.

3) Determine the spinnability of particles of similar size to API crystals and the effects of the particles on the morphology and diameter of the final fibers.

4) Develop a method for producing fibers containing crystalline API and characterize the crystal size, extent of dispersion in the polymer, and crystalline morphology of the API in the resulting fiber mat.

Chapter 2

Background

2.1 Continuous Pharmaceutical Manufacturing

A primary driving force for the work in this thesis comes from a shifting manufacturing landscape for pharmaceutical products. Traditionally, all pharmaceutical manufacturing has been done batch-wise, where operations are carried out in discrete intervals and the materials are transferred as a batch from one step to the next, as with baking, where the ingredients are mixed in one dish and then transferred to another for baking in the oven. An alternative to this, and one that is used often in both large-scale chemical production and food processing, is continuous manufacturing, where the material moves through the entire process without interruption. The pharmaceutical and fine chemical industries have been slow to adopt continuous manufacturing. As of 2008, the top 300 organic chemicals were made continuously, but 90% of the next 2700 were made batch-wise, and for numbers 3000-30,000, 97% were made batch-wise [55].

To understand this trend and the recent shift in the pharmaceutical industry towards continuous manufacturing, one must understand the differences, particularly those that affect cost and profit, between the two approaches to manufacturing a chemical product. Batch processing is often associated with greater flexibility, as it is based on stirred tank reactors that can be used for many different products and processes, whereas for continuous manufacturing the equipment is more variable

and is designed around the chemistry of each product [55]. What follows from this is that one must have a better process understanding in order to run a continuous manufacturing plant well enough to compensate for the flexibility provided by the batch processes. This is both due to a need to design equipment properly as well as a need to be able to quickly fix a problem in the line before large amounts of product are ruined; for continuous manufacturing, a batch cannot be thrown out and a new one started [55]. This can be particularly challenging for pharmaceutical manufacturers who rely on high quality in the production line and have little time to develop process understanding for each product due to the pressure to bring a product to market. The United States Food and Drug Administration (FDA) has recently recognized this, and as of 2005 began an initiative encouraging process analytical technology (PAT), aiming to increase in-line analysis of product quality and increase the understanding of the behavior of the operations [56].

Continuous manufacturing in general can have many advantages over batch. Equipment utilization tends to be higher, as particular operations do not shut down and restart after discrete intervals as they do in batch manufacturing. The equipment also tends to be smaller; many of the first manufacturing processes being implemented continuously in the pharmaceutical industry are based on microreactor designs [55]. This can be advantageous for capital costs associated with building and operating a chemical plant.

For many continuous manufacturing operations, the scale-up from a lab scale to a production scale is relatively simple compared to that for batch operations. For the chemical reaction steps of API production, when microreactors are used for the operation, they can be scaled up by running multiple units in parallel [56]. For electrospinning, the scale-up is similar, by the use of additional electrode length, either by increasing the length within a single piece of equipment or by adding multiple units in parallel.

One of the key traits of continuous manufacturing is that the processes often have better mixing, and thus better heat and mass transfer. This allows each molecule to experience a similar environment, contrary to problems with dead spots in vessel-

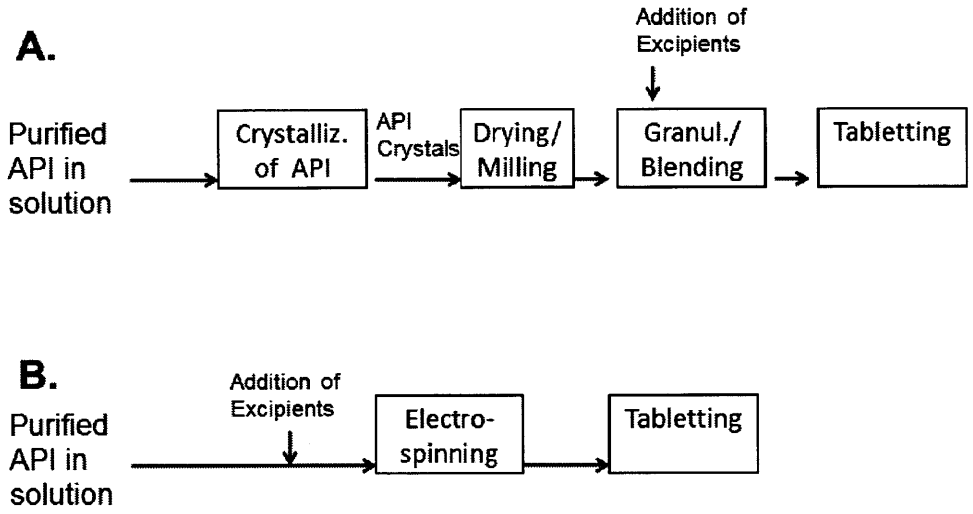

Figure 2-1: A. Traditional downstream manufacturing process, B. Proposed continuous downstream manufacturing process with electrospinning

type reactors and crystallizers, and increases quality as well as yield of the final product. For downstream manufacturing, mixing is a great concern, as the materials are generally in the solid form where it is much more difficult to achieve uniform mixing. A typical downstream process consists of crystallization, drying, milling, granulation, blending and tabletting steps (Figure 2-1-A). In developing continuous processes, we aim to remove many of these time-consuming correction steps. For the electroprocessing work, we envision a manufacturing line more like that in Figure 2-1-B. This would allow us to remove many solid handling steps and improve mixing of API and excipients, but most importantly it would replace downstream batch processes with a new continuous manufacturing process.

2.2 Electrospinning

Electrospinning refers to the process of using electrostatic forces to produce fibers from a polymer solution. First patented as a "Method of Dispersing Fluids" by William Morton [57], electrospinning has only recently begun to be applied to manufacturing products such as membranes and coatings and be explored for applications in tissue engineering and pharmaceuticals.

Various configurations may be used for electrospinning, which we will discuss later, but for a majority, the process begins with a charged droplet some distance away from a grounded electrode. At sufficient applied potential, the charge repulsion forces at the surface of the drop become great enough to overcome the surface tension forces and deform the droplet into a Taylor cone. At slightly higher applied fields, a jet is emitted from the apex of the cone, sending a fiber towards the grounded plate [58].

During the initial period, just after the jet is emitted from the cone, the fluid accelerates towards the grounded plate due to the influence of the electric field [59]. Little solvent evaporation occurs during this time [60]. At a point between the apex of the cone and arrival at the grounded plate, the charge repulsion in the jet leads to instabilities. Multiple types of instabilities are possible, but the so-called "whipping instability" is the most common for electrospinning [59]. The whipping instability was treated rigorously by Hohman *et al.* [61, 62]. During the whipping portion of electrospinning, the jet thins rapidly and significant solvent evaporation occurs [59]. As the jet diameter decreases, the effects of the acceleration of the jet in the electric field and the bending of the electric field lines become insignificant, and at small jet diameters, the charge repulsion forces decrease until they exactly balance the surface tension. This point signals the end of thinning and the diameter at this point is the terminal jet diameter [63]. However, various conditions, including solvent evaporation effects and elastic forces may cause the final fiber diameter to be larger than the predicted terminal jet diameter. If applicable, the jet then travels the remaining distance to the grounded plate and is collected as a non-woven mat.

The typical electrospinning set-up is referred to as "single-needle electrospinning", and it is illustrated in Figure 2-2. It consists of a container for the spinning solution, in our case a syringe attached to a pump, and a needle through which the fluid is pumped and at the end of which a droplet forms. A high voltage power supply provides charge to the solution and a grounded surface, often a flat metal plate, serves as the collection plate.

Alternative designs have been used, particularly ones whose aim is to increase the production rate of the electrospun fibers. The scale-up designs typically fall into

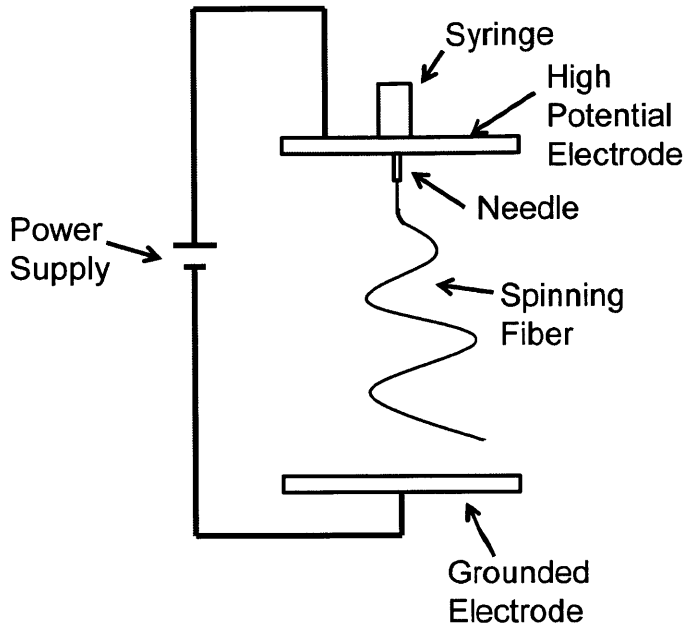

Figure 2-2: Single needle electrospinning apparatus consisting of a syringe and needle, a high voltage power supply and a grounded electrode

two categories: multi-needle or free surface (needleless) electrospinning. Multi-needle approaches aim to utilize a similar set-up to single-needle electrospinning, but with an array of needles. A key concern with this method, however, is the interaction between the electrospinning jets. Careful design of the configuration of needles and control of the electrospinning parameters is necessary to obtain spinning from all needles and a desired distribution of collected fibers [64–66].

Free surface approaches, on the other hand, rely on the self-organization of droplets on a thin liquid surface. This surface can take the form of a gaseous bubble [18] or a film on a rotating drum, disk, or wire electrode [9–17]. An illustration of a free surface electrospinning apparatus with a wire electrode is shown in Figure 2-3. During operation, the wire spindle rotates and the wire electrodes move through the liquid bath, entraining a layer of fluid on the wire as it passes the air/fluid interface. Due to Plateau-Rayleigh instabilities the fluid layer breaks into droplets, and, when sufficient electric field is applied, these droplets jet and electrospin until either the critical electric field condition is no longer met or the droplet volume is depleted (Figure 2-4). This process through fluid entrainment and jetting is discussed extensively in

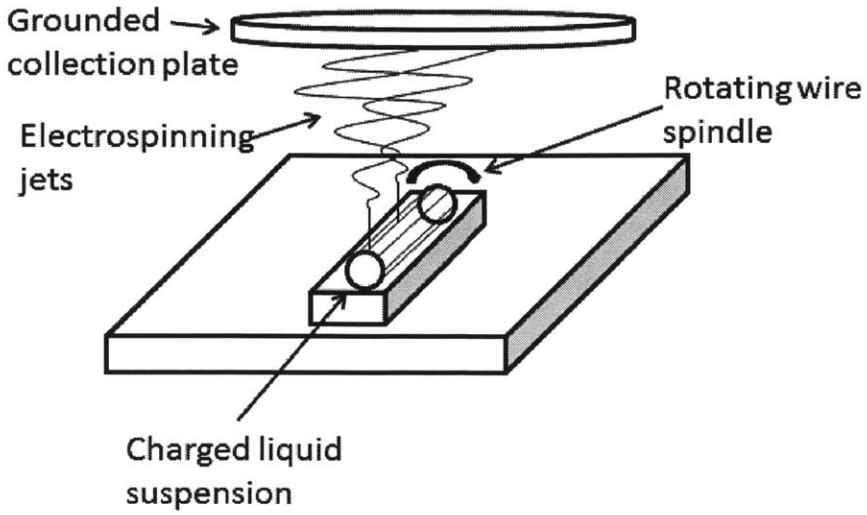

Figure 2-3: Free surface electrospinning apparatus consisting of a charged liquid bath, a grounded collection plate, and a wire spindle type of electrode.

Forward and Rutledge, 2012 [17].

2.3 Pharmaceutical Formulation Development

Though developing an effective active pharmaceutical ingredient (API) is an important part of designing a new pharmaceutical, developing an appropriate final drug product, complete with excipients, is also essential. The release rate of an API in the

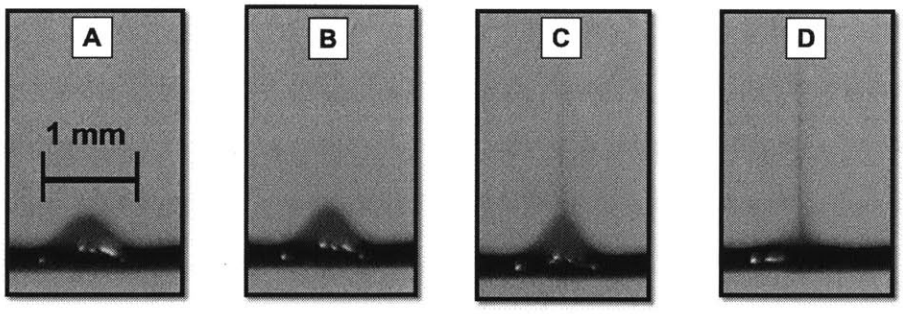

Figure 2-4: Free surface electrospinning off of a wire electrode. A. Conical droplet on the wire in the presence of an electric field at time t = 0 ms. B. Extended conical droplet at time t = 33 ms. C. Jetting droplet at time t = 66 ms. D. Depletion of droplet at time t = 99 ms.

body, as well as its solubility can depend on the API particle size, the interactions between the API and excipients, the crystallinity of the API, the dispersability of the solid dosage form, etc. These considerations can cause considerable difficulty in developing a new drug product, and work in this area is called pharmaceutical formulation development.

In this work, we have chosen a particular blending and drying method, electrospinning, and we explore ways to make it applicable to a wide variety of formulation needs. Most importantly, we aim to make it applicable to forming both amorphous and crystalline solid dispersions.

2.3.1 Amorphous Pharmaceutical Formulations

The amorphous form of an API, also referred to as a glass, is one in which there is no long range order, contrary to crystalline forms, where each polymorph has a unique, repeating configuration of molecules. Much research has been done on preparing and understanding the amorphous form for pharmaceuticals, driven primarily by one property of amorphous materials: the free energy of the amorphous state is higher than that of the crystalline state, and thus the solubility of an amorphous material is higher than that of its crystalline counterparts [67]. In 1995, Amidon and co-workers developed a method of classifying API based on their solubility and permeability to be able to predict how well *in vitro* dissolution studies would correlate with *in vivo* behavior of the drug, and this is called the biopharmaceutical classification system (BCS) [68]. API fall into one of 4 classes: I. high solubility, high permeability, II. low solubility, high permeability, III. high solubility, low permeability, and IV. low solubility, low permeability. It is the class II and IV APIs that are the target of much of the research on formulating API in the amorphous form.

Utilizing the amorphous form for drug products, however, is challenging. Thermodynamically, the crystalline form is more favorable, and this often leads to the crystallization of the amorphous form over time, thereby a change in solubility over time. In working with amorphous formulations, the stability of the amorphous form is more broadly defined than merely the thermodynamic stability; it refers to how well

the amorphous form resists crystallization, either by being more thermodynamically stable or by being kinetically stable. Despite being thermodynamically unfavorable, the amorphous form can be obtained for many compounds for one or both of the following reasons [69]:

1) The amorphous form is nearly as thermodynamically stable as the crystalline form, possibly due to poor molecular packing.

2) The time required to form a crystal is long, allowing one to use a preparation method that traps the molecule in the amorphous form for a desired period of time.

For method (1), if the thermodynamic stability is similar to that of the crystalline form, the API may not have significantly better water solubility than the crystalline form and thus formulating it as an amorphous form would be unnecessary. However, one may take advantage of method (2) for formulating many APIs in their amorphous form. There are many processing methods that have been developed, including rapid drying techniques such as lyophilization, spray drying, and electrospinning, and rapid cooling techniques such as melt quenching with liquid nitrogen [69]. These methods begin with the molecules in a liquid state where they are disordered and rapidly bring them to a solid state without leaving time for the molecules to order themselves before they are limited by low mobility [70].

Not only is it necessary to properly prepare the amorphous form, but it is essential to stabilize it, i.e. keep it from crystallizing, for the desired shelf life. For pharmaceutical products this may be on the order of 2-3 years. Often additional excipients are added to the amorphous API to further decrease its molecular mobility, either by hydrogen bonding with the API or by being a physical barrier between API molecules [22–25]. Formulations of this type, where one or more excipients are blended to some degree with the API are called solid solutions or dispersions, depending on the mixing level.

For crystalline systems, the distinction between a solid solution and solid dispersion is clear, as a crystal has a rigid structure and the dispersed molecules will exist as distinct molecules in either interstitial spaces or as substitutes for the carrier molecules. For amorphous materials on the other hand, the amorphous API molecules

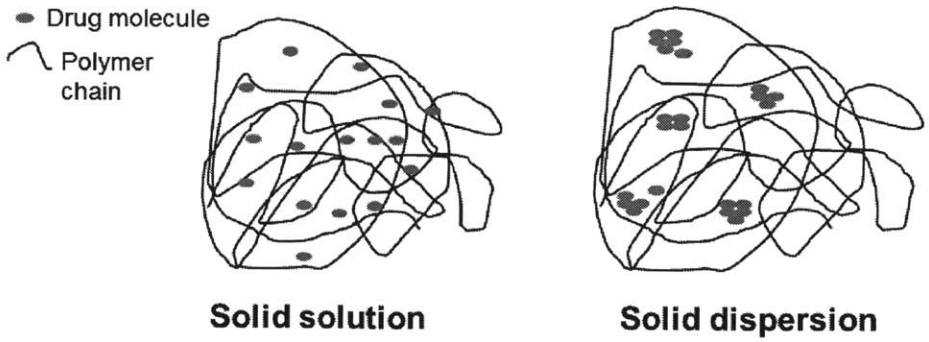

Figure 2-5: Illustration of a solid solution, where API and polymer are molecularly mixed and a solid dispersion, where clusters of API exist within the polymer

within an amorphous polymer carrier will be disordered and will be irregularly dispersed throughout the carrier [71]. By the strictest definition, a mixture is called a solid solution when there is molecular level mixing and a solid dispersion when clusters of API molecules exist (illustrated for a drug and polymer in Figure 2-5) [71].

The strict definition is difficult to use, as there are no techniques that can identify true molecular level mixing [71]. Table 2.1 lists some of the techniques used to analyze solid solutions and dispersions and their limits. In this work, we use the solid state NMR technique due to its low spacial limit, applicability to our samples, and our ease of access to the equipment through the Francis Bitter Magnet Lab (FBML) at MIT. Because of this, we define a solid dispersion as a mixture having phase separated domains greater than 2-10 nm and a solid solution as being homogeneous down to a length scale of 2-10 nm.

For stabilizing an amorphous API, it is most desirable to have a solid solution. This will allow the maximum contact between the excipient and API for hydrogen bonding as well as provide the best physical barrier to the API molecules forming clusters and, subsequently, crystals.

2.3.2 Crystalline Pharmaceutical Formulations

Similar to considerations when developing amorphous pharmaceutical formulations, one must choose materials and processing methods for crystalline formulations such

Technique	Spacial Limit (approx. domain size measurable)	Practical Limits
Scanning Electron Microscopy	50 nm	No contrast between amorphous polymer and amorphous API
Transmission Electron Microscopy	< 1 nm [72]	Different domains must have different electron densities in order to contrast
X-ray Diffraction	1 μm	Can only determine particle/domain size for crystals
Raman Mapping	2 μm [73]	Difficult to focus for spot sizes < 2 μm
Fluorescence Resonance Energy Transfer	1-10 nm [74]	Requires fluorescent materials, measures only fraction of molecules present as clusters, for low API concentrations
Solid State Nuclear Magnetic Resonance	2-10 nm	Time consuming, specialty equipment
Atomic Force Microscopy with Fourier Transfer Infrared Spectroscopy	100 nm [75]	Difficult to mount electrospun materials for AFM, mainly a surface technique

Table 2.1: Methods of analyzing solid dispersions. Where cited, spacial limit is from literature, otherwise it is from experience with available instruments.

that the final drug product has a desired bioavailability and is stable in the chosen form over time. Primary factors affecting bioavailability (i.e. solubility in the body and permeability of membranes) are the crystalline polymorph and crystal size.

Polymorphism is the ability of a molecule to exist in more than one crystal structure (long range ordered repeating arrangement of molecules). Like amorphous API, some polymorphs have higher internal energy than others, and thus the solubility and bioavailability of a drug product may be different depending on which polymorph is present. It is essential in formulation development to be aware of the polymorphism of the APIs and control the polymorph obtained such that the bioavailabilities of the APIs are constant over time.

Crystalline particle size affects the dissolution rate of an API primarily through the surface area available to dissolve, as predicted by the Noyes-Whitney equation:

$$\frac{dm}{dt} = \frac{DA}{h}(C_{sat} - C) \tag{2.1}$$

where $\frac{dm}{dt}$ is the dissolution rate, D is the diffusion coefficient, A is the surface area for diffusion, h is the diffusional path length, C_{sat} is the solubility and C is the concentration in solution [71]. Small particles have a larger surface area for a given volume and thus will have a higher dissolution rate than large particles.

When formulating poorly water soluble APIs, there are many options for producing small particles to increase the dissolution rate including wet media milling [76], sonication [77], antisolvent precipitation [78–81], and other rapid precipitation techniques [82–86]. Often when these formulations are prepared, they are made using polymer excipients or surfactants, forming some type of solid dispersion. This is done for two reasons:

1) the polymers or surfactants are chosen such that they interact with the crystal surface, hampering growth during precipitation [80–82, 86]

2) the excipients separate the API particles in the solid form and keep them from aggregating [84, 87].

Careful consideration of the polymorphism and particle size distribution is essen-

tial to properly formulate a drug product for the final oral dosage form. Thus, when exploring the use of electrospinning for producing fibers containing crystalline API (Chapter 5), we examine these properties in order to determine whether the method is viable as a pharmaceutical manufacturing process.

2.4 Solid State Nuclear Magnetic Resonance

A large part of this thesis utilizes solid state NMR analysis techniques. In this section, we will describe the basics of NMR, the application of NMR to studying solid samples, and the specific techniques used in this work.

The use of NMR is based on the principle that a spinning charge generates a magnetic field. Any nucleus that has an odd mass number or atomic number (i.e. has an odd number of protons and neutrons or the sum of the number of protons and neutrons is odd) has a spin and can be analyzed using NMR. Not all of these nuclei have 1/2 spins; for example, sodium has a 3/2 spin, but is studied using NMR. In this work, however, only the most commonly studied nuclei, ^{1}H and ^{13}C, are discussed, and they both have 1/2 spins. In the presence of an applied field, the spin for these nuclei can exist either in the +1/2 or -1/2 state, where the +1/2 state is aligned with the applied field and the -1/2 state is against the applied field.

Irradiation of a sample with radio frequency (rf) energy equal to the energy difference between the +1/2 and -1/2 state will cause the spins to jump to the higher -1/2 state [88], and this is illustrated in Figure 2-6.

A key property of this phenomenon is that different atoms will make the jump at different applied rf energy. Electrons of an atom and nearby atoms can generate an additional magnetic field in the direction of the applied field. This causes the atom to require more rf energy to jump to the higher energy state than an atom with no interference from a chemical environment, and this difference is called the chemical shift. This principle is what allows us to use NMR to study chemical structures [88].

Special considerations must be made, however, for NMR of solid state samples. The chemical shift, derived from nuclear spin interactions, depends on the orientation

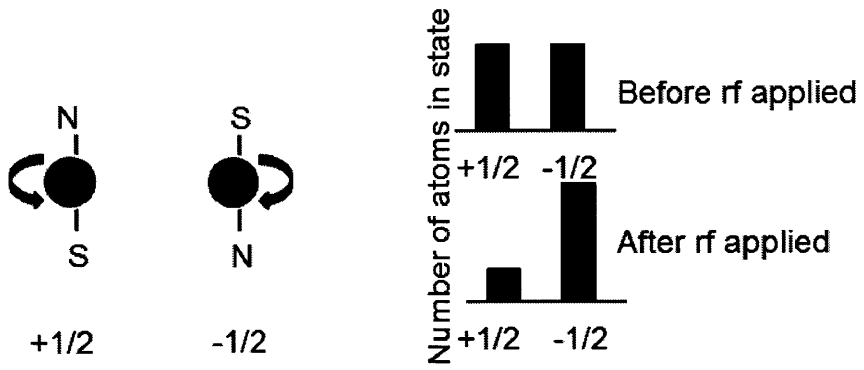

Figure 2-6: Illustration of basic principles of NMR: A spinning charge generates a magnetic field that can be aligned with (+1/2) or against (-1/2) an applied field. When radio frequency (rf) energy is applied the spins jump to a higher energy state.

of the molecule, with the nuclear spin interactions being proportional to $(3\cos^2\theta_R - 1)$, where θ_R is the angle at which the sample is inclined relative to the applied field. In a liquid, the thermal motions of the molecules cause the influences of orientation on the nuclear spin interactions to average to zero. In a solid, however, the molecules are rigid and therefore all orientations are detected and the peaks are significantly broadened. If θ_R is set to 54.74°, then $(3\cos^2\theta_R - 1)$ is equal to zero and the average orientation dependance of the nuclear spin interactions is also zero. This is only sufficient to remove the effects of orientation if the sample is not only inclined at θ_R, but also spun at a high enough rate that the angle of the spin interaction relative to the applied field is averaged rapidly compared to the orientation dependance of the nuclear spin interaction [89]. This experimental set-up, spinning the sample rapidly at an angle of 54.74° to the applied field is referred to as magic angle spinning (MAS) and is used in nearly all solid state NMR studies.

Orientation effects are not the only challenge in using solid state NMR. The technique also suffers from poor signal to noise ratio, particularly when performing ^{13}C solid state NMR. In nature, ^{13}C is only present at a rate of 1.1%, whereas ^{1}H is present at a rate of 99.9% [89]. This leads to two problems:

1) collection of sufficient data on the ^{13}C will take a very long time due to the small number of atoms

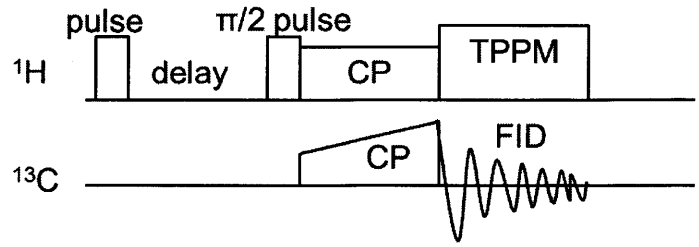

Figure 2-7: The pulse sequence for inversion recovery experiments ($T_1(^1H)$) consisting of an initial rf pulse, a delay for recovery, a second rf pulse, a cross polarization (CP) pulse and two pulse phase modulation (TPPM) during detection of the free induction decay (FID)

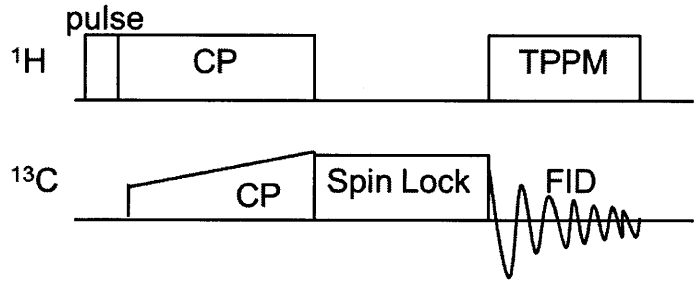

Figure 2-8: The pulse sequence for spin lock experiments ($T_{1\rho}(^1H)$) consisting of an initial rf pulse, a cross polarization (CP) pulse, a spin lock period and two pulse phase modulation (TPPM) during detection of the free induction decay (FID)

2) dipolar coupling between the far more abundant ^1H and the ^{13}C (referred to as heteronuclear coupling) will broaden the signal significantly.

To remove the effects of dipolar coupling (2), a proton decoupling (PD) sequence is used. There are many approaches to PD, most based on the same principle; applying irradiation at a very high power at the frequency of the proton resonance. The application of the irradiation at the frequency very close to the proton resonance causes the ^1H spins to repeatedly transition between +1/2 and -1/2. If the rate of transitions is fast enough (i.e. a high enough rf power is used), the coupling will average to zero [89]. Various methods can be used for PD, but in this work we use the two pulse phase modulation (TPPM) pulse sequence [90], the most commonly used pulse sequence at this time. The TPPM is generally applied during the detection time only, as can be seen in Figures 2-7 and 2-8.

A technique known as cross polarization (CP) is used to increase the signal during

^{13}C NMR experiments. A special pulse sequence for the rf energy allows the ^{13}C to obtain magnetization from ^{1}H spins, thereby increasing the ^{13}C signal. Simply, the approach is such that rf pulses are used to set the gaps between spin states of the ^{1}H and ^{13}C equal to one another. The samples are held in that position for a given contact time, allowing the transfer of magnetization, which can then be detected on the ^{13}C [89]. The incorporation of the CP pulse sequence can be seen in Figures 2-7 and 2-8.

These three techniques, MAS, TPPM, and CP are commonly used to obtain high quality solid state NMR spectra.

For the work in this thesis we use a property that can be measured by solid state NMR: spin diffusion. Like heat or mass, magnetization diffuses from areas of high magnetization to areas of low magnetization, following Fick's law [91]:

$$m(r,t) = \nabla \left[\dot{D}(r)\nabla m(r,t)\right] \tag{2.2}$$

where m is the magnetization, D is the diffusion coefficient, r is the space vector and t is the diffusion time. This diffusion is not a physical movement, but rather a transfer of magnetization between neighboring nuclei through homonuclear (same nucleus, i.e. ^{13}C and ^{13}C or ^{1}H and ^{1}H) couplings [92]. The diffusion is most efficient between protons, and we can indirectly measure that using the CP pulse sequence. We do not measure it from ^{1}H spectra directly because the signals overlap significantly, so it is much easier to use the ^{13}C spectra, where the peaks are more separated from one another [92].

When the sample is subjected to an rf pulse, we obtain a non-equilibrium distribution of spin states. It is a distribution because not all protons in the same sample are in the same chemical environment, so they have different magnetizations [92]. It is the relaxation from this distribution that we observe. By examining the magnetization change for various mixing times (delay for the inversion recovery sequence, Figure 2-7, and spin lock for the spin lock pulse sequence, Figure 2-8), we can determine a time constant for the diffusion, known as the spin lattice relaxation time ($T_1(^{1}H)$) for

the inversion recovery sequence and the spin lattice relaxation time in the rotating frame ($T_{1\rho}(^1H)$) for the spin lock sequence.

The measured time constants are dependent on the chemical environment, and thus dependent on the materials in the sample and the level of blending, if any. By solving Equation 2.2, either analytically or by using estimates, we can obtain a domain size for diffusion, L, corresponding to the time constant [92]. In this work we use a simple solution [34]:

$$L = \sqrt{6DT_i} \tag{2.3}$$

where D is the diffusion coefficient and T_i is the time constant, either $T_1(^1H)$ or $T_{1\rho}(^1H)$. If the domain size of the phase separation of the API or polymer is smaller than the diffusion length L, then all L-sized domains will have similar diffusion behavior and the value of the relaxation time will be the same whether determined from one component or the other (in our case the API or polymer peaks). This is illustrated in Figure 2-9-A, where the API (gray boxes) and polymer (white boxes) phase separation has a small domain size. If the domain size of the phase separation of the API or polymer is the same size or larger than the diffusion length L, then the L-sized domains will show different diffusion behavior and two distinct values of the time constant will be measured [91]. This is illustrated in Figure 2-9-B, where the API and polymer phase separation has a large domain size [34,91,92]. The latter case indicates phase separation of domain size L or larger and is referred to in this work as a "solid dispersion." The former case indicates no phase separation of domain size L or larger and is referred to in this work as a "solid solution."

This method of examining phase separation in mixtures was first applied to polymer blends [34], but has since been used to study API/polymer solid dispersions [4,31,32,93].

Solid state NMR is a powerful technique for examining the chemical environment of pharmaceutical formulations, including mixtures, without changing or damaging the sample. This allows us to investigate the desired properties of the actual product

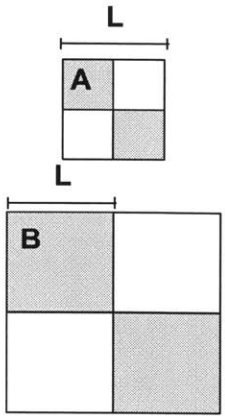

Figure 2-9: Illustrations of phase separated regions of API (gray) and polymer (white). A. Phase separated regions are smaller than length scale L, solid solution; B. Phase separated regions are as large or larger than length scale L, solid dispersion.

as it is in the final form.

Besides the relaxation time analysis used in this work, there are many other applications of solid state NMR, including two-dimensional NMR analysis that would allow us to determine which functional groups of one molecule are interacting with which functional groups in another [94]. Due to the low percentage of ^{13}C in natural abundance, these advanced techniques require ^{13}C labeling in order to provide conclusive results. Though expense and time constraints currently limit the use of solid state NMR, much research is being done to improve the signal-to-noise ratio without needing ^{13}C labeling [95–97], so it is only a matter of time before the technique is efficient enough for widespread use in the pharmaceutical industry.

Chapter 3

Methods

In this chapter we describe the methods used throughout the work this thesis, including the materials selected, electrospinning equipment and parameters, scanning electron microscopy, X-ray diffraction, differential scanning calorimetry, Fourier transform infrared spectroscopy, solid state NMR, moisture content measurements with thermogravimetric analysis, UV-visible spectroscopy, dissolution, and particle size measurements.

3.1 Materials

3.1.1 Small Molecules

Aliskiren (SPP) was kindly supplied by Novartis AG. Indomethacin (IND), carbamazepine (CBZ), ibuprofen sodium salt (IBUss), famotidine (FAM), albendazole (ABZ), ibuprofen (IBU), and lead (325 mesh) were purchased from Sigma-Aldrich (St. Louis, MO).

3.1.2 Polymers

Poly(vinyl pyrrolidone) (PVP, 1.3 MDa M_w and 55 kDa M_w), poly(ethylene oxide) (PEO, 1 MDa M_w), poly(l-lactic acid) (PLLA, 259 kDa M_w), poly(acrylic acid) (PAA, 450 kDa M_w), poly(vinyl chloride) (PVC, 62 kDa M_w), polycaprolactone (PCL, 10

kDa M_w) and polystyrene (PS, 280 kDa M_w) were purchased from Sigma-Aldrich (St. Louis, MO). Poly(methyl methacrylate) (PMMA, 300 kDa M_w) and nylon 3,6 (NY) were purchased from Scientific Polymer Products (Onterio, NY). Dry 1 μm and 3 μm polystyrene beads were purchased from Polysciences, Inc (Warrington, PA), and dry 5 μm and 10 μm polystyrene beads were purchased from Microbeads AS (Skedsmokorset, Norway).

3.1.3 Solvents

American Chemical Society grade ethanol (EtOH) and methanol (MeOH) were purchased from VWR International (West Chester, PA). Dimethyl formamide (DMF), chloroform, and tetrahydrofuran (THF) were purchased from Sigma-Aldrich (St. Louis, MO).

3.2 Electrospinning

The single needle electrospinning apparatus (Figure 2-2) was arranged in a parallel plate configuration and was equipped with a Harvard Apparatus PHD Infusion 2000 syringe pump and a Gamma High Voltage power supply model number ES30PN. Table 3.1 shows the electrospinning parameters, including concentration, flow rate, needle-to-ground distance and applied voltage for all materials electrospun on this apparatus.

The free surface electrospinning experiments (Figure 2-3) were performed on a custom-built apparatus complete with a Gamma High Voltage power supply model number RR40-1.5R/DPPM and grounded collection plate covered in aluminum foil. The wire spindle was constructed from 2 teflon disks of 3.2 cm diameter held 6.4 cm apart and connected with a center rod and wires at the outer edge. Either a 2-wire, where the wires were 180° apart, or a 6-wire, where the wires were 60° apart, configuration was used. The spindle was placed in the teflon solution bath and rotated by a small DC motor (Zheng gear box motor ZGA25RP216). The entire apparatus was located in an enclosure with low air flow. Both the wire electrode and the

Name	Polymer concentration	API concentration	Solvent	Flow rate (mL/min)	Distance (in.)	Voltage (kV)
1:4 SPP:PVP	10 wt%	2.5 wt%	MeOH	0.03	9	24
1:2 SPP:PVP	10 wt%	5 wt%	MeOH	0.02	9	24
1:1 SPP:PVP	10 wt%	10 wt%	MeOH	0.02	9	24
4:1 SPP:PVP	6 wt%	24 wt%	MeOH	0.02	9	20
1:1 IND:PVP	8 wt%	8 wt%*	EtOH	0.04	9	28
2:1 IND:PVP	6 wt%	12 wt%*	EtOH	0.05	9	28
1:1 IBU:PLLA	2.5 wt%	2.5 wt%	Chloroform	0.03	11	30
1:1 CBZ:PLLA	3 wt%	3 wt%	Chloroform	0.05	9	20
1:2 IBU:PMMA	7 wt%	3.5 wt%	DMF	0.05	9	18
1:2 CBZ:PMMA	7 wt%	3.5 wt%	DMF	0.05	9	18
1:2 IBU:NY	25 wt%	12.5 wt%	DMF	0.03	9	23
1:2 CBZ:NY	25 wt%	12.5 wt%*	DMF	0.08	9	27
1:2 IBU:PAA	5 wt%	2.5 wt%	EtOH	0.2	9	13
1:2 CBZ:PAA	5 wt%	2.5 wt%	EtOH	0.1	9	30
1:2 IBU:PVC	18 wt%	10 wt%	60% THF 40% DMF	0.1	9	27
1:2 CBZ:PVC	20 wt%	10 wt%	60% THF 40% DMF	0.03	9	26
1:2 IBU:PCL	8 wt%	4 wt%	Chloroform	0.02	9	28
1:2 CBZ:PCL	8 wt%	4 wt%	Chloroform	0.2	9	13
1:2 IBU:PS	20 wt%	10 wt%	DMF	0.02	10.5	18
1:2 CBZ:PS	23 wt%	10 wt%	DMF	0.05	9	12
1:2 IBU:PEO	2 wt%	1 wt%	MeOH	0.2	9	15
1:1 CBZ:PEO	2 wt%	2 wt%	MeOH	0.2	9	24
1:2 IBU:PVP	10 wt%	5 wt%	MeOH	0.02	11	22
1:2 CBZ:PVP	10 wt%	5 wt%	MeOH	0.02	9	19

Table 3.1: Electrospinning parameters for the formulations prepared using the single needle apparatus discussed in this work, *heated in order to dissolve

solution bath were connected to the high voltage supply [17]. For some electrospinning experiments, the conductivity of the fluid was measured prior to spinning using a VWR digital conductivity meter. The rotation rate of the wire spindle was set at 8.8 rpm, the electrode to ground distance was set at 20 cm, and the high voltage power supplied to the bath was set to obtain jetting (approximately 30 kV) for all solutions electrospun on the free surface apparatus.

3.3 Scanning Electron Microscopy

The morphology of the electrospun fibers was characterized by scanning electron microscopy (SEM). The samples were sputter coated using a Quorum Technologies SC7640 high resolution gold/palladium sputter coater and examined using a JEOL 6060 SEM at a 5 kV operating voltage. Where necessary, the fiber diameter was measured from the SEM images using ImageJ image analysis software (available through the National Institutes of Health). At least 80 measurements were analyzed per sample, and the measurements were made from multiple images.

3.4 X-ray Diffraction

X-ray diffraction (XRD) was performed on a PANalytical X'Pert Pro instrument with a reflection-transmission spinner PW 3064/60 sample stage and a Cu X-ray source with a 1.54 Å wavelength. For electrospun samples a piece of the mat was laid flat on a zero background plate for analysis, and for powder samples the powder was spread over the zero background plate and flattened with a microscope slide. Powder patterns were taken of pure materials for comparison with electrospun samples.

The limit of detection for crystalline IND in a PVP matrix is approximately 1 wt% (Figure 3-1).

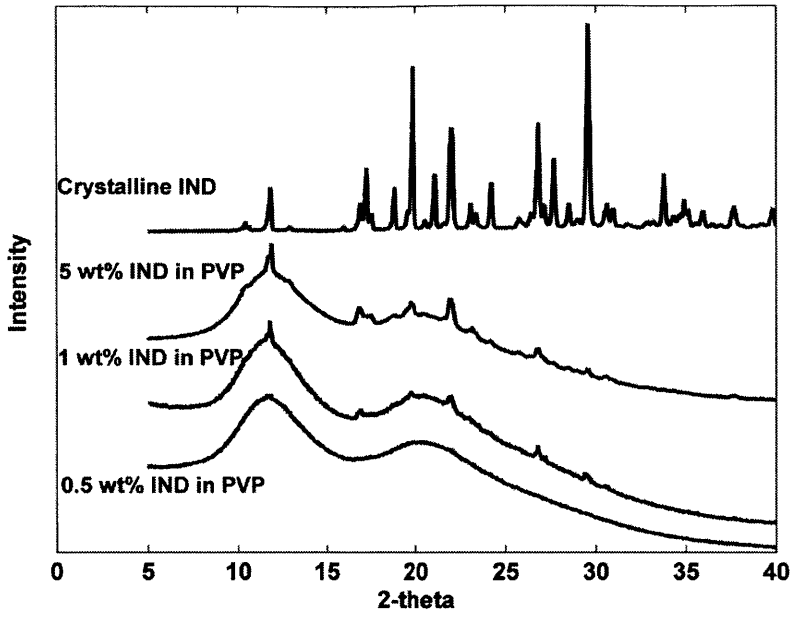

Figure 3-1: XRD powder patterns of crystalline IND and physical mixtures of 5 wt% crystalline IND in PVP, 1 wt% crystalline IND in PVP and 0.5 wt% crystalline IND in PVP. Indicates limit of detection of crystalline IND by the XRD method used is approximately 1 wt%.

3.5 Differential Scanning Calorimetry

DSC was performed on a TA DSC Q2000 instrument using a 2-6 mg sample in an aluminum sample pan. The materials were heated at 10°C/min from room temperature to approximately 20°C beyond the melting point of the API present in the sample.

The limit of detection for IND in a PVP matrix is approximately 10 wt% (Figure 3-2).

For many of the formulations (including the IND/PVP mixtures in Figure 3-2), a large, broad endotherm was present, centered around approximately 100°C. This corresponds to the release of water absorbed by the SPP (where applicable) and PVP [36], which has been confirmed by holding at 60°C for 2 hours to allow the water to release prior to ramping the temperature in the DSC experiment. After such a hold, there is no longer a broad endotherm in 50-150°C range, and these results are shown in Figure 3-3. The 2 hour hold was used to measure the Tg of SPP/PVP formulations (results in Section 4.2.2), but was not used in other experiments in this

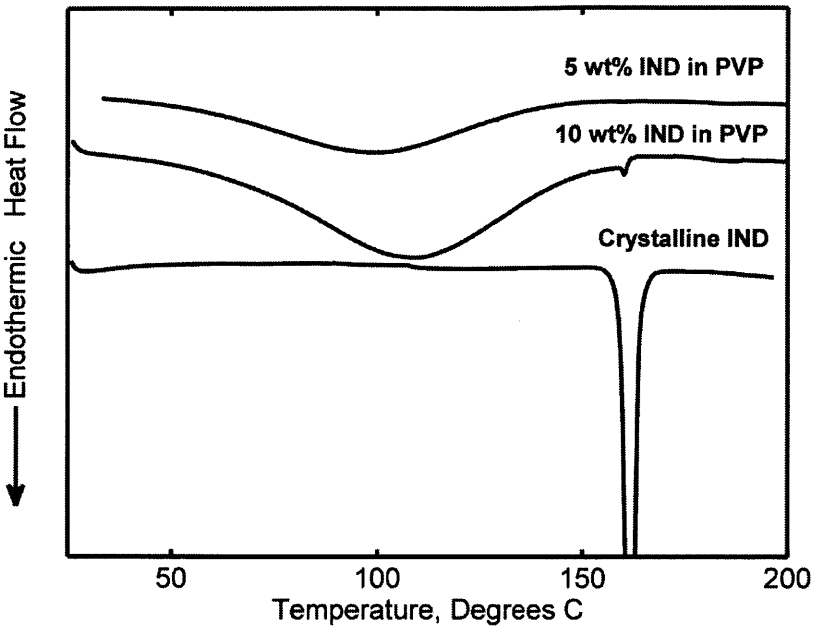

Figure 3-2: DSC curves of 5 wt% crystalline IND in PVP physical mixture, 10 wt% crystalline IND in PVP physical mixture and pure crystalline IND. Indicates limit of detection of crystalline IND in PVP by DSC is approximately 10 wt%.

work.

3.6 Fourier Transform Infrared Spectroscopy

Fourier transform infrared spectroscopy (FTIR) was performed with a Nicolet 8700 instrument (Thermo Fisher Scientific, Waltham, MA) and an Specac attenuated total reflectance (ATR) accessory (Specac, Slough, UK). Scans were pefrormed with a 2 cm^{-1} resolution, 128 scans, aperture of 69, gain of 8, and atmospheric suppression. The data was collected with and analyzed using the OMNIC software package (Thermo Fisher Scientific, Waltham, MA).

3.7 Solid State Nuclear Magnetic Resonance

To measure domain size using solid state NMR, one uses the relaxation time constant, a property of spin diffusion [31–35]. Like heat or mass, magnetization diffuses from

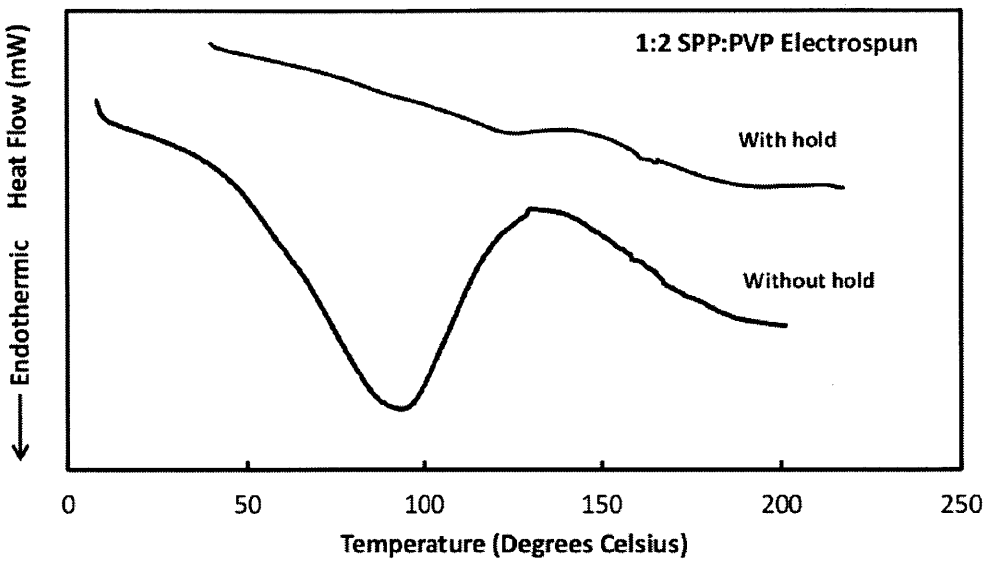

Figure 3-3: DSC curves for 1:2 SPP:PVP electrospun formulations following a 2 hour hold at 60°C for the top curve, but no hold for the bottom curve.

areas of high magnetization to areas of low magnetization. The diffusion follows Fick's law, Equation 2.2 [91].

By running experiments at different mixing times (i.e. diffusion times) and measuring the maximum peak intensities, one can generate a plot of signal intensity vs. mixing time. Figure 3-4 shows an example of experimental data for the $T_1(^1H)$ of the 1:1 SPP:PVP physical mixture. The filled symbols are the peak intensities for the corresponding PVP peaks at each mixing time, τ, and the open symbols are the peak intensities for the corresponding SPP peaks at each mixing time, τ. The peak intensities have been normalized such that they fall between zero and one in order to better show the difference in the exponential curves.

An exponential decay function of the form:

$$I(t) = I(0)exp\left(-\frac{t}{T_i}\right) \tag{3.1}$$

can be fit to the intensity data for each peak, where I is the signal intensity, t is the time and T_i is the relaxation time constant. For $T_1(^1H)$ and $T_{1\rho}(^1H)$ measurements, t is the mixing time, or τ. For the example case, the $T_1(^1H)$ relaxation times for each

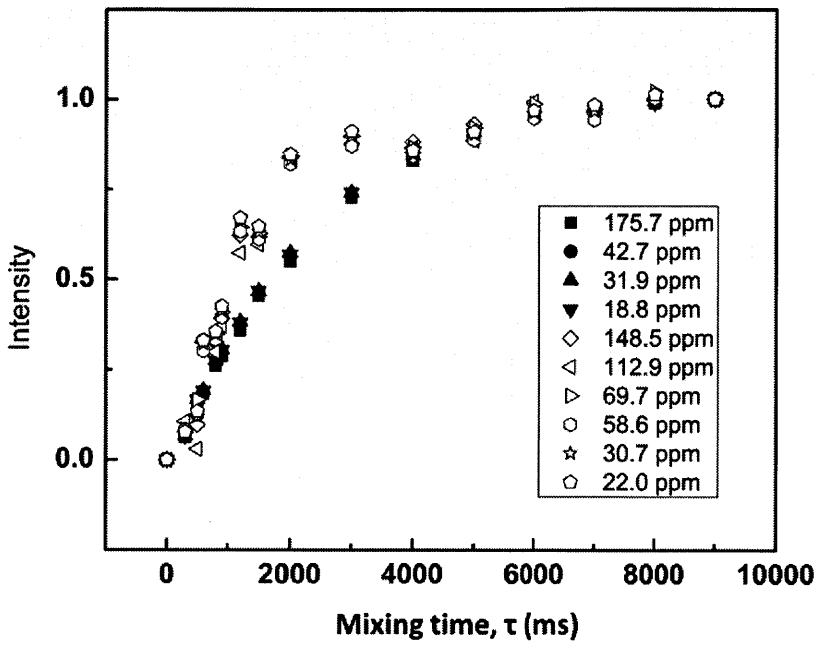

Figure 3-4: Signal intensity vs. mixing time (τ) from $T_1(^1H)$ experiments for the 1:1 SPP:PVP physical mixture. Filled symbols correspond to PVP peaks, open symbols correspond to SPP peaks.

peak are shown in Table 3.2.

There are two time constants that characterize the relaxation, $T_1(^1H)$ and $T_{1\rho}(^1H)$. $T_1(^1H)$ characterizes domains on a larger length scale (20-80 nm) while $T_{1\rho}(^1H)$ characterizes domains on a smaller length scale (2-20 nm), and the peak intensities from two different experiments, inversion recovery (Figure 2-7) and spin lock (Figure 2-8), are used to calculate each separately.

Immediately prior to solid state NMR experiments, electrospun mats were removed from the desiccator and packed into a 4 mm rotor. The mats were not milled, but placed in the rotor as is and packed tightly using a blunt rod. Approximately 40 mg material was packed into the rotor.

Experiments were performed on a custom-built spectrometer operating at 500 MHz ^1H Larmor frequency (courtesy of D. Ruben, FBML, MIT, Cambridge, MA), equipped with a 4 mm triple-resonance Varian-Chemagnetics probe (Varian Inc., Palo Alto, CA). The sample was cooled with a stream of dry air maintained at a temper-

Material	Peak (ppm)	$T_1(^1H)$ (s)
PVP	175.7	2.52 ± 0.09
	42.7	2.44 ± 0.08
	31.9	2.37 ± 0.07
	18.8	2.38 ± 0.08
SPP	148.5	1.39 ± 0.17
	112.9	1.47 ± 0.22
	69.7	1.35 ± 0.15
	58.6	1.37 ± 0.17
	30.7	1.31 ± 0.17
	22.0	1.29 ± 0.16

Table 3.2: $T_1(^1H)$ values for each peak for the 1:1 SPP:PVP physical mixture

ature of 8°C, while the sample spinning speed at the magic angle was set to 10 kHz for the SPP formulations and 8.5 kHz for the IND formulations. The spinning speeds were chosen such that the spinning side bands did not overlap with the peaks of interest. For all experiments, the ^1H, ^{13}C, and ^{15}N channel tuning and matching were optimized, the spectra were referenced to adamantane, and the alignment of the magic angle was verified.

One dimensional ^{13}C CP/MAS experiments were recorded using a CP contact time of 2 ms and 100 kHz TPPM ^1H decoupling during acquisition [98]. The relaxation delay, or the delay between scans, was 10 s for SPP formulations and 7 s for IND formulations, which were the minimum to allow full return of the magnetization to its original distribution. $T_1(^1H)$ was measured using an inversion recovery scheme employing 100 kHz ^1H pulses. The relaxation time was varied from 0 to 9000 ms for the $T_1(^1H)$ experiments. $T_{1\rho}(^1H)$ was measured using spin-lock experiments employing 100 kHz ^1H pulses. The spin-lock time was varied from 1-35 ms and 1-60 ms for SPP and IND formulations, respectively.

The free induction decays were Fourier transformed using software in the FBML to obtain the intensity vs. chemical shift NMR spectra, and the resulting data was exported for further analysis following background correction and phasing. The FBML software is not commercially available, but the Fourier transform operation, background correction, and phasing are standard in many NMR software packages, in-

cluding those for Varian and Brucker instruments and NMRPipe, a unix-based free software available through the National Institutes of Health. For background correction, the baseline was shifted up or down in order to set it to zero intensity and the phasing was adjusted until the baseline was symmetric about the peaks. To deconvolude overlapping drug and polymer peaks, MATLAB was used to fit the sum of the pure amorphous spectra to the mixture spectrum in question.

The maximum peak intensities of the strong drug and polymer peaks were determined using the deconvoluded drug and polymer spectra, and the data for intensity vs. mixing time (Figure 3-4) for each peak and each relaxation time ($T_1(^1H)$ and $T_{1\rho}(^1H)$) were then fit to the exponential function in Equation 3.1 using built in functions in Origin 8.5 (Table 3.2). We then calculated average $T_1(^1H)$ and $T_{1\rho}(^1H)$ values for the drug and polymer using the four major PVP peaks (175.7, 42.7, 31.7, and 18.8 ppm) and the six major SPP peaks (148.5, 112.9, 69.7, 58.6, 30.7, and 22.0 ppm) or six major IND peaks (156.5, 131.1, 113.9, 55.2, 29.9, and 13.3 ppm). For the example case, with the 1:1 SPP:PVP physical mixture $T_1(^1H)$, the average value from the PVP peaks is 2.47 $\pm$ 0.20 s and the average value from the SPP peaks is 1.26 $\pm$ 0.27 s.

3.8 Moisture Analysis

The weight percent water in electrospun stability samples was measured using thermogravimetric analysis (TGA). TGA experiments were performed on a TA TGA Q5000 (TA Instruments, New Castle, DE). A ramp of 20°C/min to 150°C was used and the weight percent water was calculated from the weight loss between 40-110°C using the TA Universal Analysis software (TA Instruments, New Castle, DE).

3.9 UV-visible Spectroscopy

In order to determine the actual drug loading in electrospun fibers, samples were analyzed with a Perkin-Elmer (Waltham, MA) double-beam Lambda25 UV-vis spec-

trophotometer. A standard curve was prepared for ABZ in methanol for concentrations from 0.005 mg/mL to 0.05 mg/mL at an absorbance of 295 nm and for FAM in methanol for concentrations from 0.002 mg/mL to 0.035 mg/mL at an absorbance of 286 nm. PVP does not absorb in the UV range and pure methanol was used for the background spectrum. A known mass of electrospun mat was dissolved in a known volume of methanol and diluted such that the expected concentration of API fell within the concentration ranges covered by the standard curves. From the resulting measured concentration, the mass of API in the original mat sample, and thus the weight percent API in the electrospun mat was calculated. Three measurements were made per API and were averaged to give the reported value.

3.10 Dissolution

Tablets were made from electrospun material by weighing out 150 mg of the fiber mat and pressing into a 9 mm tablet using a Gamlen Tablet Press model GTP1 in the manual mode. The material was inserted into the die randomly, it was not rolled or folded in a controlled manner. Powder tablets were prepared by weighing out 50 mg API powder and 100 mg PVP powder, mixing for 1 min, and pressing into 9 mm tablets using the same press with the same insertion depth.

Dissolution was performed using a Varian VK 7025 dissolution bath (Agilent, Santa Clara, CA) and a Cary 50 Bio UV spectrophotometer (Agilent, Santa Clara, CA). For ABZ we used the standard United States Pharmacopeia (USP) method with 900 mL 0.1 N HCl media, apparatus II, 50 rpm paddle speed and a temperature of 37°C. For FAM we used the standard USP method with 900 mL 0.1 M Phosphate buffer media, apparatus II, 50 rpm paddle speed, and a temperature of 37°C. Three tablets of each formulation were tested and the average is reported. Measurements were made every minute for 90 minutes by probes inserted into the bath and connected to the spectrophotometer by fiber optic cables.

3.11 Particle Size Measurement

Particle size analysis was performed on the applicable spinning solutions prior to sonication, after sonication, and 1 hour after sonication. A Malvern Mastersizer 2000 with a Hydro 2000µP accessory was used to measure the particle size distribution and the volume-based results were used for the analysis. Three measurements were made per sample and the average is reported in this work.

Chapter 4

Electrospinning of Fibers Containing Amorphous API

4.1 Introduction

In this chapter, solid state NMR is used to measure the spin lattice relaxation times for 1:1 SPP:PVP, 4:1 SPP:PVP, 1:1 IND:PVP, and 2:1 IND:PVP formulations prepared by electrospinning in order to determine whether the APIs and PVP are well-mixed down to small length scales (Section 4.2.3). As supporting evidence, the Tg of the mixture was determined for SPP/PVP mixtures and compared to that predicted by the Gordon-Taylor equation (Section 4.2.2).

Two other formulations were studied using solid state NMR relaxation times. The first was a 4:1 SPP:PVP solid dispersion prepared by hot melt extrusion, which was used to compare electrospinning to a second method of forming solid dispersions. A 2:1 IBUss:PVP electrospun formulation was also analyzed because it partially crystallized during electrospinning, allowing us to verify that phase separation could be determined by solid state NMR relaxation time analysis.

This study also applies solid state NMR relaxation time analysis to investigate the homogeneity of the solid solutions over 6 mo., and these results are presented in Section 4.3. Since physical stability is enhanced in a solid solution, it is desirable that the two components remain intimately mixed over a typical shelf life, preventing an

opportunity for crystallization. We also use FTIR to probe the interactions between SPP-PVP and IND-PVP and determine whether interactions contribute to stability in addition to the decreased mobility due to the high mixing level.

4.2 Results and Discussion: Homogeneity of the API/Polymer Solid Mixture

Electrospinning was used to prepare solid dispersions of unknown mixing level of a polymer, PVP, with either SPP, IND, or IBUss. The water-soluble polymer PVP was chosen as the excipient because it is known to hydrogen bond with many APIs, including IND [25], and it has a high Tg, so will act as a strong antiplasticizer. SPP was chosen as one model compound because it will only crystallize in the presence of certain solvents, allowing us to investigate a case where only phase separation and not crystallization would occur. The second API, IND, was chosen due to its ability to remain amorphous during the 1 week NMR analysis time for the pure sample, but still crystallize over time under some conditions. IBUss was chosen to demonstrate that solid state NMR relaxation time analysis can show when phase separation occurs in electrospun samples, as IBUss is partially crystalline following electrospinning. The $T_1(^1H)$ and $T_{1\rho}(^1H)$ relaxation times were measured for 1:1 SPP:PVP, 4:1 SPP:PVP, 1:1 IND:PVP, 2:1 IND:PVP, and 2:1 IBUss:PVP electrospun formulations, as well as a 4:1 SPP:PVP extruded formulation. In addition, the glass transition temperature for the mixture was determined for SPP formulations and compared to that predicted by the Gordon-Taylor equation.

4.2.1 Morphology of Electrospun Fibers

The morphology of electrospun fibers containing amorphous API and polymer was examined using SEM. In particular, we used SEM micrographs to verify that we obtained smooth fibers without any beads or protrusions. The micrographs are shown in Figure 4-1.

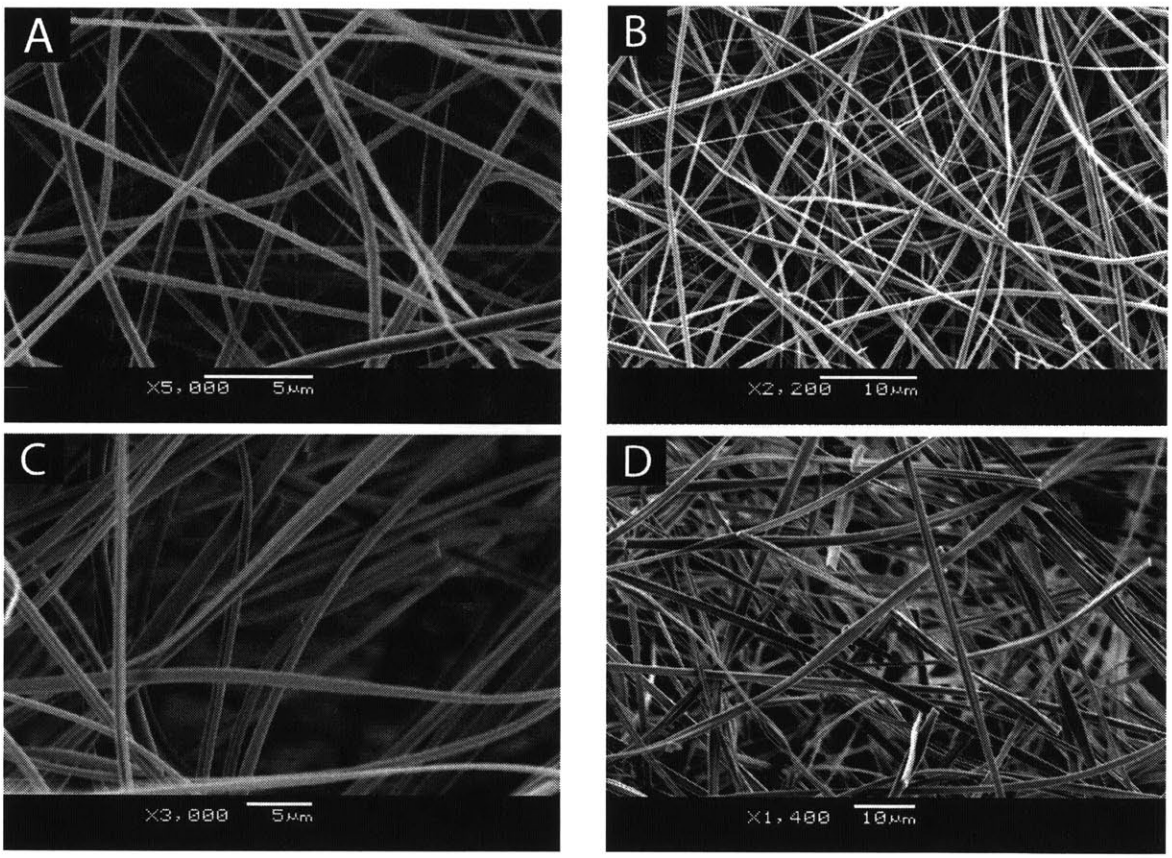

Figure 4-1: SEM images of electrospun A. 1:1 SPP:PVP, B. 4:1 SPP:PVP, C. 1:1 IND:PVP, and D. 2:1 IND:PVP

4.2.2 Glass Transition Temperature and the Gordon-Taylor Equation

The glass transition temperature has often been used as an indicator of miscibility of multiple components in a mixture [8, 26, 99]. For a two component system, well-mixed materials will exhibit only one Tg for the mixture, whereas phase separated materials will exhibit two Tgs. For an ideal system with no interaction between the components, the Tg of the homogeneous mixture can be predicted by the Gordon-Taylor equation [26]:

$$T_g = \frac{w_1 T_{g1} + K w_2 T_{g2}}{w_1 + K w_2} \tag{4.1}$$

where w_1 and w_2 are the weight fractions of components 1 and 2, Tg_1 and Tg_2 are the glass transition temperatures of components 1 and 2, and K is $\rho_1 T_{g1}/\rho_2 T_{g2}$, where ρ_1 and ρ_2 are the densities of components 1 and 2. Though only sensitive to a domain size of approximately 30 nm, the technique is a simple method to determine whether an API and polymer in a solid mixture are phase separated [8, 27].

To examine the use of this method, we measured the Tg for various SPP/PVP electrospun mixtures (Figure 4-2). We did not include results for SPP drug loadings above 50% because the degradation of SPP occurs in the same temperature range as the expected Tgs and the DSC scans are not smooth enough in that region at high loadings to conclusively determine a Tg. The spikes in the DSC cures for the pure PVP and 1:2 SPP:PVP samples are due to instrument error and the non-smooth character of the curve above 150°C for the 1:1 SPP:PVP is due to SPP degradation at high temperatures. From these results we see that only one Tg is present for each of the mixtures, indicating that the SPP and PVP are in close contact and likely a homogeneous solid solution.

Figure 4-3 shows a comparison of the measured Tgs to the Tgs calculated using the Gordon-Taylor equation and assuming that the density of the amorphous SPP is equal to the density of the amorphous PVP. The calculated and measured Tg values are quite close for all three mixtures, indicating that, if interactions between

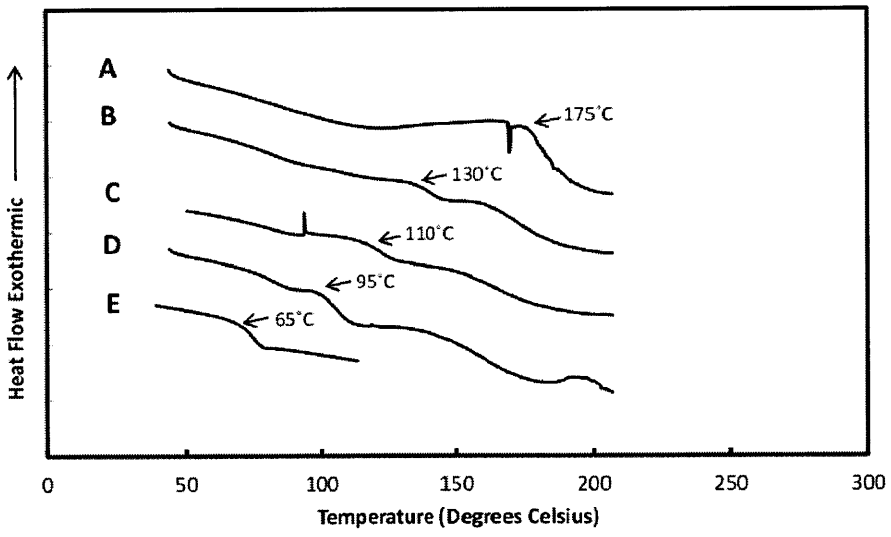

Figure 4-2: DSC curves for electrospun SPP formulations with glass transition temperatures labeled; A. PVP, B. 1:4 SPP:PVP, C. 1:2 SPP:PVP, D. 1:1 SPP:PVP, and E. Amorphous SPP

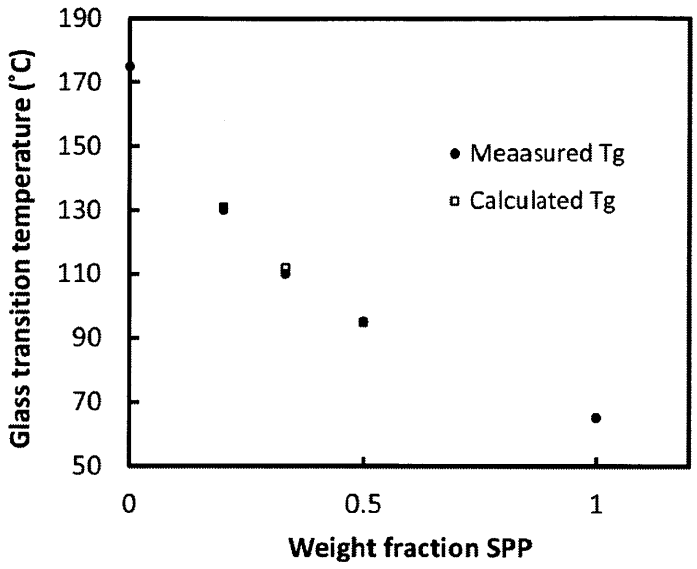

Figure 4-3: Comparison of measured glass transition temperatures (filled circles) with those calculated from the Gordon-Taylor equation (open squares)

the SPP and PVP are present, they are of the same order of magnitude as SPP-SPP interactions and PVP-PVP interactions, allowing the volume additivity assumption of the Gordon-Taylor equation to hold.

The Tg of the IND/PVP mixtures was too weak to be measured for most cases, so a similar study could not be done with the electrospun IND formulations. However, due to enthalpy relaxation [70], the signal for the Tg of the 2:1 IND:PVP was strong enough to measure after 6 months of storage at 40°C and was found to be 81°C. Using the Gordon-Taylor equation, the Tg of pure IND from the literature, 42°C [100], and again making the assumption that the densities of the two materials are equal, the calculated Tg is 56°C. In this case, the measured and calculated Tgs are different, indicating that there are likely significant interactions between the IND and the PVP in the mixture (the interactions will be discussed further in Section 4.3.3).

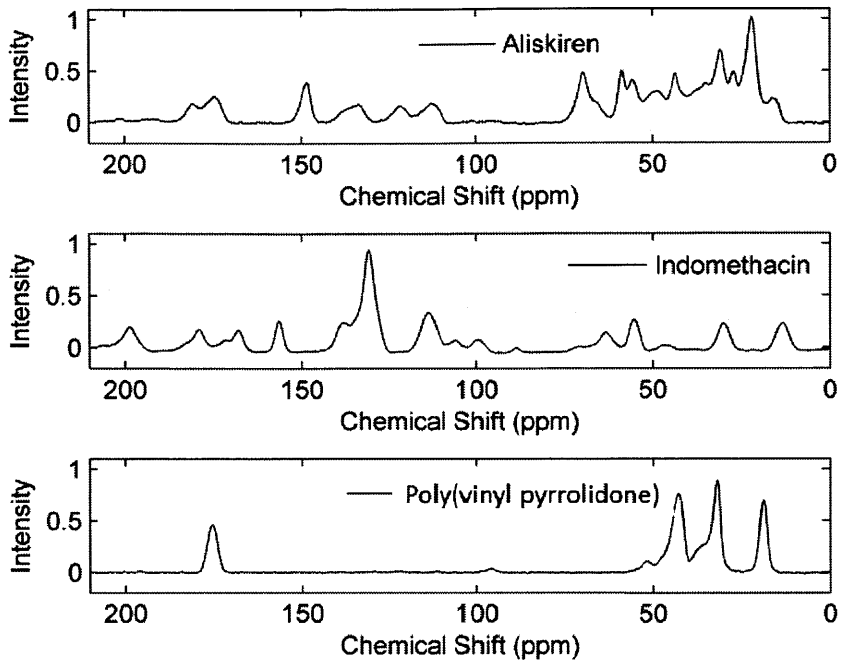

Figure 4-4: Solid state NMR spectra for amorphous SPP, amorphous IND and PVP

4.2.3 Solid State Nuclear Magnetic Resonance Analysis of Phase Separation

One dimensional ^{13}C solid state NMR spectra were obtained for amorphous SPP, IND, and PVP (Figure 4-4). From these spectra, we were able to identify the strongest peaks for the materials (Table 4.1). The peaks at 198.7 and 63.9 ppm for IND are spinning side bands. Peaks in the 170 ppm range were not included for IND or SPP because the intensity was too low to analyze at many time points. $T_1(^1H)$ and $T_{1\rho}(^1H)$ were measured for each of these peaks for the pure materials and the error was determined using the uncertainty in the exponential fit. They are listed in Table 4.1.

The $T_1(^1H)$ and $T_{1\rho}(^1H)$ values vary slightly from one peak to another for each compound. To account for this variance when performing the deconvolution fitting, spectra of the pure components from the time point closest to that for the mixture being analyzed were used for deconvolution.

The $T_1(^1H)$ and $T_{1\rho}(^1H)$ relaxation times were measured for pure compounds,

Material	Peak (ppm)	$T_1(^1H)$ (s)	$T_{1\rho}(^1H)$ (ms)
PVP	175.7	2.33 ± 0.60	20.9 ± 0.6
	42.7	2.30 ± 0.66	20.7 ± 0.5
	31.9	2.41 ± 0.82	20.1 ± 0.4
	18.8	2.37 ± 0.83	21.3 ± 0.6
SPP	148.5	1.07 ± 0.41	8.8 ± 0.3
	112.9	1.02 ± 0.53	9.7 ± 0.8
	69.7	1.05 ± 0.29	8.5 ± 0.2
	58.6	1.07 ± 0.29	8.6 ± 0.4
	30.7	1.05 ± 0.29	8.4 ± 0.2
	22	1.05 ± 0.25	8.3 ± 0.2
IND	156.5	2.61 ± 0.16	34.4 ± 2.0
	131.1	2.53 ± 0.15	38.2 ± 2.3
	113.9	2.51 ± 0.13	38.4 ± 2.7
	55.2	2.53 ± 0.15	31.2 ± 2.1
	29.9	2.57 ± 0.13	34.1 ± 2.1
	13.3	2.63 ± 0.15	33.4 ± 2.3

Table 4.1: $T_1(^1H)$ and $T_{1\rho}(^1H)$ for the major peaks of PVP, SPP, and IND

physical mixtures, electrospun formulations and an extruded formulation, and they are reported in Table 4.2. The relaxation times reported for the mixtures are the averages of the PVP peaks (top number) and of the API peaks (bottom number). The reported uncertainty is determined from the largest deviation from the average using the uncertainty from the exponential fits. In the cases where the average relaxation time from the PVP peaks is within the uncertainty of the average relaxation time from the API peaks, no minimum domain size was calculated, and where there was a difference in the relaxation times, the minimum domain size is listed in Table 4.2.

The $T_1(^1H)$ and $T_{1\rho}(^1H)$ relaxation times can be correlated to a length scale of phase separation. In time $T_1(^1H)$ or $T_{1\rho}(^1H)$, diffusion occurs across a length, L, which can be calculated from the diffusion coefficient D and the relaxation time T_i [91] using Equation 2.3. In calculating the length scale, the diffusion coefficient plays an important role. However, it is not practical to measure a diffusion coefficient for the particular materials under consideration, as we are not able to prepare a sample with a known domain size. Two diffusion coefficients are commonly used in the literature, 8.0 x 10^{-16} m^2/s for rigid systems [92] and 0.5 x 10^{-16} m^2/s for mobile systems [91].

Formulation	$T_1(^1H)$ (s)	Minimum domain size	$T_{1\rho}(^1H)$ (ms)	Minimum domain size
SPP	1.05 ± 0.08	NA	8.7 ± 1.8	NA
PVP	2.37 ± 0.15	NA	20.7 ± 1.1	NA
IND	2.56 ± 0.22	NA	35.0 ± 6.1	NA
Amorph. 1:1 SPP:PVP Physical Mixture	2.47 ± 0.20 and 1.26 ± 0.27	20-110 nm	23.6 ± 1.8 and 12.6 ± 3.7	2-11 nm
Amorph. 1:1 IND:PVP Physical Mixture	2.44 ± 0.24 and 2.67 ± 0.43	30-110 nm	18.8 ± 0.5 and 29.8 ± 6.3	2-11 nm
1:1 SPP:PVP Electrospun	1.56 ± 0.10 and 1.40 ± 0.29	NA	11.1 ± 0.3 and 9.9 ± 1.7	NA
1:1 IND:PVP Electrospun	2.11 ± 0.17 and 2.15 ± 0.32	NA	29.2 ± 2.3 and 28.9 ± 4.2	NA
4:1 SPP:PVP Extruded	2.27 ± 0.21 and 1.32 ± 0.20	20-100 nm	12.4 ± 0.63 and 9.0 ± 1.4	2-8 nm
4:1 SPP:PVP Electrospun	1.31 ± 0.09 and 1.33 ± 0.25	NA	8.3 ± 0.3 and 7.9 ± 1.0	NA

Table 4.2: Relaxation time constants for SPP/PVP and IND/PVP formulations; the top number in mixtures is measured from the PVP peaks and the bottom number is measured from the API peaks, NA = No separated domains

In this work, L is calculated using both diffusion coefficients and is presented as a range.

For the SPP/PVP amorphous physical mixtures, the relaxation times measured from the SPP and PVP peaks were different for both $T_1(^1H)$ and $T_{1\rho}(^1H)$, with corresponding minimum domain sizes of 20-110 nm and 2-11 nm, respectively. For the electrospun 1:1 SPP:PVP formulation, the relaxation times calculated from the SPP and PVP peaks were within experimental error of each other, meaning that the components were well mixed down to a length scale of 2-11 nm and indicating that the electrospun formulation is a solid solution down to these length scales.

For the IND/PVP formulations, there was no difference in the $T_1(^1H)$ values within the experimental uncertainty for either the physical mixture or the electrospun formulation. This is to be expected, as the values for the pure amorphous IND and PVP are 2.56 $\pm$ 0.22 s and 2.37 $\pm$ 0.15 s, respectively, which are within experimental uncertainty of each other. For the $T_{1\rho}(^1H)$, on the other hand, the values for the pure components are 35.0 $\pm$ 6.1 ms and 20.7 $\pm$ 1.1 ms, respectively, which are sufficiently different. For the 1:1 IND:PVP physical mixture, the $T_{1\rho}(^1H)$ values measured from the IND and PVP peaks differed, whereas for the 1:1 IND:PVP electrospun formulation, the $T_{1\rho}(^1H)$ values calculated for the IND and PVP peaks were equal within experimental error. With a calculated domain size of 2-11 nm, it is clear from these results that the electrospun formulation is a solid solution down to a length scale of 2-11 nm.

To demonstrate that electrospinning is a strong technique for forming solid solutions, we compared it to hot melt extrusion, a technique commonly used to form solid solutions or dispersions [1, 101]. We performed the relaxation time analysis on a 4:1 SPP:PVP mixture prepared by hot melt extrusion and a 4:1 SPP:PVP mixture prepared by electrospinning. For the extruded formulation, two significantly different values were measured for both the $T_1(^1H)$ and $T_{1\rho}(^1H)$, indicating that there was separation of the SPP and PVP with domain sizes greater than 20-100 nm. For the electrospun formulation, the two measured values for both the $T_1(^1H)$ and $T_{1\rho}(^1H)$ were within experimental uncertainty, indicating that the drug and polymer are well-

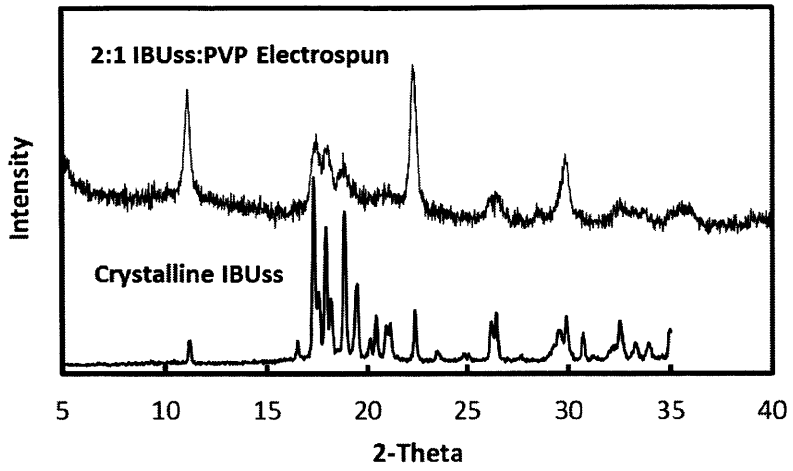

Figure 4-5: XRD powder patterns of electrospun 2:1 IBUss:PVP and crystalline IBUss.

mixed on a domain size of 2-11 nm or less. The reason for this difference in mixing levels is due to a key difference in the processes. For extrusion, the SPP and PVP begin as separate powders and are gradually mixed near the melting point of SPP (but below the Tg of PVP), making it difficult to form a molecular-level mixture. Electrospinning, on the other hand, begins with a well dispersed solution of solvent with the SPP and PVP and the solvent is removed through rapid evaporation, making it difficult for the SPP and PVP to phase separate.

This study was further extended to examine a partially amorphous formulation, 2:1 IBUss:PVP, in order to demonstrate that phase separation can occur with electrospinning and that it can be measured using the solid state NMR techniques applied here. When electrospun in a ratio of 2 to 1 drug to polymer, the IBUss is partially crystalline in the fibers, as can be seen from XRD powder pattern in Figure 4-5.

Solid state NMR was performed on the electrospun samples and the NMR spectrum with primary peaks numbered is shown in Figure 4-6. These peaks were chosen for analysis because they remained clearly non-overlapping for all mixing times.

Table 4.3 lists the values of $T_1(^1H)$ and $T_{1\rho}(^1H)$ measured for each peak labeled in Figure 4-6. For the $T_1(^1H)$ values, a slight difference is seen in those measured from the PVP peaks (average of 1.04 $\pm$ 0.07 s) and those measured from the IBUss peaks

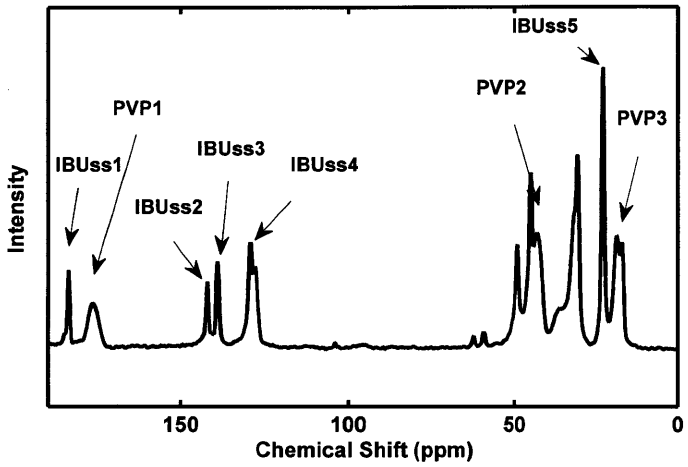

Figure 4-6: Solid state NMR spectrum of electrospun 2:1 IBUss:PVP.

Peak	$T_1(^1H)$	$T_{1\rho}(^1H)$
PVP1	1.04 ± 0.06 s	11.2 ± 0.5 ms
PVP2	1.07 ± 0.04 s	11.6 ± 0.3 ms
PVP3	1.01 ± 0.04 s	11.2 ± 0.3 ms
IBUss1	0.90 ± 0.03 s	4.7 ± 0.2 ms
IBUss2	0.89 ± 0.04 s	5.2 ± 0.3 ms
IBUss3	0.88 ± 0.03 s	6.1 ± 0.2 ms
IBUss4	0.91 ± 0.03 s	6.8 ± 0.1 ms
IBUss5	0.88 ± 0.02 s	6.6 ± 0.1 ms

Table 4.3: Relaxation time constants for 2:1 IBUss:PVP for each peak labeled in Figure 4-6.

(average of 0.89 ± 0.04 s). This indicates that there is phase separation between the PVP and IBUss of the domain size 20-90 nm or larger, as is expected given that the IBUss is partially crystalline. For the $T_{1\rho}(^1H)$ values, the difference in the $T_{1\rho}(^1H)$ between the PVP and IBUss is larger, with the average $T_{1\rho}(^1H)$ for the PVP peaks being 11.3 ± 0.6 ms and for the IBUss being 5.9 ± 1.0 ms. Therefore, the conclusion of phase separation in this sample is further supported by the $T_{1\rho}(^1H)$ data, and we know that electrospinning can produce phase separated solid dispersions and solid state NMR can be used to identify them.

4.2.4 Summary

From the results of the solid state NMR relaxation time studies reported above, we can conclude that 1:1 electrospun formulations of SPP or IND with PVP, as well as 4:1 SPP:PVP and 2:1 IND:PVP are miscible to a length scale of 2-10 nm immediately after electrospinning. This illustrates the potential of electrospinning to be used to make solid solutions for final solid dosage forms. For SPP, this conclusion is supported by the measurement of only one Tg for the electrospun mixtures.

A 2:1 IBUss:PVP formulation was used to demonstrate that the solid state NMR relaxation time analysis will show the presence of phase separation when the components are not intimately mixed. IBUss is partially crystalline in the formulation studied, and both $T_1(^1H)$ and $T_{1\rho}(^1H)$ measurements showed that the IBUss and PVP were phase separated.

We have also shown that a 4:1 SPP:PVP electrospun formulation is miscible to the 2-10 nm domain size, whereas a 4:1 SPP:PVP extruded formulation is phase separated with domain sizes of 20-100 nm or larger. The impact of this is two-fold. First, it shows that solid state NMR can be used to compare the phase separation in different solid dosage forms when the products appear similar using other techniques. Second, it shows that electrospinning a drug and polymer from a solution forms solid solutions at a high drug loading and can be a useful process for formulating amorphous API.

4.3 Results and Discussion: Physical Stability of Amorphous API in Electrospun Fibers

Typical physical stability studies of pharmaceutical products involve storage at high temperatures and/or high humidity and analysis via XRD and DSC to determine crystallinity as a function of time [36]. Solid state NMR has also been used in stability studies to examine crystallization over time. Crystallinity of an API has been evaluated using solid state NMR at late time points [102, 103], which was advantageous over XRD or DSC due to the increased sensitivity of solid state NMR for detecting crystalline material and crystal defects.

In this section, we apply solid state NMR relaxation time analysis to investigate the homogeneity of solid solutions over time, rather than only examining the crystallization of the API over time. Since physical stability is enhanced in a solid solution, it is desirable that the two components remain intimately mixed over a typical shelf life, preventing an opportunity for crystallization. Stability can also be enhanced when the amorphous API and polymer excipient are able to interact. In this section, we utilize FTIR spectral analysis to identify hydrogen bonding in the electrospun formulations. Extending the solid state NMR study from Section 4.2, the $T_1(^1H)$ and $T_{1\rho}(^1H)$ relaxation times were measured for 1:1 SPP:PVP, 4:1 SPP:PVP, 1:1 IND:PVP and 2:1 IND:PVP formulations after 0 mo., 3 mo., and 6 mo. storage at 40°C and 0% relative humidity (RH) to determine the physical stability of the solid solution. As supporting evidence, we also used XRD and DSC to verify that no crystallization occurred during the 6 mo. analysis period.

4.3.1 Moisture Analysis

It is well known that water acts as a plasticizer and increases mobility of components in a solid dispersion [104]. Due to the increased mobility, this can also cause the relaxation times measured in solid state NMR to decrease [105, 106]. In order to remove the known effect of water on mobility and the relaxation times, we stored our

Sample	Weight Percent Water
1:1 SPP:PVP 3 mo.	1.2
1:1 IND:PVP 3 mo.	1
4:1 SPP:PVP 3 mo.	1.1
2:1 IND:PVP 3 mo.	1.1
1:1 SPP:PVP 6 mo.	3.5
1:1 IND:PVP 6 mo.	0.2
4:1 SPP:PVP 6 mo.	1.3
2:1 IND:PVP 6 mo.	0.2

Table 4.4: Weight percent water in stability samples as measured by TGA

Sample	Weight Percent Water
1:1 SPP:PVP	1.7
1:1 IND:PVP	1.8
4:1 SPP:PVP	1.1
2:1 IND:PVP	2.0

Table 4.5: Weight percent water in electrospun samples as measured immediately after electrospinning by TGA

samples in a desiccator with a humidity of less than 5% RH in the stability chamber. Prior to solid state NMR analysis of the 3 mo. and 6 mo. samples, we measured the weight percent water present in the fibers in order to confirm that water was not the key factor affecting the measured relaxation times (Table 4.4). The weight percent water was not measured for initial samples because previous tests, whose results are shown in Table 4.5, showed approximately 1-2 wt% water when spun in the controlled humidity environment of the lab.

As can be seen in Table 4.4, for all cases the water content is generally low, so the effect of water on the relaxation times should be minimal. The 1:1 SPP:PVP sample measured after 6 mo. storage had slightly high water content, which was due to the analysis being carried out over multiple days and the sample being exposed to high humidity.

4.3.2 Stability of the Amorphous Form

DSC and XRD experiments were performed on all samples in order to determine whether crystalline API was present in the fibers. For IND, the limit of detection

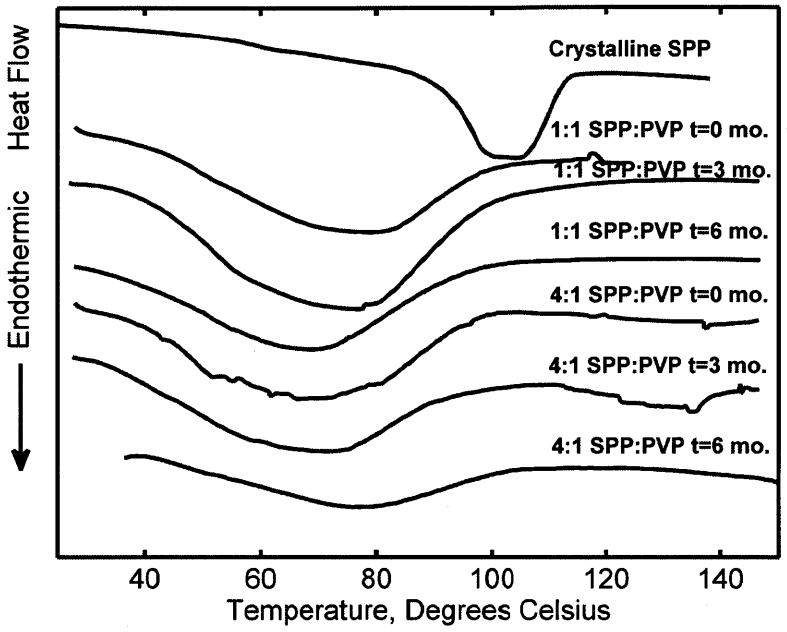

Figure 4-7: DSC curves for 1:1 SPP:PVP and 4:1 SPP:PVP at 0, 3, and 6 mo. For scale reference, the depth of the SPP crystalline melting endotherm is approximately 0.5 W/g.

for DSC is 10 wt% crystalline material and for XRD is 1 wt% crystalline material; demonstration of these limits may be found in Figures 3-2 and 3-1, respectively. SPP will not crystallize unless in the presence of specific solvents, so will not crystallize over time in our system. The DSC curves for SPP formulations are shown in Figure 4-7, while those for the IND formulations are shown in Figure 4-8.

For scale reference, the depth of the crystalline IND endotherm is approximatley 6 W/g and the depth of the crystalline SPP endotherm is approximately 0.5 W/g. The crystalline IND standard peak was obtained by testing the crystals as-received, and is assumed to correspond to 100% crystalline material. For SPP, the crystalline standard peak was also obtained by testing the crystals as-received from Novartis. The material is not 100% crystalline, but is approximately 85% crystalline. None of the DSC curves for the SPP/PVP or IND/PVP formulations show endotherms in the range of the melting peak measured from the crystalline standards, indicating that neither SPP nor IND is crystalline in the fibers for any sample.

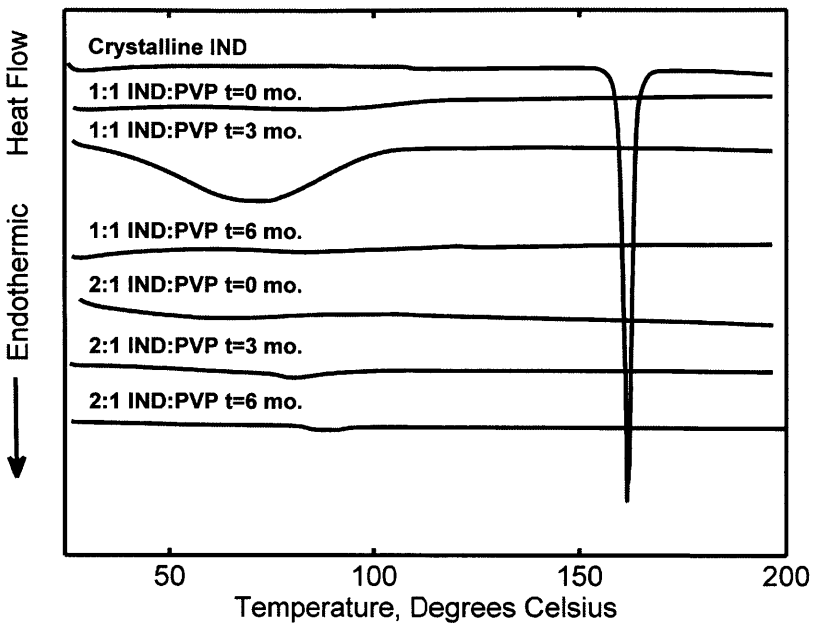

Figure 4-8: DSC curves for 1:1 IND:PVP and 2:1 IND:PVP at 0, 3, and 6 mo. For scale reference, the depth of the crystalline IND melting endotherm is approximately 6 W/g.

All of the DSC curves for the SPP formulations display a broad endotherm at low temperatures. This endotherm corresponds to the release of water absorbed by the SPP and PVP [36], as was discussed in Section 3.5. This same endotherm is also present in the 1:1 IND:PVP 3 mo. sample. For many of the SPP formulations, there are also disturbances in the curve at temperatures above 110°C, which are due to chemical degradation of the SPP at those temperatures.

The XRD powder patterns for the SPP formulations are shown in Figure 4-9 and the XRD powder patterns for the IND formulations are shown in Figure 4-10.

All formulations of SPP/PVP and IND/PVP at all times show an amorphous hump and no defined peaks. This indicates that there is no detectable crystalline drug present in the fibers. The 1:1 IND:PVP 6 mo. and 2:1 IND:PVP 6 mo. samples (Figure 4-10-D and -G) were measured on a different instrument than the other samples, hence the sloped curve at low values of 2-theta.

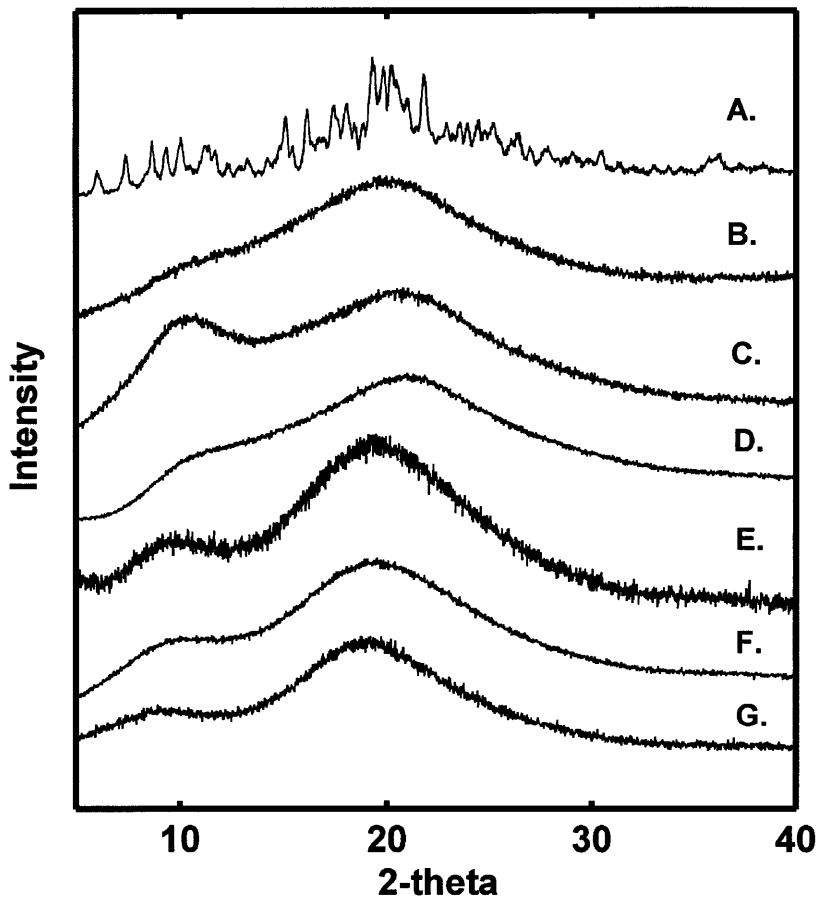

Figure 4-9: XRD powder patterns for A. Crystalline SPP, B. 1:1 SPP:PVP at 0 mo., C. 1:1 SPP:PVP at 3 mo., D. 1:1 SPP:PVP at 6 mo., E. 4:1 SPP:PVP at 0 mo., F. 4:1 SPP:PVP at 3 mo., G. 4:1 SPP:PVP at 6 mo.

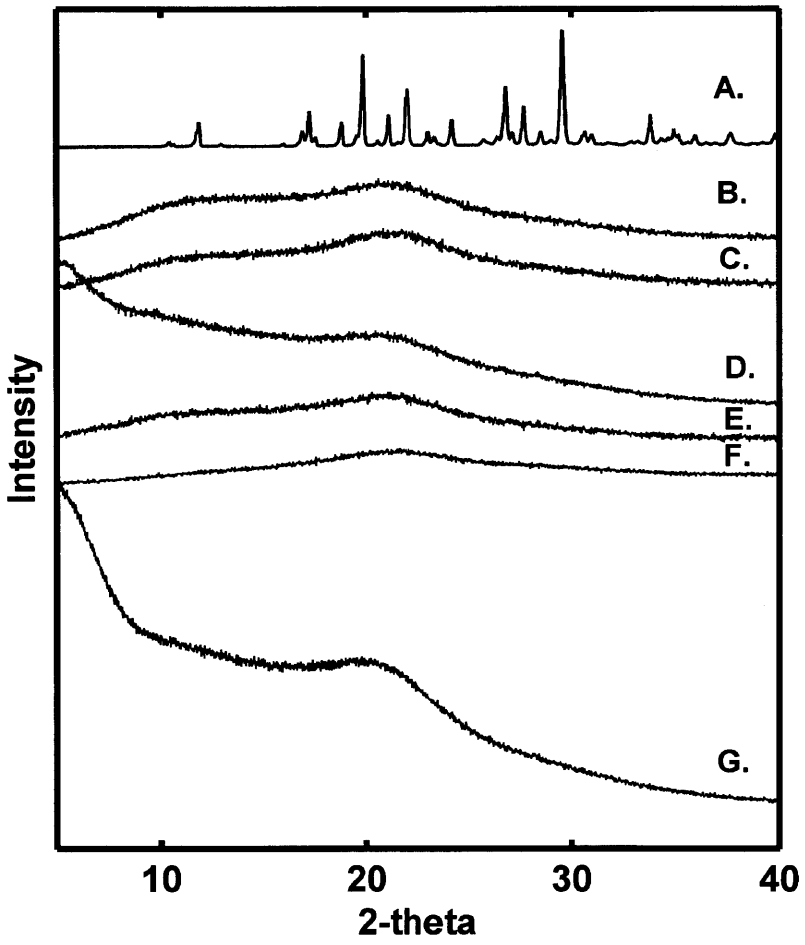

Figure 4-10: XRD powder patterns for A. Crystalline IND, B. 1:1 IND:PVP at 0 mo., C. 1:1 IND:PVP at 3 mo., D. 1:1 IND:PVP at 6 mo., E. 2:1 IND:PVP at 0 mo., F. 2:1 IND:PVP at 3 mo., G. 2:1 IND:PVP at 6 mo.

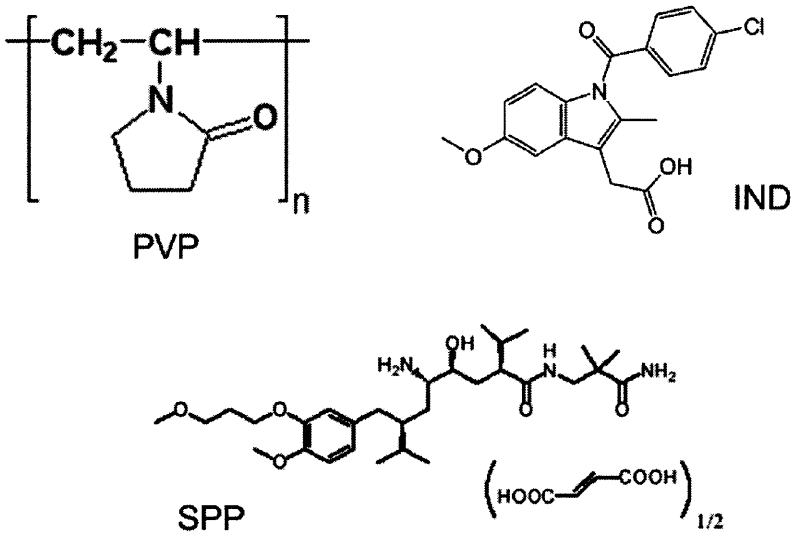

Figure 4-11: Chemical structures of IND, SPP, and PVP

4.3.3 Interactions Between API and Excipients

As mentioned in Section 2.3.1, close contact between an API and excipient can lead to hydrogen boonding interactions, which can stabilize an amorphous API. This has been demonstrated for CBZ and hydroxypropyl methylcellulose (HPMC) [107], felodipine and PVP [24], felodipine and HPMC [24], and IND and PVP [25], among others. We investigated the interactions for three of the electrospun formulations discussed here, 1:1 IND:PVP, 2:1 IND:PVP, and 1:1 SPP:PVP. The chemical structures of IND, SPP, and PVP are shown in Figure 4-11.

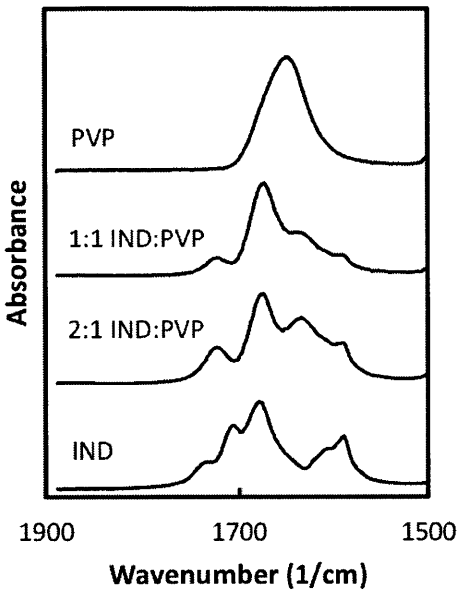

Figure 4-12: FTIR spectra of PVP, 1:1 IND:PVP electrospun, 2:1 IND:PVP electrospun, and amorphous IND

Solid dispersions of IND/PVP prepared by solvent evaporation with a rotary evaporator were studied previously [25]. It was found that there is a peak for PVP at 1679 cm^{-1} corresponding to the vibrations of the amide carbonyl when not hydrogen bonded, a peak for amorphous IND at 1710 cm^{-1} corresponding to the vibrations of the carboxylic acid when IND is present as hydrogen bonded dimers and a peak for solid dispersions at 1726 cm^{-1} corresponding to the vibrations of the IND carboxylic acid when hydrogen bonded with PVP [25].

Figure 4-12 shows the FTIR spectrum for IND formulations in the 1500-1900 cm^{-1} range. In both the 2:1 and 1:1 IND:PVP electrospun formulations, the peak at approximately 1710 cm^{-1} disappears (it is present in the amorphous IND at 1706

cm^{-1}) and the peak at approximately 1723 cm^{-1} (corresponding to the peak at 1726 cm^{-1} in [25]) appears for both samples. This indicates that the amorphous IND in the fibers no longer exists as cyclic dimers, but instead is hydrogen bonded with PVP.

SPP is a more complicated molecule and much of the FTIR spectrum is difficult to interpret due to overlapping peaks, particularly in the 1500-1900 cm^{-1} range. One area that can be examined is 500-1200 cm^{-1}, where the C-N vibrations, O-H vibrations, and ring and C-H deformation vibrations for the aromatic ring occur. These functional groups could all interact in with PVP, and so would change if interactions occurred. The spectra for SPP, PVP and the 1:1 SPP:PVP physical mixture are shown in Figure 4-13, and the spectra for SPP, PVP and the 1:1 amorphous SPP:PVP electrospun are shown in Figure 4-14.

If interactions were occurring between SPP and PVP, one would expect changes in the FTIR peaks for the functional groups participating in the interactions. In Figure 4-13, the spectrum of the 1:1 SPP:PVP amorphous physical mixture is nearly identical to that of SPP, which is to be expected, as the spectrum would be a sum of the SPP and PVP spectra for a physical mixture and the PVP barely absorbs in this range. For the 1:1 SPP:PVP electrospun sample, there is less definition in the peaks, but the strong peaks (those labeled in Figure 4-14) remain and do not shift significantly. Thus, there is no clear evidence of interactions. However, because there is still a difference between the electrospun and physical mixture spectra, interactions cannot be conclusively ruled out based on these results.

4.3.4 Stability of the Solid Solution

Solid state NMR $T_1(^1H)$ and $T_{1\rho}(^1H)$ measurements were made of pure components, physical mixtures and the electrospun formulations at the storage times of 0, 3, and 6 mo., and they are reported in Table 4.6. The reported times are the averages for the PVP peaks (top number) and API peaks (bottom number). The uncertainty is determined from the largest deviation from the average using the raw values and the uncertainty in the exponential fits.

Both the $T_1(^1H)$ and $T_{1\rho}(^1H)$ relaxation times for the pure amorphous SPP and

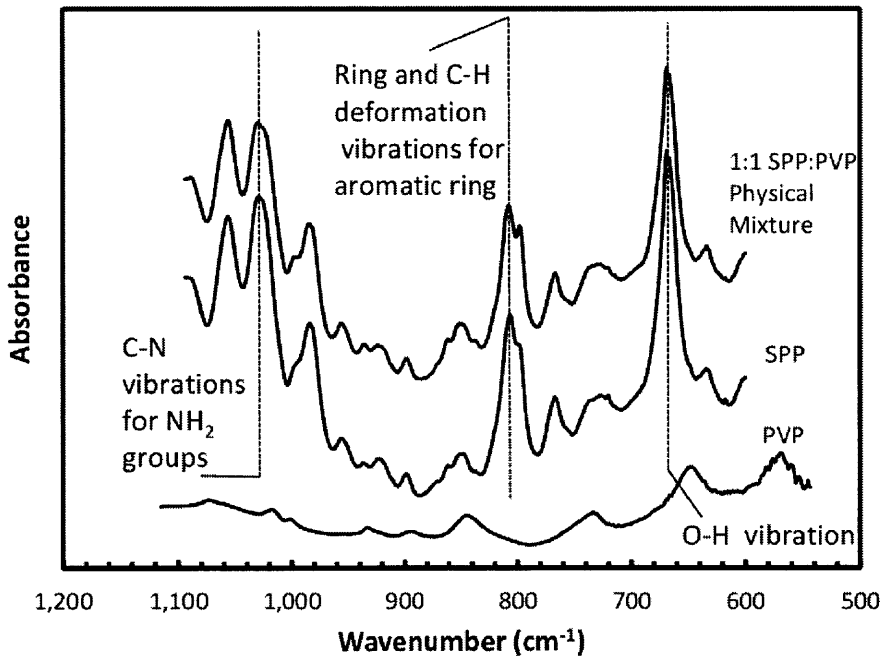

Figure 4-13: FTIR of PVP (bottom), SPP (middle), and 1:1 SPP:PVP amorphous physical mixture (top) with peaks for vibrations of important functional groups marked.

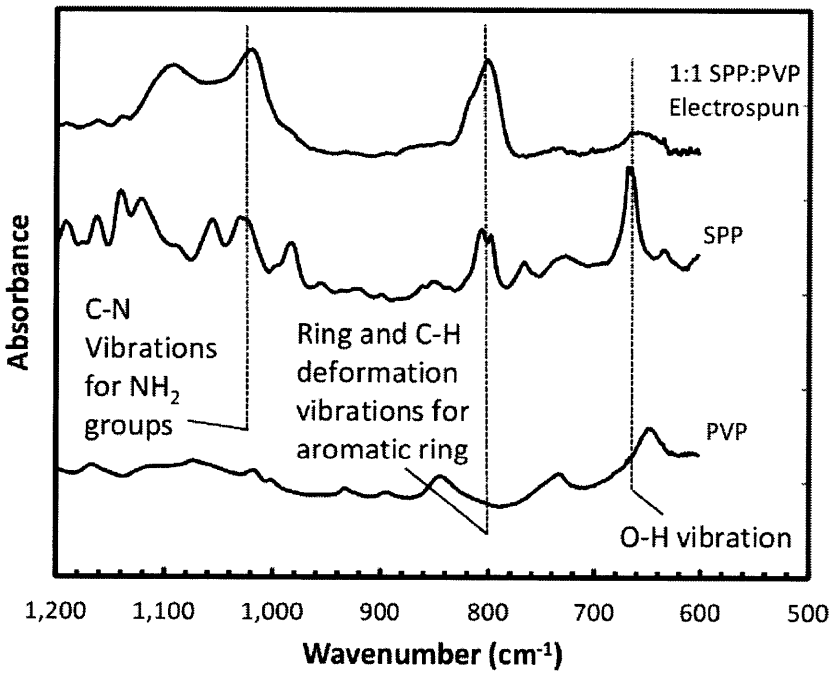

Figure 4-14: FTIR of PVP (bottom), SPP (middle), and 1:1 SPP:PVP electrospun material (top) with peaks for vibrations of important functional groups marked.

Formulation	$T_1(^1H)$ (s) 0 months	$T_1(^1H)$ (s) 3 months	$T_1(^1H)$ (s) 6 months	$T_{1\rho}(^1H)$ (ms) 0 months	$T_{1\rho}(^1H)$ (ms) 3 months	$T_{1\rho}(^1H)$ (ms) 6 months
SPP	1.05 ± 0.08	NA	NA	8.7 ± 1.8	NA	NA
IND	2.56 ± 0.22	NA	NA	35.0 ± 6.1	NA	NA
PVP	2.37 ± 0.15	NA	NA	20.7 ± 1.1	NA	NA
Amorphous 1:1 SPP:PVP	2.47 ± 0.20	NA	NA	23.6 ± 1.8	NA	NA
Physical Mixture	1.26 ± 0.27			12.6 ± 3.7		
Amorphous 1:1 IND:PVP	2.44 ± 0.24	NA	NA	18.8 ± 0.5	NA	NA
Physical Mixture	2.67 ± 0.27			29.8 ± 6.3		
1:1 SPP:PVP	1.54 ± 0.14	1.48 ± 0.10	1.60 ± 0.10	11.2 ± 0.9	9.7 ± 0.7	7.1 ± 0.6
Electrospun	1.36 ± 0.16	1.29 ± 0.21	1.29 ± 0.31	10.3 ± 3.5	9.7 ± 3.2	5.9 ± 1.7
1:1 IND:PVP	2.44 ± 0.21	2.51 ± 0.20	2.45 ± 0.18	16.8 ± 1.2	15.3 ± 1.0	16.9 ± 1.0
Electrospun	2.48 ± 0.26	2.37 ± 0.43	2.42 ± 0.19	15.8 ± 2.2	14.2 ± 2.2	17.2 ± 1.8
4:1 SPP:PVP	1.34 ± 0.24	1.25 ± 0.19	1.17 ± 0.11	8.2 ± 1.1	7.8 ± 0.5	9.3 ± 1.2
Electrospun	1.35 ± 0.28	1.13 ± 0.12	1.08 ± 0.11	7.6 ± 1.1	8.0 ± 1.5	9.4 ± 2.1
2:1 IND:PVP	2.19 ± 0.24	2.46 ± 0.23	2.28 ± 0.17	33.5 ± 5.8	34.2 ± 3.5	40.5 ± 12.4
Electrospun	2.20 ± 0.23	2.55 ± 0.29	2.33 ± 0.32	34.7 ± 7.3	38.1 ± 7.1	48.0 ± 16.2

Table 4.6: Relaxation time constants for stability studies, top number in mixtures is from the polymer peaks and bottom number is from the drug peaks. NA = No separated domains

PVP are sufficiently different to distinguish between them. This is demonstrated by the amorphous 1:1 SPP:PVP physical mixture, where the $T_1(^1H)$ and $T_{1\rho}(^1H)$ values as measured from the PVP peaks differed from those measured from the SPP peaks. For IND, however, the $T_1(^1H)$ values were not sufficiently different to distinguish; 2.37 $\pm$ 0.15 s and 2.56 $\pm$ 0.22 s are within the experimental error of each other. Thus, the analysis of the IND formulations was based only on the $T_{1\rho}(^1H)$ values.

For both the 1:1 SPP:PVP and 4:1 SPP:PVP electrospun formulations, the $T_1(^1H)$ values measured from the PVP peaks are within experimental error of the $T_1(^1H)$ value measured from the SPP peaks. The domain size associated with these values can be calculated using Equation 2.3. We report the domain size as a range using each diffusion coefficient discussed previously (Section 4.2.3). For the $T_1(^1H)$ values measured from the SPP/PVP formulations, we conclude that the materials are homogeneous to a domain size of 20-80 nm and remain as such throughout the 6 mo. stability study.

The $T_{1\rho}(^1H)$ relaxation times for the SPP/PVP formulations measured from the SPP and PVP peaks also remain within experimental error of each other throughout the 6 mo. study period. This indicates that the materials are in a solid solution with no phase separation of 2-10 nm or greater. The 6 mo. sample for the 1:1 SPP:PVP has lower values of the $T_{1\rho}(^1H)$ than the 0 mo. or 3 mo. sample, which is likely due to its higher water content, approximately 3.5 wt% versus 1.1 wt%.

For the IND formulations, the $T_{1\rho}(^1H)$ values remain within experimental error of each other, indicating that the solid solutions retain their homogeneity down to a 2-10 nm domain size for the entire 6 mo. storage period. The value of the $T_{1\rho}(^1H)$ increases significantly from the 3 mo. sample to the 6 mo. sample. This may be due to the decrease in the water content (1.1 wt% to 0.2 wt%) and subsequent increase in the Tg from approximately 75°C to 80°C, which can be seen in Figure 4-8. The $T_{1\rho}(^1H)$ values measured for the 2:1 IND:PVP formulation have a large experimental error associated with them, which is because the $T_{1\rho}(^1H)$ is large and experiments could not be run for long enough spin-lock times to allow the signal to decrease to zero, as they could for the other formulations. This experimental limit, due to a limit

in the amount of time a high power could be applied in the NMR, required us to calculate a $T_{1\rho}(^1H)$ value from an incomplete exponential curve, resulting in greater error.

4.3.5 Summary

Solid state NMR relaxation time measurements were used to study the stability of solid solutions prepared by electrospinning over 6 mo. at an elevated temperature. It was found that for all four formulations studied, 1:1 SPP:PVP, 4:1 SPP:PVP, 1:1 IND:PVP and 2:1 IND:PVP, the mixture remained homogeneous down to a 2-10 nm domain size throughout the study period. XRD and DSC analyses were used as complementary tools, showing that the drug in the fibers remains amorphous over the time period. FTIR results indicated that for the IND formulations, IND-PVP hydrogen bonding occurs, contributing to the stability of the amorphous IND in the electrospun fibers. These results show that the technique of electrospinning may be a good method to produce physically stable, amorphous solid solutions.

With this work, we have also shown that solid state NMR allows us to verify that an amorphous mixture remains a solid solution throughout a stability study. Techniques that measure the crystallinity, such as XRD and DSC, do not show when phase separation occurs, which is a likely precursor to crystallization. By using SSNMR relaxation time analysis, we are able to obtain a more comprehensive understanding of the physical stability of amorphous solid solutions.

4.4 Conclusions

Due to the rapid solvent evaporation rate, electrospinning a solution of dissolved API and polymer often results in amorphous API in the fibers. In Chapter 4, we present a detailed study of electrospun formulations containing amorphous API, in particular 1:1 SPP:PVP, 4:1 SPP:PVP, 1:1 IND:PVP and 2:1 IND:PVP.

We found that, following electrospinning, these formulations are present as a solid solution down to a 2-10 nm length scale, and remain as such for 6 mo. storage at 40°C.

During that time, there is also no evidence that crystallization occurs. One reason for the high stability of the amorphous form is that the PVP acts as an antiplasticizer and, since it is mixed to a 2-10 nm length scale or smaller with the API, keeps the API molecules from arranging into clusters and, subsequently, crystals.

An additional reason for the stability of the amorphous form is hydrogen bonding of the API with PVP. For the IND formulations, we used IR spectral analysis to show that hydrogen bonding is, indeed, occurring between the carboxylic acid of the IND and the amide carbonyl of the PVP. This was supported by the Tg of 2:1 IND:PVP; the measured Tg was significantly different than that predicted by the Gordon-Taylor equation.

For the SPP formulations, interactions between the SPP and PVP could not be conclusively proven. In fact, FTIR analysis showed no peak shifts in some regions that would be expected to hydrogen bond and the measured Tgs of the electrospun SPP/PVP mixtures correlated well with those predicted by the Gordon-Taylor equation. This is logical because SPP is a bulky molecule with much steric hindrance to hydrogen bonding. It may be, then, that SPP and PVP do not interact via hydrogen bonding and the stability can be explained only by the decrease in mobility due to the antiplasticizing effect of PVP.

Electrospinning has been shown here to be a method of producing stable amorphous formulations and, for the same materials, is superior to hot melt extrusion. Though it can also produce phase separated solid dispersions in some cases, as with IBUss and PVP, the rapid evaporation rate from an initial well-mixed solution aids the formation of a homogeneous solid solution. Hot melt extrusion, which starts with a phase separated powder blend is unable to provide the same level of mixing. Application of electrospinning to manufacturing of amorphous API formulations is promising and, for some API/polymer mixtures, would result in an acceptably stable final product.

Chapter 5

Electrospinning Fibers Containing Crystalline API

5.1 Introduction

For electrospinning to become generally applicable as a manufacturing process, it must also be able to produce fibers containing crystalline API. A few studies on electrospinning of API have found that the API is partially crystalline immediately after electrospinning [37–39]. They test only one API/polymer formulation each and do not examine the effect of API/polymer properties on crystallinity in depth. In Section 5.2 of this chapter, we extend these studies to explore the percent crystallinity of IBU and CBZ with a wide variety of polymers.

Due to the difficulties in obtaining fully crystalline drug for a variety of APIs and drug loadings, however, we have also developed a new approach to electrospin crystalline API. We use free surface electrospinning to spin suspensions of API particles in a PVP/ethanol solution. To develop an understanding of the spinnability of microparticles, we first use 1, 3, 5, and 10 μm polystyrene spheres (Section 5.3) as model particles. We then apply the method to electrospinning API crystals (Section 5.4). If a solvent is chosen in which the API is insoluble, the API will maintain its crystallinity during the electrospinning process, resulting in electrospun mats containing crystalline API dispersed within the polymer fibers. For this work, we selected two

APIs that are insoluble in ethanol, ABZ and FAM, and chose PVP as the polymer due to its acceptability as a pharmaceutical excipient and the ease of electrospinning.

5.2 Results and Discussion: Fibers Containing Crystalline API from Solutions of API and Polymer

Though it has often been demonstrated that amorphous API can be produced in electrospun fibers [6,7,108,109], few have studied the crystallization of the API during electrospinning. Three studies have mentioned crystalline API in the electrospun fibers [37–39], and only one has attempted to explain why crystallization occurs [39]. Since the evaporation rates are high during spinning, crystallization is rare. Yet, amorphous dispersions are difficult to stabilize and many drugs have sufficiently high bioavailability in their crystalline form, so developing a method of producing fibers containing crystalline API is appealing.

In this section, various polymers with two APIs, IBU and CBZ, are electrospun from fully dissolved solutions. The focus here is on drug and polymer properties, neglecting for the time being solvent effects, concentration and drug loading. Many material properties may affect whether the API crystallizes in the fibers during spinning. With respect to the API, these include glass transition temperature, solubility in solvent, hydrogen bonding capabilities (donor/acceptor) molecular weight, charge, and ability to form a solvate. With respect to the polymer, the important properties include hydrogen bonding capabilities (donor/acceptor), glass transition temperature, solubility in solvent, molecular weight, melting temperature (or whether crystalline or amorphous at room temperature), and miscibility with the drug.

5.2.1 Selection of Polymers and API

A variety of polymers have been selected based on their hydrogen bonding capabilities, crystallinity at room temperature, molecular weight, glass transition temperature and melting temperature. These are summarized in Table 5.1. The API used in this study

Polymer	Tm (°C)	Tg (°C)	Hydrogen Bonding	State at 25°C	Molecular Weight (Da)
Poly(l-lactic acid) (PLLA)	173-178	50-80	Acceptor	Slightly Crystalline	103,000
Poly(methyl methacrylate) (PMMA)	n/a	85-165	Acceptor	Amorphous	300,000
Nylon 3,6 (NY)	190-350	45	Acceptor	Amorphous	
Poly(acrylic acid) (PAA)	n/a	79-100	Donor/Acceptor	Amorphous	450,000
Poly(vinyl chloride) (PVC)	100-260	80	Neither	Slightly Crystalline	62,000
Polycaprolactone (PCL)	60	-60	Acceptor	Crystalline	70-90,000
Polystyrene (PS)	n/a	100	Neither	Amorphous	280,000
Poly(ethylene oxide) (PEO)	65	-20	Acceptor	Crystalline	1,000,000
Poly(vinyl pyrrolidone) (PVP)	n/a	190	Acceptor	Amorphous	1,300,000

Table 5.1: Melting temperature (Tm), glass transition temperature (Tg), hydrogen bonding behavior, state at room temperature (25°C) and molecular weight of polymers used in electrospinning experiments.

API	Tm (°C)	Tg (°C)	Hydrogen Bonding	Molecular Weight (Da)
CBZ	190	53	Donor/acceptor	236
IBU	75	-45	Acceptor	206

Table 5.2: Melting temperature (Tm), glass transition temperature (Tg), hydrogen bonding behavior, and molecular weight of CBZ and IBU

are IBU and CBZ, and their properties are listed in Table 5.2.

Though we aimed to electrospin 1:1 API:polymer in all cases, due to solubility issues, we were often not able to obtain such a high API loading. The exact solutions electrospun for these studies and the electrospinning parameters may be found in Table 3.1.

5.2.2 Morphology of Electrospun Fibers Containing Crystalline API

The morphology of all formulations electrospun were analyzed using SEM. For most formulations, the resulting fibers were similar to those containing amorphous API (Figure 4-1): smooth, relatively uniform diameter, and lacking protrusions from the fiber. For a few cases, however, the morphology was distinctly different, and these are shown in Figure 5-1.

For the 1:2 IBU:PEO fibers, the mat was stretched upon mounting on the SEM stage, providing the pulled-apart look along the fibers. What is obvious from Figure 5-1-A is that the fibers contain rough, stiff regions where crystalline material exists.

CBZ tends to crystallize in a needle shape, and Figure 5-1-B of 1:2 CBZ:PEO clearly shows small, needle-like protrusions along the length of the fiber, indicating that there is very clear phase separation between CBZ and PEO and the CBZ crystals have grown through the polymer.

Two other formulations that display interesting morphology are 1:2 IBU:PCL and 1:2 CBZ:PCL (Figure 5-1-C and 5-1-D, respectively). The first observation of note from these images is that the fibers are very thick compared to other fibers electrospun in this work. This is likely due to a combination of the low dielectric constant and the low boiling point of the solvent, chloroform [110, 111]. The dielectric constant is

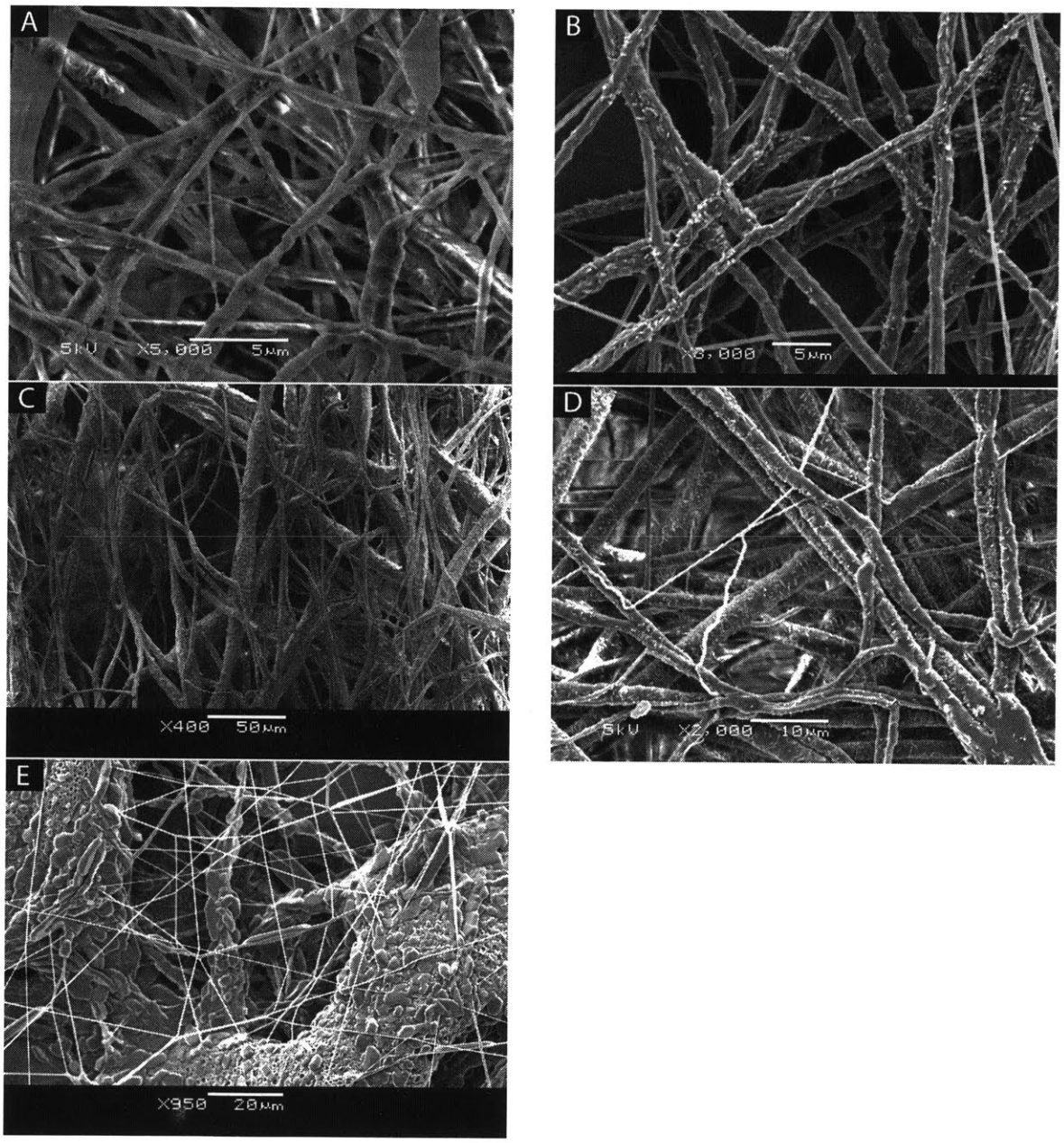

Figure 5-1: SEM images of electrospun A. 1:2 IBU:PEO, B. 1:2 CBZ:PEO, C. 1:2 IBU:PCL, D. 1:2 CBZ:PCL, and E. 1:1 IBU:PLLA

a measure of how well a material can polarize, and a solvent with a low dielectric constant will have a lower charge density during spinning and thus experience weaker elongation forces [111]. Due to the low boiling point, evaporation is more rapid, leaving less time for the weak elongation forces to act and resulting in thicker fibers. Often, to improve the dielectric constant of the spinning solution, a co-solvent is used [110]. That was not done here, however, so as not to add additional solvent effects.

For the IBU/PCL fibers, distinct plate-shaped crystals are visible on the surface of the fibers. These are likely IBU crystals, as it tends to adopt a plate-like morphology. The CBZ/PCL fibers looked very similar to the CBZ/PEO fibers, with needle-like protrusions along the length of the fiber. Both of these images suggest that the API is significantly phase separated from the polymer and crystallizes either through the surface of the fiber or solely on the surface of the fiber.

Finally, we were unable to obtain uniform fibers for 1:1 IBU:PLLA, and the best morphology electrospun can be found in Figure 5-1-E. In general, the electrospun mat was comprised of large portions of IBU/PLLA containing significant IBU crystals and small fibers with no visible crystals.

5.2.3 Crystallinity of Formulations Electrospun from an API/Polymer Solution

Both XRD and DSC were used to evaluate the crystallinity of IBU and CBZ in electrospun fibers. XRD was used primarily to confirm the conclusions drawn from DSC scans, while the DSC data was used to quantitatively determine the percent crystallinity of the API in the fibers. The percent crystallinity can be estimated by integrating the area under the melting endotherm for the pure crystalline material ($\triangle h_{melt,API}$), the melting endotherm for the unknown sample ($\triangle h_{melt,samp}$), and any recrystallization exotherm ($\triangle h_{recryst}$) and using the following equation [86]:

$$\%cryst = \frac{\triangle h_{melt,samp} - \triangle h_{recryst}}{\triangle h_{melt,API}} \tag{5.1}$$

Formulation	IBU % crystallinity	CBZ % crystallinity
1:1 API:PLLA	30, SC	0, AM
1:2 API:PMMA	10, SC	15, SC
1:2 API:NY	0, AM	0, AM
1:2 API:PAA	20, SC	0, AM
1:2 API:PVC	40, SC	40, SC
1:2 API:PCL	XRD cryst., HC	70, HC
1:2 API:PS	10, SC	20, SC
1:2 IBU:PEO, 1:1 CBZ:PEO	XRD cryst., HC	65, HC
1:2 API:PVP	0, AM	0, AM

Table 5.3: Percent crystallinity of the IBU and CBZ in electrospun fibers prepared from many polymers. AM=amorphous, SC=slightly crystalline, and HC=highly crystalline

This calculation method is only a rough estimate, for it relies on the assumption that the heat necessary to melt 1 g of crystalline API is equal to the heat necessary to crystallize 1 g of amorphous API [86], which may not always be the case. In addition, the sensitivity of the DSC is only 5-10 wt% (see Section 3.5), and since the API is only approximately 33 wt% of the entire sample, accuracy will suffer at lower crystallinities.

The measured percent crystallinity for each formulation tested is listed in Table 5.3. Because of the high error associated with using this method to calculate percent crystallinity for low amounts of crystalline material, we sort the results into three categories to draw conclusions; amorphous API (AM), less than 50% crystalline API (slightly crystalline, SC), and greater than 50% crystalline API (highly crystalline, HC).

For most formulations, we were able to calculate a percent crystallinity from the DSC data. For 1:2 IBU:PEO and 1:2 IBU:PCL, however, the melting peaks of IBU and the polymer were too close to separate for analysis. For these formulations, we rely on XRD powder patterns to conclude that the API in the fibers is highly crystalline (Figures 5-2 and 5-3).

Only 4 formulations displayed high crystallinity immediately following electrospinning, and all 4 were API with crystalline polymer (PCL or PEO). The two slightly crystalline polymers, PVC and PLLA, had varying results when spun with API; for

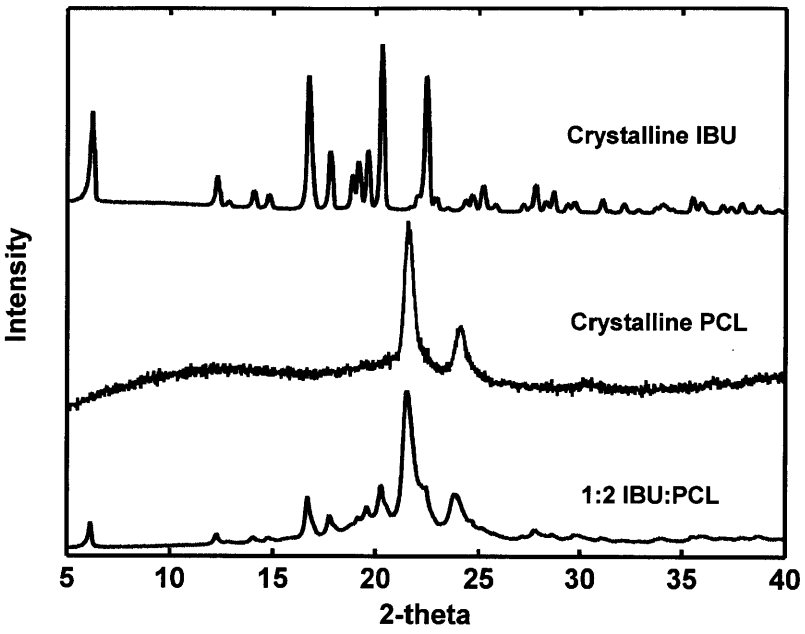

Figure 5-2: XRD powder patterns for crystalline IBU, crystalline PCL, and 1:2 IBU:PCL

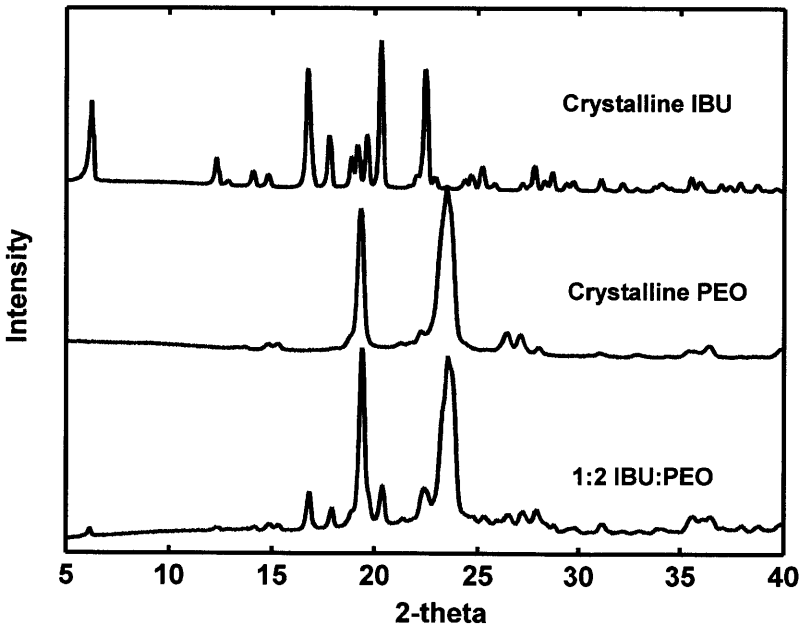

Figure 5-3: XRD powder patterns for crystalline IBU, crystalline PEO, and 1:2 IBU:PEO

PVC both API were slightly crystalline and for PLLA the IBU was slightly crystalline, but CBZ was amorphous. For the remainder of the API/polymer combinations, there is no clear pattern with any of the polymer or API properties.

It is clear from these results that crystallization of an API during electrospinning is dependent on more factors than merely the API and polymer properties. For one, the solvent effects cannot be neglected, as solvent properties, such as dielectric constant and boiling point, have a large effect on the behavior of the fiber during electrospinning. In addition, interactions between the solvent and polymer as well as solvent and API will affect the phase separation during spinning and thus the likelihood of crystallization occurring.

In addition, recent studies on the crystallization of a polymer during electrospinning have shown that concentration and viscosity play a role in crystallization of the polymer. The morphology of polymer crystals (whether the chain layering is parallel to the fiber length or perpendicular to it) depends on how quickly the fiber dries and the mobility of the chains during drying [112]. These properties were not controlled for these studies, as the different API/polymer solutions were only spinnable in a small window of concentrations near that chosen for the experiments.

A final issue encountered in this work is that it is unknown whether crystallization takes place while the jet is electrospinning or after collection, but before XRD and DSC experiments can be performed. Though the samples were all analyzed as soon as possible after electrospinning was completed, the time required to spin enough material for analysis was on the order of hours. In some cases, this could be sufficient for an initially amorphous API to crystallize. Better analysis techniques are required in order to truly understand when crystallization is occurring.

5.2.4 Summary

For the many API/polymer combinations studied, only 4 displayed highly crystalline API in the fibers: 1:2 IBU:PCL, 1:2 CBZ:PCL, 1:2 IBU:PEO, and 1:1 CBZ:PEO. These also correlated with the only polymers that themselves crystallized readily, indicating that electrospinning with a polymer that tends to crystallize during elec-

trospinning can lead to crystallization of the API. More work is necessary to understand the mechanism behind the crystallization and to determine to what extent crystallization takes place before collection versus after collection but before analysis.

Additionally, it was shown here that crystallization of an API during electrospinning is dependent on more parameters than merely the API and polymer properties. Besides all of the conditions that play a role in traditional crystallization via solvent evaporation, including temperature, solvent-API interactions, API concentration, etc., other parameters will have a strong effect during electrospinning, particularly on the evaporation rate and elongation forces. Further investigation into these alternate parameters will help determine which conditions are necessary in order to produce fibers containing crystalline API via electrospinning of a solution of API, polymer, and solvent.

5.3 Results and Discussion: Spinnability of Particles using Polystyrene Beads as Model API

One attractive attribute of electrospinning is that other materials can be added to the polymer/solvent solution and incorporated into the electrospun fibers in order to make composite fibers. In this section we investigate the spinnability of 1-10 μm PS beads suspended in an ethanol/PVP solution in order to better understand the use of free surface electrospinning for suspensions of large particles. With the knowledge gleaned from this work, the technique can be applied to producing fibers containing large API particles for application to pharmaceutical manufacturing.

5.3.1 Theory of the Spinnability of Microparticles

For single needle electrospinning of both the 1.3 MDa and 55 kDa PVP solutions in ethanol, particles should be spinnable at all sizes up to the diameter of the nozzle at sufficiently low loadings, but for the free surface approach, the particles must remain suspended in the solution bath, be entrained on the wire along with the fluid and must

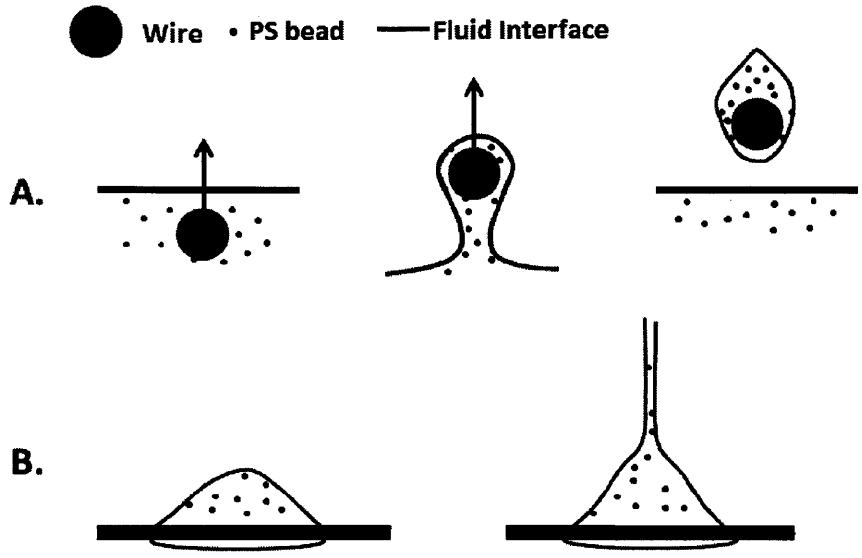

Figure 5-4: A. Fluid entrainment on the wire in the presence of an electric field. The large circle represents the wire viewed end-on, the small circles are the microparticles and thin line is the fluid/air interface. The middle image illustrates entrainment of the fluid with a trailing film. The rightmost image illustrates droplet formation after breakup of the trailing film; the droplet is drawn asymmetrically about the wire to represent the influence of the electric field. B. Jetting of the fluid. The small circles are the microparticles, the thick line is the wire viewed perpendicular to its axis, and the thin line is the fluid/air interface. The left image represents the droplet profile prior to jetting, while the right image shows the profile during jetting. The beads are not drawn to scale.

also remain with the fluid during jetting. The latter two processes are illustrated in Figure 5-4.

In the entrainment process, the wire electrode experiences several forces (capillary, inertial, viscous, and gravitational forces) as it travels vertically through the air/liquid interface of the bath. As the wire approaches the interface, the interface deforms and coats the upper hemisphere of the wire. Once the wire has passed through the original position of the interface, liquid begins to drain from the wire, causing a trailing film to form. At a distance several times larger than the diameter of the wire, the trailing

film ruptures, leaving liquid entrained on the wire. It is important to note that this configuration is distinct from previous studies of coating and liquid entrainment on a cylinder where the cylinder axis is oriented parallel to the interface normal as it is drawn through the interface. The latter configuration has been described by Landau and Levich [113], and Derjaguin [114] and more recently for a fiber by Quéré [115].

The configuration employed here is similar to studies where spherical particles are drawn through an interface by mechanical forces [116,117] or buoyancy forces [118] and entrain liquid through the draining and rupture of a trailing filament. Computational studies have shown that the liquid entrainment on a sphere at low Reynolds number (Re) is highly dependent on the capillary number (Ca), a measure of the viscous force relative to the surface force, of the system [119–121]. All of the previous studies describe the entrainment of a liquid on a spherical surface, whereas here we consider entrainment on a cylindrical surface. To the best of our knowledge, analysis of a cylinder traveling horizontally through a deformable interface has not been described prior to a recent study on free surface electrospinning [17], where it was found that the amount of liquid entrained on the wire could be described by the relation:

$$\frac{z}{r_w} = aCa^b \tag{5.2}$$

where z is the thickness of the uniform liquid film entrained on a wire of radius r_w, and a=0.78±0.03 and b=0.21±0.01 for solutions of PVP in ethanol.

Here we consider whether the polystyrene beads are entrained with the fluid or remain in the solution bath. In this analysis, we use only the wire electrode type of free surface electrospinning and assume the particles are perfect spheres of density equal to that of polystyrene, 1.05 g/cm^3. Due to the low Re of the fluid during entrainment, it is possible to assume that the beads behave as a dilute suspension of spheres in a large fluid bath, and the flow can be approximated by Stokes's flow, given that the bead diameter is much less than the wire diameter. In this work, the wire diameter is 200 μm, and the largest bead diameters are 10 μm, so the assumption is reasonable. The main forces acting on the bead are the force due to gravity and the

Fluid	Density (g/cm^3)	Viscosity (Pa.s)	Surface tension (mN/m)
1.3 MDa PVP in ethanol (8.6 wt%)	0.82	0.137	23
55 kDa PVP in ethanol (20 wt%)	0.85	0.028	23
1.3 MDa PVP (8.6 wt%), 10 μm PS beads (4.3 wt%) in ethanol	n/a	0.154	n/a
55 kDa PVP (20 wt%), 10 μm beads (10 wt%) in ethanol	n/a	0.035	n/a

Table 5.4: Physical properties of the PVP solutions, 8.6 wt% 1.3 MDa PVP with 4.3 wt% 10 μm PS bead in ethanol and 20 wt% 55 kDa PVP with 10 wt% 10 μm PS beads in ethanol

drag force on the bead due to the liquid. We ignore any electrical forces that may arise due to accumulation of charge on the PS microparticle itself.

The force due to gravity, taking into account buoyancy, can be determined by:

$$F_g = (\rho_{part} - \rho_{fluid}) \frac{4}{3} \pi r_p^3 g \tag{5.3}$$

where ρ_{part} is the particle density, ρ_{fluid} is the fluid density, r_p is the radius of the particle and g is the gravitational acceleration. The drag force can be calculated by Stoke's law:

$$F_{drag} = 6\pi\eta r_p v_{rel} \tag{5.4}$$

where η is the viscosity of the fluid and v_{rel} is the relative velocity between the fluid (v_{fluid}) and particle (v_{part}):

$$v_{rel} = v_{fluid} - v_{part} \tag{5.5}$$

In order to determine whether the particles will be entrained on the wire or jet with the fluid during electrospinning, we calculate v_{part} and determine whether it is positive (travels with the fluid) or negative (left behind). The physical properties of the polymer solutions used for calculations are listed in Table 5.4.

We deal first with the settling of the beads in the fluid bath, where v_{fluid} is equal to zero. In this case, the settling velocity of the PS beads in 1.3 MDa PVP and 55 kDa PVP, determined by equating F_g and F_{drag} and solving for v_{part}, is very small. For the largest bead size used in this study, 10 μm, the settling velocity is calculated to be -3.5 x 10^{-5} cm/s and -1.5 x 10^{-5} cm/s for the 1.3 MDa and 55 kDa solutions, respectively. This is very slow, and means that it would take more than 6 hours for a particle to travel the depth of the solution bath, 0.8 cm. Since our experiments run for 30 min, this is not a large concern for this work. For larger particles, the settling becomes a greater issue, as 100 μm particles are expected to settle out in less than 4 min.

Next we examine the entrainment process. The velocity of the fluid away from the fluid bath during entrainment can be approximated by the velocity of the wire. This can be calculated by:

$$v_{fluid} = 2r_s\pi\Omega \tag{5.6}$$

where r_s is the radius of the spindle and Ω is the rotation rate. Equating F_g and F_{drag} (Equations 5.3 and 5.4) and using Equations 5.5 and 5.6 for the relative velocity, the velocity of the particle can be caculated as a function of the particle diameter, allowing us to determine whether the particle will remain entrained on the wire.

The predicted velocity of the particle during entrainment was calculated using the parameters from the experiments. The diameter of the wire was 200 μm, the radius of the spindle was 3.2 cm, and the rotation rate was 8.8 rpm. The calculated particle velocity for the 55 kDa PVP and 1.3 MDa PVP solutions was 2.92 cm/s and did not change appreciably as a function of particle diameter for particle diameters up to 100 μm. This indicates that for particle diameters up to one half the wire diameter, the velocity is positive and the particles will remain within the fluid during entrainment.

For the inclusion of the beads during jetting, determining the precise velocity of the fluid is non-trivial. Many researchers have developed methods to analyze the flow of an electrospinning jet, but they involve complex numerical simulations, which

are outside the scope of this paper. In lieu of calculating the precise velocity, many authors estimate the velocity based on the volumetric flow rate (Q):

$$v_{fluid} = QA \tag{5.7}$$

where A is the area of the jet, determined from the radius of the jet immediately past the Taylor cone. In our case this is approximately 10 μm, based on image analysis. For needle elctrospinning with a metering pump, Q is a known input parameter, but for free-surface electrospinning Q is unknown. In order to estimate it, we use the lifetime of a jet and the volume of the drop, assuming that the flow rate is approximately the volume of the drop (V_{drop}) divided by its lifetime (t_{jet}).

$$Q = \frac{V_{drop}}{t_{jet}} \tag{5.8}$$

The lifetime of the jet was determined to be 1.28 s for a 30 wt% solution of 55 kDa PVP in ethanol electrospun at an applied voltage of 30 kV [17]. To determine the volume of the drop, V_{drop}, we use the correlation reported previously [17]:

$$V_{drop} = \frac{2\pi^2 r_w^3 \left[(1+0.78Ca^{0.21})^3 - 0.78Ca^{0.21} - 1\right]}{0.0028V_A + 0.5} \tag{5.9}$$

where $Ca = \frac{v_{fluid}\eta}{\gamma}$, V_A is the applied voltage in kV, r_w is the radius of the wire in km, v_{fluid} is the velocity of the fluid during entrainment and γ is the surface tension of the fluid. The solutions employed in Ref [17] are similar to the 20 wt% 55 kDa and 8.6 wt% 1.3 MDa PVP solutions used in this work and were also spun at approximately 30 kV, so the values and correlations reported there are taken as a first approximation here as well.

Equating F_g and F_{drag}, Equations 5.3-5.5 and 5.7-5.9 may be solved to yield the velocity as a function of particle diameter, allowing us to determine whether the particles remain in the fluid during entrainment and jetting. This results in a velocity of approximately 10.6 cm/s for particle diameters up to 100 μm for both polymer solutions, indicating again that PS particles up to a 100 μm diameter should be

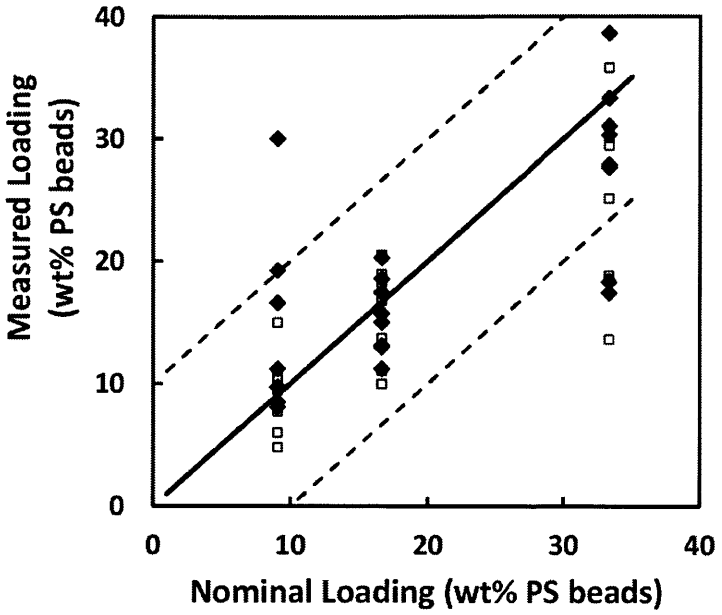

Figure 5-5: Measured mass loading of polystyrene beads in electrospun fibers as a function of the nominal mass loading for both free surface (filled diamonds) and single needle (open squares) electrospinning. The parity line assuming complete and uniform entrainment is shown by the solid line, and the dotted lines represent ± 10 wt%.

spinnable with the PVP/ethanol solutions.

5.3.2 Loading of Polystyrene Beads in Electrospun Fibers

One way of assessing whether the particles were actually entrained in the fluid on the wire or remained with the fluid during jetting is to examine the final loading of PS in the fiber mat. To do this, we measured the weight percent of the PS in the fiber mats for both the free surface and single needle electrospinning. Approximately 30 mg of the solid fibers were washed with ethanol, dissolving the PVP and washing it through a filter (1 µm pore size for the 3, 5, 10 µm PS beads and 0.45 µm pore size for the 1 µm bead size). The final mass of the filter was determined after drying under vacuum, and the mass of the PS beads was calculated by subtracting the initial mass from the final mass. The measured mass loading is plotted in Figure 5-5 against the nominal mass loading for all solutions electrospun in this study.

The method for determining loading results in an error of approximately ± 10

wt%, due to the low mass being analyzed and the uncertainty of the balance, so we have included the +10 wt% and -10 wt% boundaries (dotted lines) in Figure 5-5. The limited accuracy of the measurement is confirmed by the single needle electrospinning results, where entrainment is not an issue and all points should fall on the parity line, according to conservation of mass. In order to evaluate how well particles are spun in free surface electrospinning, then, we can compare it to single needle electrospinning. Most points for both cases fall within the 10 wt% error boundaries. There are two points that fall outside of the boundaries for the single needle electrospinning and three points that fall outside for free surface, an insignificant difference. Thus, we conclude that there are no large deviations of the loading from the expected loading, and the solutions are spinnable. This is also consistent with observations from SEM.

5.3.3 Fiber Morphology and Diameter

All samples were examined by SEM to determine their morphology. In Figures 5-6 and 5-7, sample SEM images are shown from free surface electrospun fiber mats. Figure 5-6 shows images of the 1.3 MDa PVP, 1:5 PS:PVP mass loading mats for all four different PS bead sizes. It can be seen from these images that the fibers have a mostly smooth morphology and their diameters are smaller than the size of the beads.

Figure 5-7 shows images for the 1.3 MDa PVP, 3 μm beads for the three different mass loadings used in the experiments: 1:10, 1:5, and 1:2 PS:PVP. It is obvious from these images that the fiber morphologies, i.e. smooth and uniform between beads, with fiber diameters smaller than the bead size, are very similar from one sample to the next, independent of the mass loading of the PS beads. From this we conclude that the loading has no effect on fiber morphology up to a 1:2 PS:PVP ratio.

An average fiber diameter calculated from at least 80 measurements was determined for each of the samples. From the results in Table 5.5, one can see that the fiber diameter is independent of the PS bead diameter within each similar group (same PVP base solution and same bead loading). For all cases, the average fiber diameters fall within the widths of the fiber diameter distributions of one another.

To examine the effect of bead loading, we compared the fiber diameters to the fiber

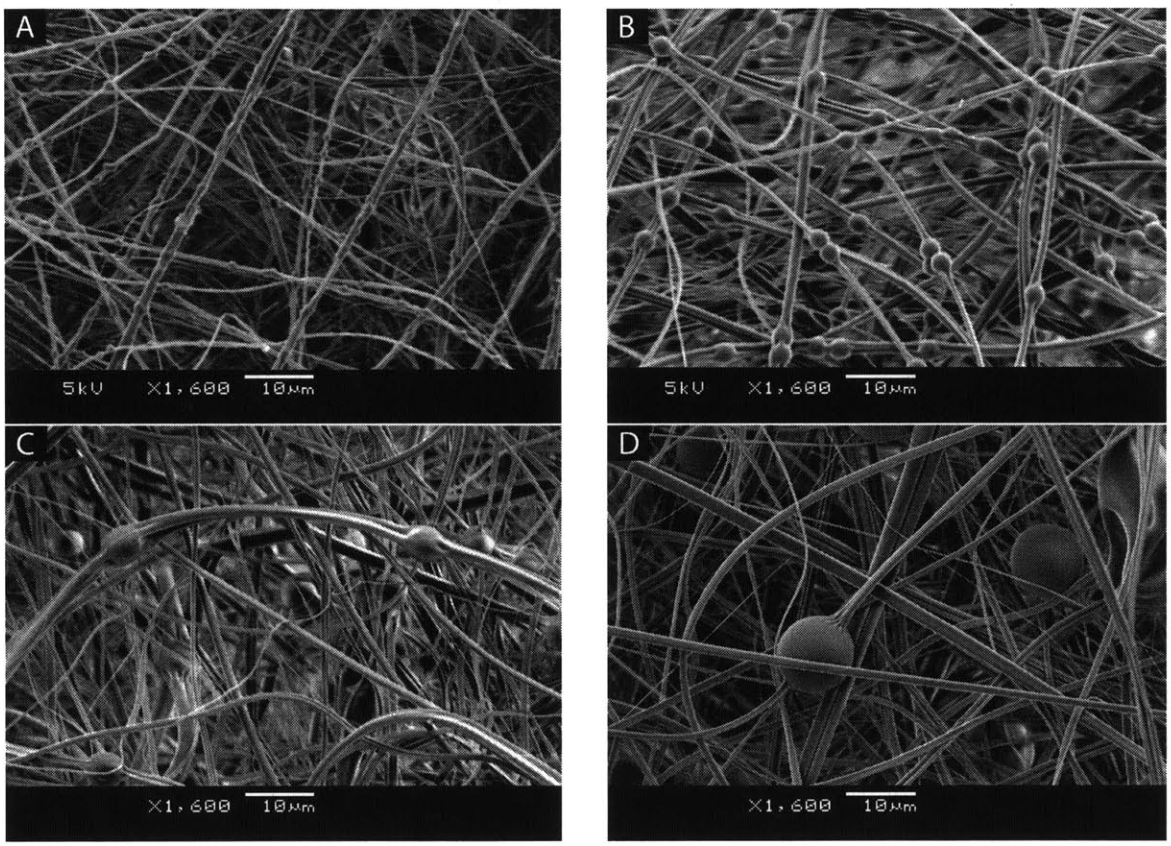

Figure 5-6: SEM images of electrospun A. 1 μm beads, 1:5 loading, 1.3 MDa PVP, average fiber diameter 1.07 $\pm$ 0.17 μm; B. 3 μm beads, 1:5 loading, 1.3 MDa PVP, average fiber diameter 1.17 $\pm$ 0.23 μm ; C. 5 μm beads, 1:5 loading, 1.3 MDa PVP, average fiber diameter 0.97 $\pm$ 0.32 μm; and D. 10 μm beads, 1:5 loading, 1.3 MDa PVP, average fiber diameter 1.05 $\pm$ 0.32 μm

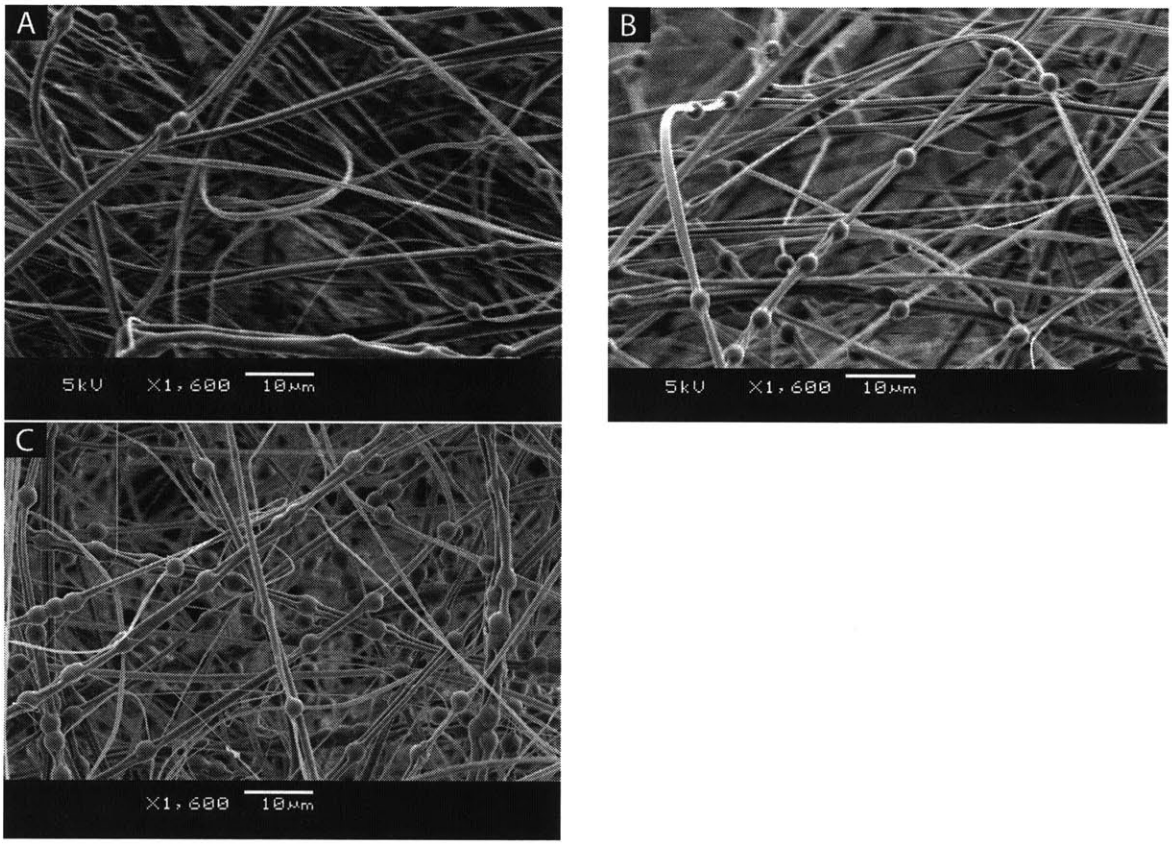

Figure 5-7: SEM images of electrospun A. 1:10 loading, 3 μm beads, 1.3 MDa PVP, average fiber diameter 1.33 $\pm$ 0.25 μm; B. 1:5 loading, 3 μm beads, 1.3 MDa PVP, average fiber diameter 1.23 $\pm$ 0.18 μm; and C. 1:2 loading, 3 μm beads, 1.3 MDa PVP, average fiber diameter 0.97 $\pm$ 0.22 μm

Bead Diameter (μm)	PS:PVP loading	PVP M_W	Diameter (μm) +/- width of distribution
1	1:10	1.3 MDa	1.11 ± 0.22
3	1:10	1.3 MDa	1.33 ± 0.25
5	1:10	1.3 MDa	1.17 ± 0.30
10	1:10	1.3 MDa	0.94 ± 0.21
1	1:5	1.3 MDa	1.13 ± 0.23
3	1:5	1.3 MDa	1.19 ± 0.22
5	1:5	1.3 MDa	0.88 ± 0.22
10	1:5	1.3 MDa	0.98 ± 0.30
1	1:2	1.3 MDa	n/a*
3	1:2	1.3 MDa	0.96 ± 0.18
5	1:2	1.3 MDa	0.88 ± 0.15
10	1:2	1.3 MDa	1.11 ± 0.34
1	1:10	55 KDa	0.66 ± 0.08
3	1:10	55 KDa	0.48 ± 0.16
5	1:10	55 KDa	0.56 ± 0.10
10	1:5	55 KDa	0.47 ± 0.11
1	1:5	55 KDa	0.66 ± 0.15
3	1:5	55 KDa	0.84 ± 0.27
5	1:5	55 KDa	0.50 ± 0.12
10	1:5	55 KDa	0.60 ± 0.22
1	1:2	55 KDa	0.56 ± 0.10
3	1:2	55 KDa	0.56 ± 0.12
5	1:2	55 KDa	0.53 ± 0.11
10	1:2	55 KDa	0.54 ± 0.14
None	None	1.3 MDa	1.19 ± 0.44
None	None	55 KDa	0.72 ± 0.23

Table 5.5: Average diameter of the fibers for each solution electrospun, *Could not be measured due to aggregation, see Figure 5-10-B.

diameters for PVP fibers containing no PS beads. The average fiber diameter for 1.3 MDa PVP fibers containing no beads spun under the same conditions is close to that for all bead-containing fibers electrospun from the 1.3 MDa PVP base solution. In addition, all values for the 55 kDa PVP containing beads fall near the average for 55 kDa fibers containing no beads. These results indicate that the fiber diameter is independent of the bead size as well as bead loading for the materials studied. The fiber diameter can thus be adjusted independently of the diameter of the bead and bead loading, up to a 10 μm bead diameter and a 1:2 bead to polymer loading, by adjusting the base solution properties, for example by changing the concentration or molecular weight of the polymer. Further work is necessary to determine whether the relationship between fiber diameter and the various solution properties follow identical trends as for solutions without particles, as this study examined only a small subset of solution properties.

5.3.4 Discussion

All formulations chosen for this work were "electrospinnable". This is consistent with the predictions based on particle settling, fluid entrainment and jetting. In fact, for a scenario where the polymer fluid was the 8.6 wt% 1.3 MDa PVP used in this study and the particle density was as high as lead (approximately 12 g/cm^3), the beads would still be expected to be entrained in the fluid up to a diameter of 100 μm, as can be seen in Figure 5-8.

For a particle of such high density, however, the settling velocity becomes very high. For the case of 8.6 wt% 1.3 MDa PVP and a lead particle, the settling velocity for a 5 μm particle is -2 x 10^{-4} cm/s, for a 30 μm diameter particle is -0.007 cm/s and for a 100 μm particle is -0.08 cm/s , corresponding to complete settling times of 4000 s, 110 s, and 10 s, respectively. To test whether lead particles would be entrained in the fluid and jet, we scattered lead particles of diameter less than 44 μm onto the top of the fluid bath and immediately began spindle rotation and application of the electric field. We allowed the spinning to progress for approximately 30 s and then analyzed the as-received powder and fibers via SEM (Figure 5-9).

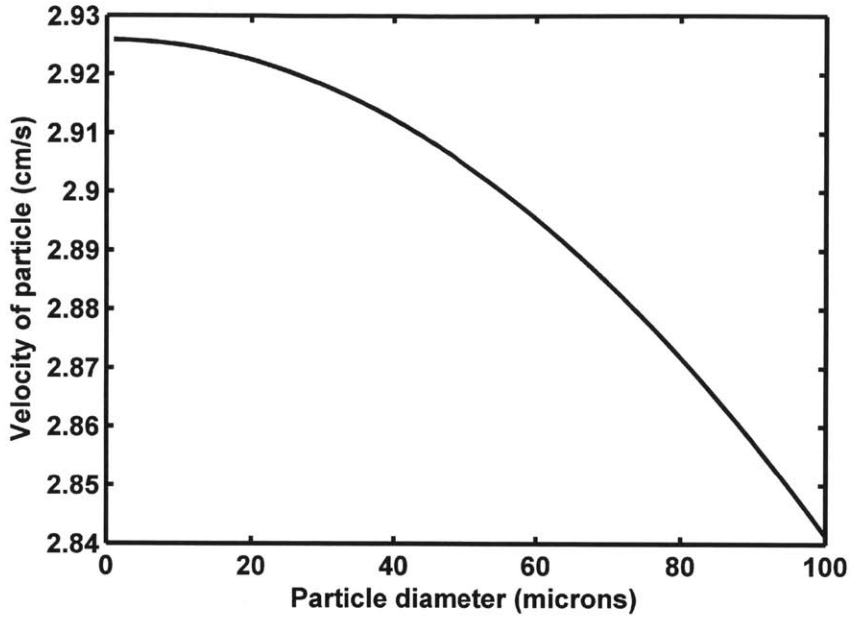

Figure 5-8: Predicted velocity of particles during fluid entrainment as a function of particle diameter for a solution of 8.6 wt% 1.3 MDa PVP and a particle with the density of lead

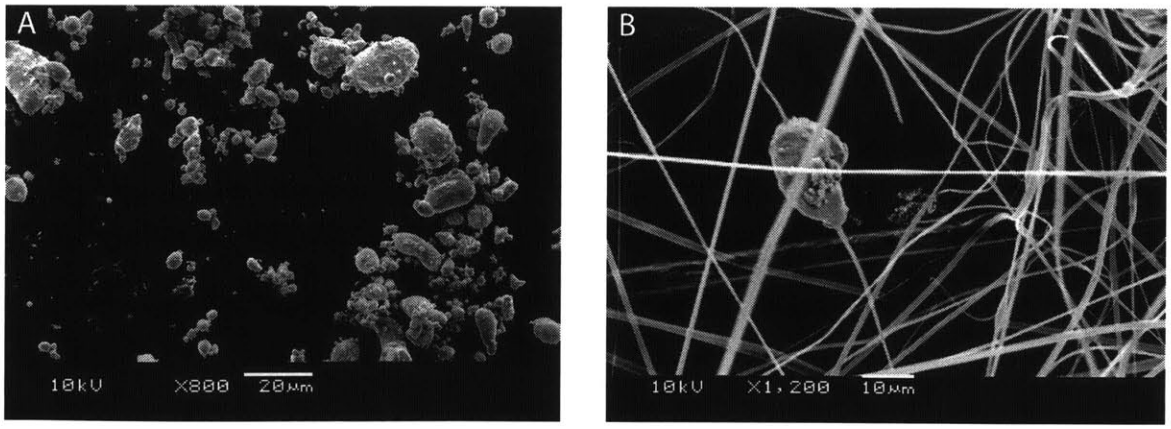

Figure 5-9: SEM images of lead particles as received (left) and electrospun 1.3 MDa PVP/lead fibers (right)

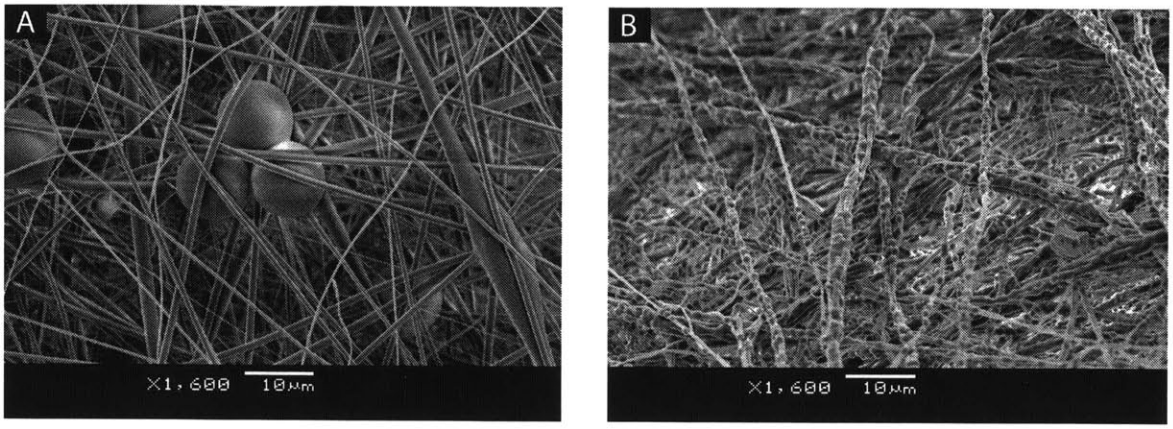

Figure 5-10: SEM images of A. aggregation of particles for single needle electrospinning of 1:2 loading, 1.3 MDa PVP and 10 μm beads and B. aggregation of particles for free surface electrospinning of 1:2 loading, 1.3 MDa PVP and 1 μm beads

It is clear from Figure 5-9 that lead particles of greater than 10 μm are spinnable with 8.6 wt% 1.3 MDa PVP if the particles can be made to remain suspended in the fluid bath.

One additional challenge identified in these studies is aggregation of the particles. For some of the single needle formulations, the spinning was so slow that aggregation of particles occurred in the syringe prior to spinning, resulting in aggregates present in the fibers rather than single, separated beads. This is illustrated in Figure 5-10-A for 10 μm PS beads in a 1:2 PS:PVP mass loading prepared by single needle electrospinning.

Aggregation may also be an issue in free surface electrospinning, as can be seen in Figures 5-6-B, 5-7-C and 5-10-B. Though not performed in this study, this challenge could be addressed through use of agitation in the solution bath during spinning or incorporation of a surfactant in the electrospinning solution.

In addition, high bead loadings could also produce challenges, both with respect to aggregation, as seen in Figure 5-10-B, as well as with respect to fluid entrainment, as all of the entrainment predictions in this work applied the assumption of a dilute solution. Further work is necessary to understand the behavior of particles during electrospinning at high particle loadings.

5.3.5 Summary

Electrospinning has been a useful tool for producing nanofibers for a number of years, and here we present a case for its application to create fibers with more complex geometries by electrospinning microparticles up to a diameter of 10 μm. Various bead diameters and polymer molecular weights were shown to be spinnable up to a 1:2 PS:PVP mass loading. The final fiber diameters were independent of the bead size and bead loading, but were dependent on the solution properties, such as viscosity and conductivity, and similar to fibers spun without any beads at all. This indicates that a wide variety of particles can be electrospun for many applications and the final bead and fiber dimensions can be controlled. In addition, this is manageable using the high-throughput free surface electrospinning apparatus, meaning it has a greater potential for application to an industrial process.

5.4 Results and Discussion: Fibers Containing Crystalline API from Suspensions

Due to the difficulties in obtaining fully crystalline drug for a variety of APIs and drug loadings (Section 5.2), we developed a new approach to electrospin fibers containing crystalline API. It has previously been demonstrated that nano- and microparticles can be electrospun starting from a dispersion of the particles in a polymer solution. The particles can be very small, 20 nm or less, as with magnetite [40], TiO_2 [41, 42] and carbon black [45] or larger, 1-10 μm, as with bacteria and viruses [50], clays [51, 52] and polystyrene beads [122] (Section 5.3). Though most work has been done electrospinning particles using a single needle apparatus, we recently demonstrated that polystyrene beads of 1-10 μm diameter can be electrospun from PVP solutions using free surface electrospinning (Section 5.3).

In this section, we use free surface electrospinning to spin suspensions of API crystals in a PVP/ethanol solution. If a solvent is chosen in which the API is insoluble, the API will maintain its crystallinity during the electrospinning process, resulting in

electrospun mats containing crystalline API dispersed within the polymer fibers. For this work, we selected two poorly water soluble APIs that are insoluble in ethanol, albendazole (ABZ) and famotidine (FAM), and chose PVP as the polymer due to its acceptance as a pharmaceutical excipient and the ease of electrospinning. We demonstrate that the API crystals are entrained within the fibers, retain their crystalline morphology during spinning, and exhibit improved dissolution rates when compared to compressed powder tablets.

5.4.1 Particle Size Analysis

The particle size distributions of the API crystals suspended in the PVP/ethanol solution were measured prior to sonication, after sonication and after standing for 1 hour, approximately the length of time to electrospin the mat for analysis. The distributions for the ABZ and FAM suspensions are shown in Figures 5-11 and 5-12.

For ABZ, the sonication greatly decreases the crystal size. This is likely due to dispersal of aggregates rather than crystal breakage, as SEM images of the ABZ crystals show agglomerates of smaller crystals (Figure 5-13-A). The FAM particle size distribution does not show a strong change following sonication. This is likely because the FAM crystals are less agglomerated in the powder, as can be seen in Figure 5-13-B. Following 1 hour of standing, both suspensions retain their particle size distribution, indicating that the suspensions electrospun will retain their particle size distribution throughout the entire 1 hour electrospinning process.

5.4.2 Characterization of Fibers Containing Crystalline API

The morphologies of the electrospun fibers were examined by SEM and the images are shown in Figure 5-14.

In both cases, the API crystals present in the electrospun fibers are easily visible. For the ABZ dispersed in the PVP mat, the crystals are present in the fibers as small agglomerates as well as dispersed crystals, which can be seen by careful examination of the roughness of the fibers. FAM dispersed within PVP, on the other hand, shows

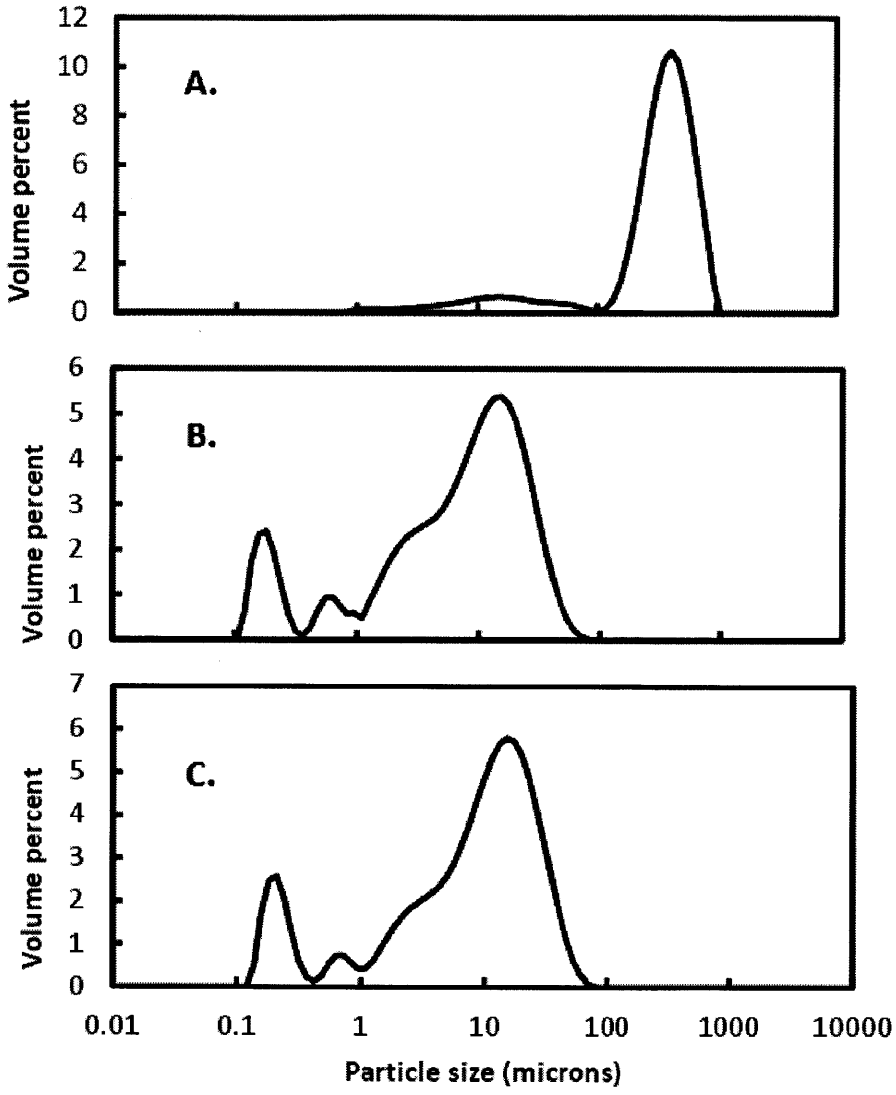

Figure 5-11: Particle size distributions by volume of 4.3 wt% ABZ crystals suspended in 8.6 wt% PVP in ethanol A. before sonication, B. after sonication, and C. after 1 hour

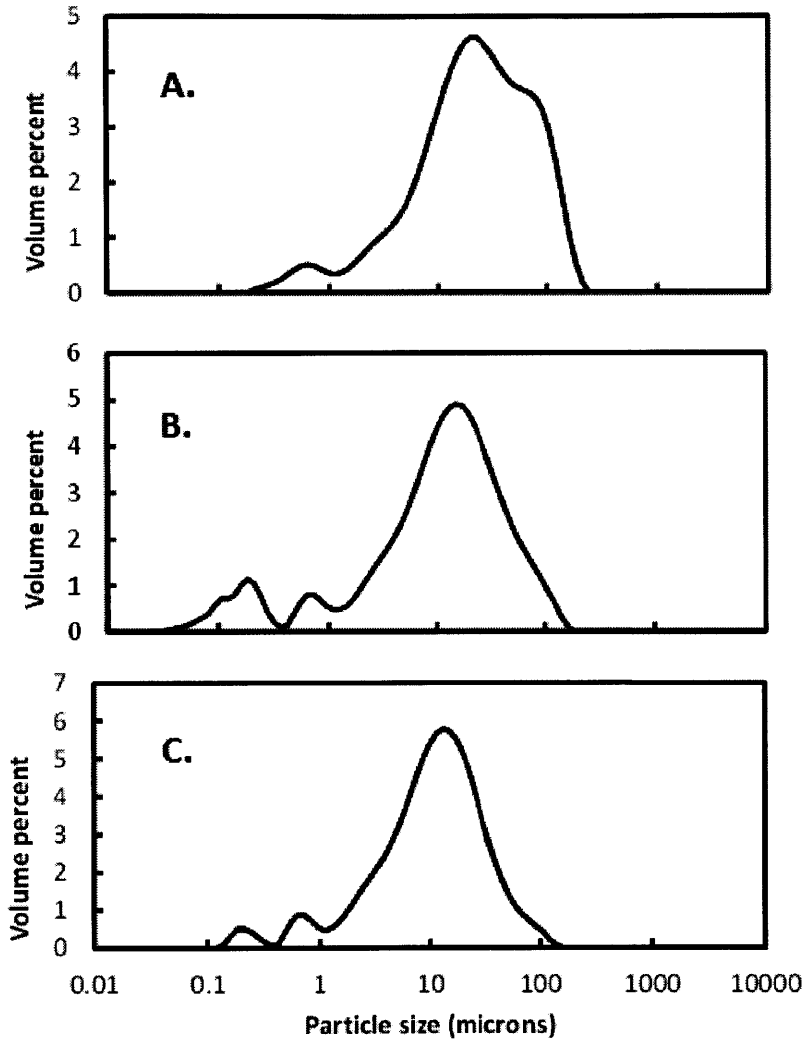

Figure 5-12: Particle size distributions by volume of 4.3 wt% FAM crystals suspended in 8.6 wt% PVP in ethanol A. before sonication, B. after sonication, and C. after 1 hour

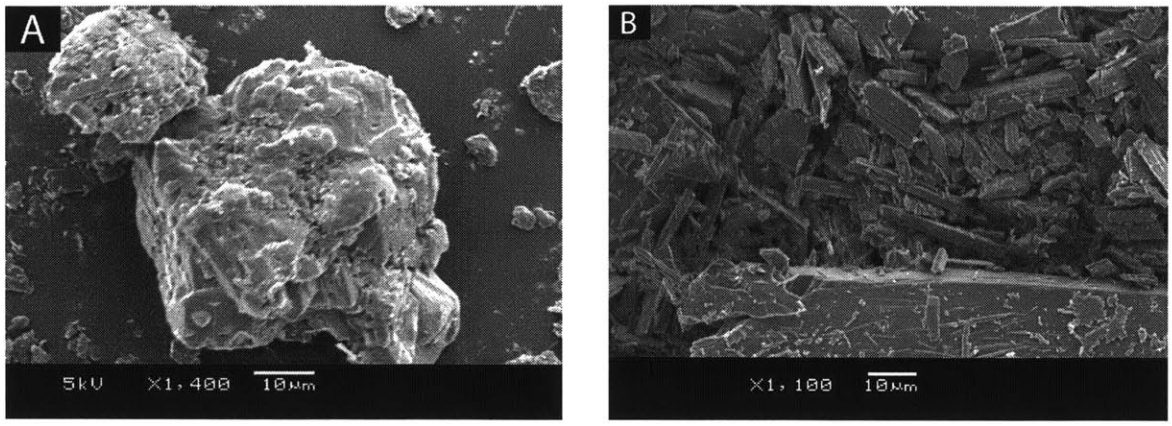

Figure 5-13: SEM images of A. ABZ crystals as received and B. FAM crystals as received

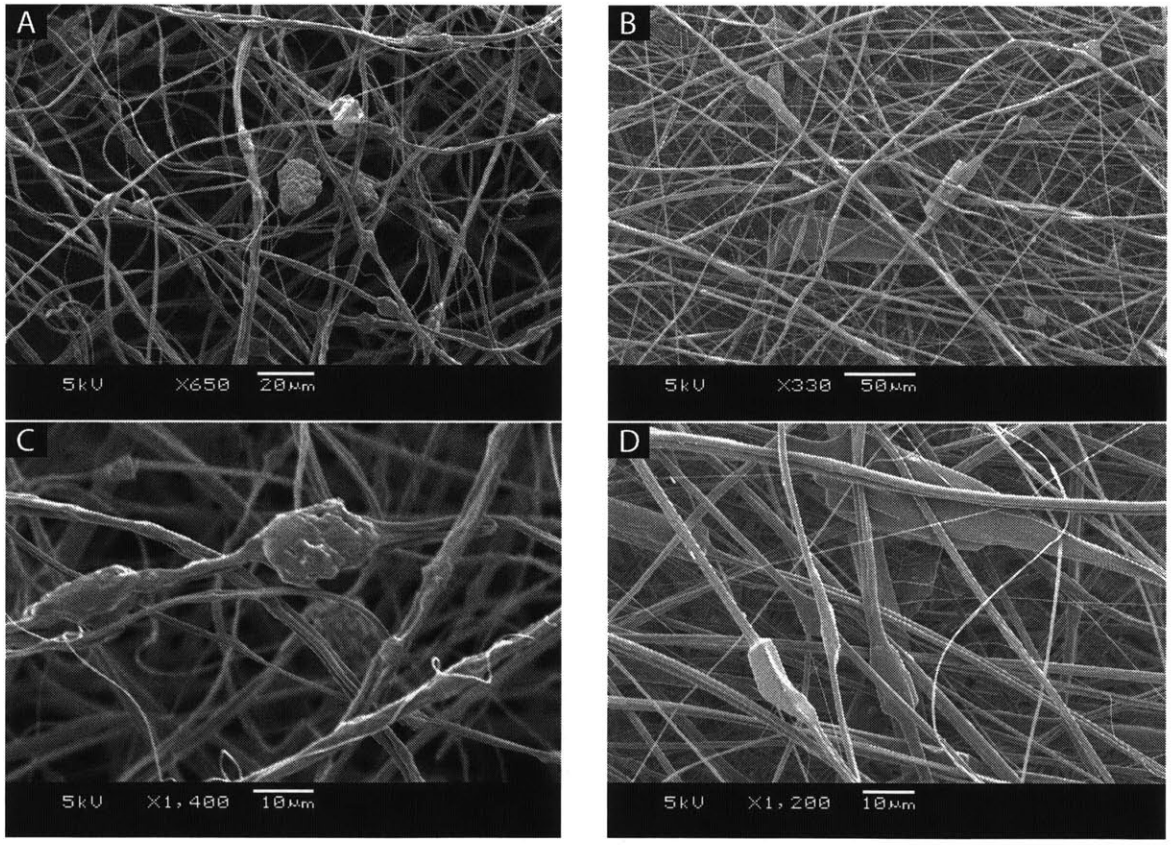

Figure 5-14: SEM images of A. 1:2 ABZ:PVP electrospun, B. 1:2 FAM:PVP electrospun, C. 1:2 ABZ:PVP electrospun at higher magnification, D. 1:2 FAM:PVP electrospun at higher magnification

little agglomeration and good dispersion of the API in the fibers. It is interesting to note that the FAM crystals are always distributed with their longest side parallel to the fiber. This can be attributed to the high shear forces during jetting [48].

XRD and DSC were both used to examine the crystallinity of the API within the electrospun fibers. For 1:2 ABZ:PVP, the melting endotherm is broad with an onset melting point of 165°C, indicating that the ABZ is crystalline in the fibers (Figure 5-15). The onset melting point is depressed from that of the crystalline ABZ as received, 190°C. The onset melting of ABZ is consistent with that of Form I of ABZ shown in the literature [123].

The first onset melting point for crystalline FAM as received is 160°C, and based on the DSC results (Figure 5-16), there is a broad melting endotherm for the 1:2 FAM:PVP with an onset at 150°C. This melting point corresponds to polymorph B [124]. There is a second melting endotherm for the crystalline material as received with on onset at 167°C corresponding to polymorph A [124]. This melting endotherm is also present for the 1:2 FAM:PVP electrospun material with an onset at 167°C. This indicates that both the crystalline material as received and the FAM in the final electrospun fibers are mixtures of polymorphs A and B.

The DSC scans also provide evidence that the APIs are well-dispersed within the fibers. The depression of the melting points of the APIs and the broadening of the melting endotherms indicate that the APIs are well-dispersed and form a partially miscible blend with the polymer as the APIs melt during the temperature ramp of the DSC experiment [125].

XRD powder patterns were used to determine which crystalline polymorph is present following electrospinning. Figures 5-17 and 5-18 compare the experimental powder patterns to the calculated powder patterns from the Cambridge Structural Database.

For ABZ, both the crystalline material as received and the 1:2 ABZ:PVP electrospun powder patterns show the same peaks as the calculated powder pattern for form I from the Cambridge Structural Database (Figure 5-17), reference code BOGFUZ. The powder patterns for the crystalline ABZ as-received and 1:2 ABZ:PVP electro-

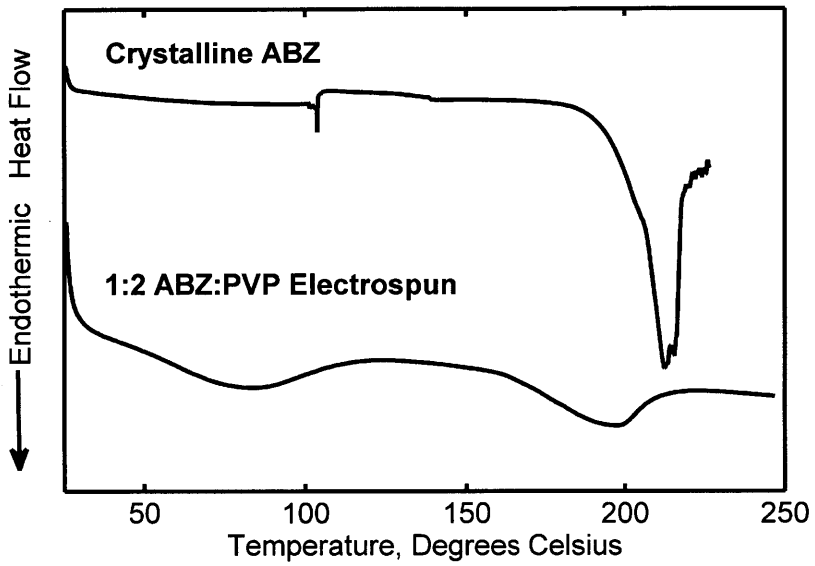

Figure 5-15: DSC scan of crystalline ABZ powder and 1:2 ABZ:PVP electrospun

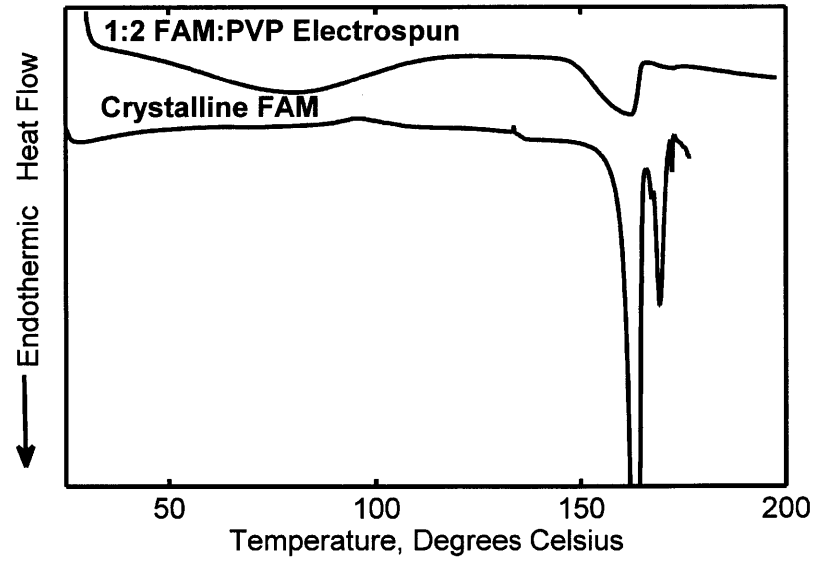

Figure 5-16: DSC scan of crystalline FAM powder and 1:2 FAM:PVP electrospun

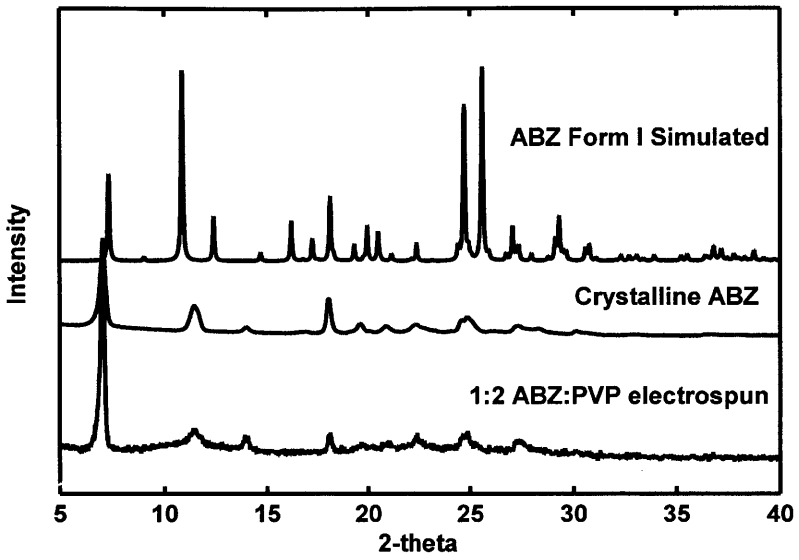

Figure 5-17: XRD powder pattern of crystalline ABZ powder, 1:2 ABZ:PVP electrospun and a calculated powder pattern for ABZ form I

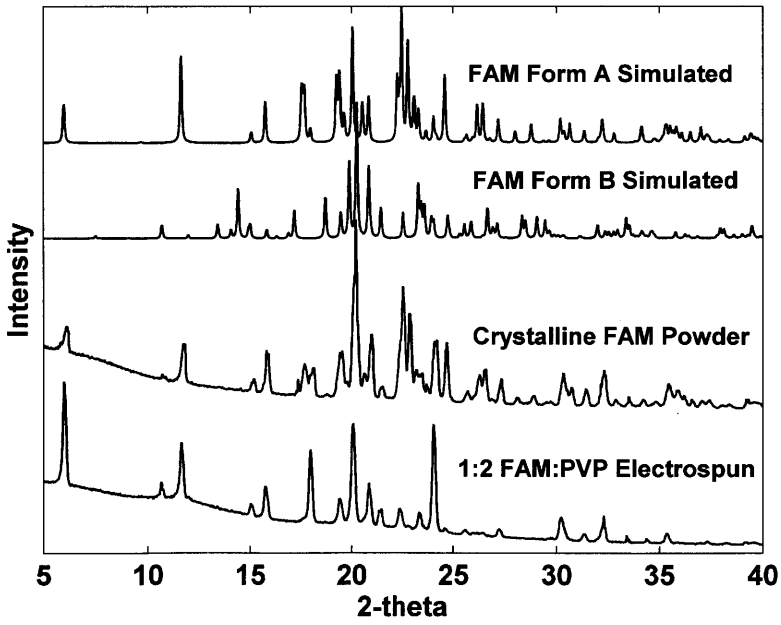

Figure 5-18: XRD powder pattern of crystalline FAM powder, 1:2 FAM:PVP electrospun and calculated powder patterns of polymorphs A and B

spun are also consistent with the experimental powder patterns of the commercial form (form I) as presented by Pranzo *et al* [123]. The polymorph of the ABZ was not affected by the electrospinning process.

The powder patterns for the crystalline FAM as received and 1:2 FAM:PVP electrospun are mixtures of polymorphs A and B (Figure 5-18), as can be seen by comparing them to the calculated powder patterns from the Cambridge Structural Database (reference codes FOGVIG06 and FOGVIG07 for polymorphs A and B, respectively). Though many peaks are overlapping, the presence of peaks at both 10.7 degrees 2-theta and 11.7 degrees 2-theta confirm the presence of both polymorphs. Differences in relative peak intensities can be attributed to the difference in sample preparation. The powder samples were flattened onto the zero background plate in a disordered manner, while the electrospun mat was laid onto the plate with all the fibers parallel to the flat plate.

5.4.3 Loading of API in Electrospun Fibers

The weight percent API in the electrospun fibers was determined using UV-vis spectrophotometry. The average loading of ABZ in the fibers was 31 wt% and the average loading of FAM in the fibers was 26 wt %. Compared to the nominal API loading of 33 wt%, both cases showed lower loading than expected.

In order to examine why the loading is lower than expected, we can calculate the settling velocity, v_s as a function of the particle radius using equation :

$$v_s = \frac{2}{9}\frac{(\rho_{part} - \rho_{fluid})}{\eta} g r_p^2 \tag{5.10}$$

where ρ_{fluid} is the fluid density, ρ_{part} is the particle density, μ is the viscosity, g is the gravitational acceleration and r_p is the particle radius. The fluid density and viscosity used were the same as 8.6 wt% 1.3 MDa PVP in ethanol used previously (Section 5.3.1). The particle densities were taken from the Cambridge Structural Database and were 1.56 g/cm^3 and 1.38 g/cm^3 for FAM and ABZ, respectively (reference codes BOGFUZ, FOGVIG06 and FOGVIG07 for ABZ, FAM polymorph A and

FAM polymorph B, respectively). This velocity is based on Stoke's law and thus is for spherical particles. Though our particles are more plate-shaped, we use a spherical approximation here for simplicity.

From the settling velocity, we can determine the time required for a particle of a given radius to settle to the bottom of the electrospinning bath. The distance between the top of the fluid level when full and the lowest point of the wire rotation is 0.8 cm. Since the particles are dispersed evenly within the fluid at the start of the experiment, we assume that an average particle must travel 0.4 cm, or half the depth of the bath.

Once the time required to settle is determined for a range of particle diameters, we determine the smallest particle diameter that we expect to settle out in 1 hour, the length of our experiment. For ABZ that is 82.5 μm and for FAM that is 70.8 μm. The particle size distribution based on volume percent is known for these solutions from the Malvern results discussed previously, and we have determined that 0.1 vol% ABZ and 4.5 vol% FAM (0.14 wt% ABZ and 7.1 wt% FAM) is expected to settle out during the experiment time. These values are merely an estimate, due to the assumptions of spherical particles and the average distance traveled and the time, but they provide insight into the difference in the final API loading in the fibers for the two API chosen for this study. For this method to be applied to a large continuous process, a stirring mechanism in the bath or a surfactant must be used to keep the particles suspended. In a larger, continuous operation set-up, the suspension will be continuously pumped into the fluid bath, which itself may be sufficient to remove the effects of settling out.

5.4.4 Dissolution of Electrospun Formulations Containing Crystalline API

Tablets prepared from a powder mixture and electrospun material were subjected to USP dissolution tests to compare the release behavior of the two preparation methods. Market formulations of the APIs were not used for comparison because we aim to examine only the effects of using the electrospinning preparation method compared

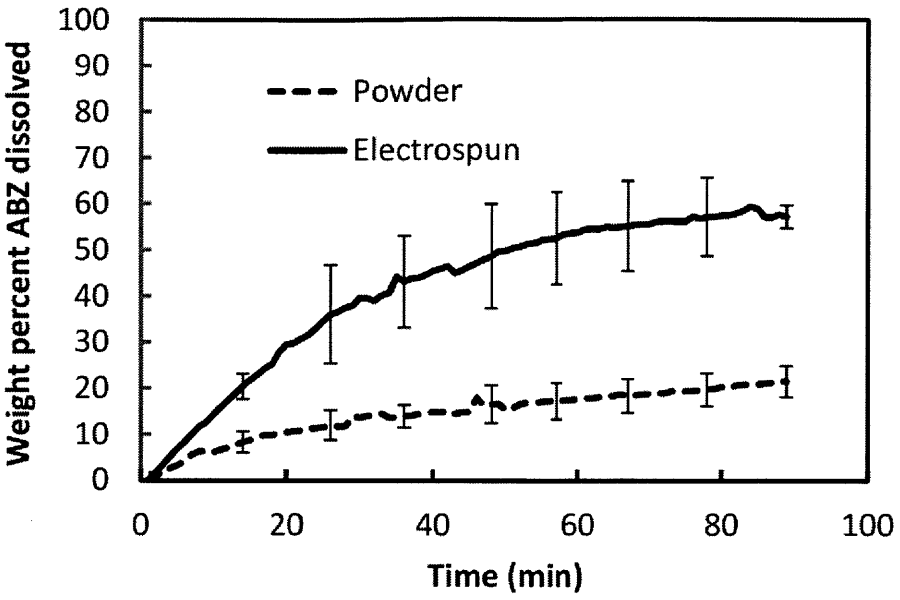

Figure 5-19: Dissolution of 1:2 ABZ:PVP tablets made from compressed powder (dashed line) and electrospun material (solid line) over time

to a powder-based preparation method. Electroprocessed materials may be further optimized for better dissolution through the use of additional excipients in the same manner as is done for a market formulation and then the two may be compared.

All tablets tested had the same mass and were prepared using the same insertion depth, meaning that the surface area and volume of the tablets is the same for all tested. The dissolution curves for ABZ are shown in Figure 5-19 and for FAM are shown in Figure 5-20.

For both ABZ and FAM, the electrospun formulations showed marked improvement in the dissolution rate over the compressed powder tablets. The crystal size, the extent of dispersion in the polymer and the crystalline morphology are essential properties of the electrospun API/polymer mixture that will have an effect on the dissolution of the APIs, and thus on the effectiveness of the final formulation. Understanding these properties is essential to the application of this process in a pharmaceutical manufacturing line.

From both the particle size analysis of the spinning suspension and the SEM im-

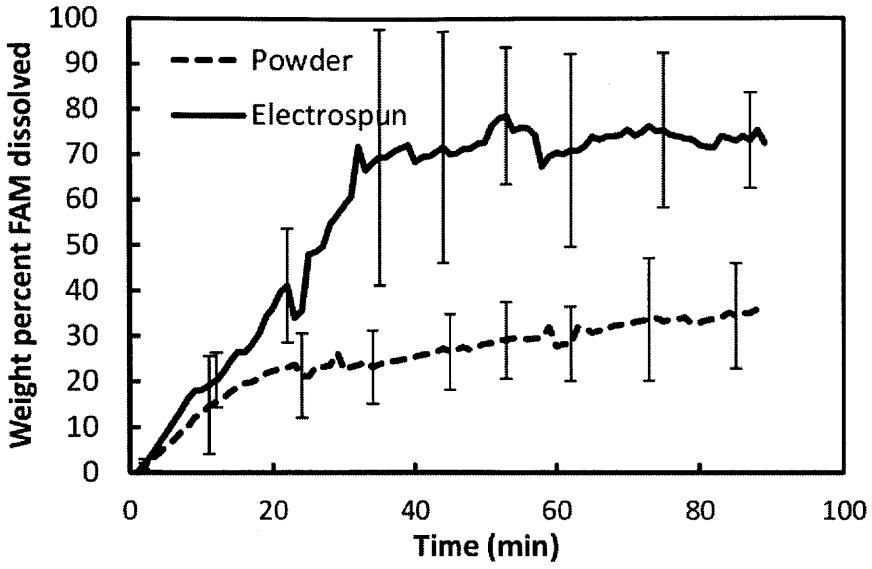

Figure 5-20: Dissolution of 1:2 FAM:PVP tablets made from compressed powder (dashed line) and electrospun material (solid line) over time

ages we have determined that the crystals range in size from 0.1-100 μm, with a volume percent-based mean of approximately 10 μm. For ABZ in particular, sonication treatment prior to electrospinning decreased the measured particle size by breaking up aggregates. The crystals are relatively small, and thus are expected to enhance the dissolution rate through an increase in the surface area, as predicted by the Noyes-Whitney equation, Equation 2.1.

In order to take advantage of the small crystal size to enhance the dissolution rate, the particles must be kept from aggregating. Using electrospinning, this is done by trapping the particles within the small polymer fibers. The SEM images in Figure 5-14 show that the particles are present and separated in the polymer fibers. This occurs due to the rapid solvent evaporation following the dispersion using sonication. Once in the dried solid form, the particles remain dispersed until the polymer begins to dissolve during dissolution testing.

As predicted by the Noyes-Whitney equation and supported by the evidence of formation of a well-dispersed solid mixture, the dissolution rate of the API from

compressed electrospun tablets is significantly higher than from compressed powder tablets. As the highly soluble polymer in the electrospun fibers dissolves, the API crystals are released as individual crystals and the exposed surface area is larger than that for agglomerates of API in the compressed powder tablets, resulting in an increased dissolution rate.

5.4.5 Summary

Nanofibers containing a well-mixed dispersion of crystalline API and a polymer were prepared by electrospinning a suspension of crystals in a polymer solution using a high-throughput free surface electrospinning process. The final loading in the fibers was 31 wt% and 26 wt% for 1:2 ABZ:PVP and 1:2 FAM:PVP, respectively, and the APIs retained their crystalline morphology throughout the electrospinning process. Due to the small particle size and dispersion of the particles in the polymer, the dissolution rate was enhanced for compressed electrospun tablets when compared to compressed powder tablets. This study proposes a novel process for preparing solid dispersions of crystalline API via electrospinning and demonstrates that the APIs are well-dispersed, retain their polymorphism, and have a high dissolution rate compared to compressed powder tablets and thus that electrospinning would be a viable option for a downstream pharmaceutical manufacturing process.

5.5 Conclusions

For electrospinning to be accepted as a viable pharmaceutical manufacturing process, it must be sufficiently flexible to produce API formulations with many properties, including both amorphous and crystalline API. In this section, we explore two methods to electrospin materials containing crystalline API. The first is spinning from a fully dissolved solution of API and polymer and the second is from suspensions of crystalline API in a dissolved polymer solution.

Electrospinning fibers containing crystalline API from fully dissolved solutions has been demonstrated previously [37–39], but here we extend the study to include a wider

variety of polymers. From this work we found that electrospinning solutions with a polymer that crystallizes readily can result in highly crystalline API in the polymer fibers. Besides that particular polymer property, there were no clear correlations between polymer or API properties and the crystallinity of the API in the final fibers. This is because many other conditions, including the solvent properties, interactions between the solvent and polymer or API, polymer concentration, etc., will affect the crystallization of the API. In addition, further work is necessary to develop a method to measure the crystallization occurring during spinning, rather than after hours of collection.

The crystallinity of API in the electrospun fibers following electrospinning of a solution of API, polymer and solvent was found to depend on many factors and often result in only partially crystalline materials. To provide an alternative method of manufacturing fibers containing crystalline API, we explored a method of spinning a suspension of particles in a dissolved polymer solution. The particles were placed in a solution of polymer and a solvent in which they were insoluble, sonicated to disperse them evenly, and the solution was electrospun on a free surface apparatus.

To develop an understanding of the spinnability of particles of the same order of magnitude as API crystals, we used spherical polystyrene beads of 1, 3, 5, 10 μm diameter. These were found to be spinnable at loadings up to 1:2 PS:PVP for two different PVP molecular weights, 1.3 MDa and 55 kDa. Even a particle with the density of lead (12 g/cm^3) was found to be spinnable using free surface electrospinning, provided it can remain suspended in the fluid bath for the entire experiment time. The fiber diameter was found to be independent of PS bead diameter and bead loading, but dependent on the base polymer solution (8.6 wt% 1.3 MDa PVP or 20 wt% 55 kDa PVP).

With the knowledge of spinnability of particles obtained from the PS bead work, we applied our study to electrospinning suspensions of API crystals in a polymer solution. ABZ and FAM, poorly water soluble APIs, were electrospun in a 1:2 API:polymer ratio with a PVP/ethanol solution, and the final fibers contained 31 wt% ABZ and 26 wt% FAM, slightly lower than expected due to particles settling

out during the experiment time. The resulting crystals were well-dispersed in the polymer and maintained their crystalline morphology throughout the electrospinning process. Dissolution studies showed that tablets prepared from electrospun materials had a higher dissolution rate than those prepared from blended powder, likely due to the fine dispersion of small crystals in the water-soluble polymer.

A free surface electrospinning process has been shown to be useful for preparing pharmaceutical formulations containing crystalline API with improved dissolution properties compared to compressed powder. With further refinement, this could lead to the application of electrospinning as a unit operation in a pharmaceutical continuous manufacturing process.

Chapter 6

Conclusions and Recommendations

Through the results in this thesis, we have demonstrated the utility of electrospinning as a method of preparing drug products that may be applied to a continuous manufacturing process. Formulations containing amorphous or crystalline API can be prepared using the same equipment, and selection of the spinning method, by spinning a solution or suspension, and appropriate polymers will determine whether crystalline or amorphous API will be present in the fibers.

By studying the amorphous solid mixtures formed by electrospinning in depth, we were able to come to the following conclusions:

1) Electrospun API/polymer formulations are homogeneous down to a 2-10 nm length scale for 1:1 SPP:PVP, 4:1 SPP:PVP, 1:1 IND:PVP, and 2:1 IND:PVP, as demonstrated using solid state NMR relaxation time analysis.

2) Electrospinning may be used to prepare homogeneous solid solutions in situations where hot melt extrusion results in phase separated mixtures.

3) The electrospun API/polymer formulations in (1) remain homogeneous to a 2-10 nm length scale for 6 months when stored in a desiccator at 40°C due to the antiplasticizing effect of the PVP and, for IND, the PVP-IND hydrogen bonding interactions.

4) SSNMR relaxation time analysis may be used to detect phase separation in electrospun mixtures as well as compare methods of forming solid dispersions.

Overall, the studies have demonstrated that electrospinning has great potential

as a method for forming amorphous solid solutions that may be used as final drug products. However, additional work would be useful to better understand the stability of the API/polymer solutions. Though the FTIR studies gave some indication of the presence or absence of hydrogen bonding, they were not completely conclusive, particularly for SPP/PVP formulations. Further study with 2D solid state NMR correlation spectroscopy would greatly improve the understanding of interactions. 2D NMR can show which carbons are within close proximity to one another and has been used to elucidate the structure of complicated molecules [126, 127]. The disadvantage of 2D NMR is that the sensitivity must be very high, and thus the sample must be ^{13}C labeled, an expensive process. However, the depth of information that may be obtained from 2D NMR correlation spectroscopy would add significant understanding to the chemical environment in the electrospun fibers.

Additional solid state NMR relaxation time stability studies would also be beneficial to aid in understanding the crystallization of an API over time in the solid state. Both formulations studied in this work were stable over the 6 mo. analysis time. Choosing materials that are unstable over time, such as ones that cannot hydrogen bond and have a Tg closer to the storage temperature, may result in phase separation over time. Solid state NMR relaxation time analysis performed frequently on such a sample would determine when phase separation occurs, and that could be correlated with the time crystalline material is first detected in the sample. This would show whether the API molecules form a significant solid state cluster prior to crystallization or whether the crystallization occurs prior to the formation of the 2-10 nm clusters.

The work in this thesis pertaining to forming fibers containing crystalline API by electrospinning resulted in the following conclusions:

1) Electrospinning a fully-dissolved solution of API, polymer, and solvent can result in crystalline API in the fibers, particularly when a crystalline polymer is used, but the crystallinity of the API depends on more factors than merely the API and polymer properties.

2) Microparticles up to a 10 μm diameter are electrospinnable using free surface electrospinning provided they are able to remain suspended in the fluid bath.

3) The fiber diameter of fibers containing microparticles up to a 10 μm diameter and 1:2 particle:polymer loading is independent of the particle diameter and particle loading.

4) Fibers containing well-dispersed API crystals with improved dissolution properties over compressed powder can be prepared by free surface electrospinning of API crystal suspensions.

The method of electrospinning suspensions has great promise for use in a continuous pharmaceutical manufacturing process, as it is simple and easily combined with upstream processes. Prior to application, however, additional polymer/API systems must be studied. In particular, additional polymers that would make good carriers must be identified, as not all APIs are insoluble in ethanol or other solvents in which PVP is soluble. In addition, for some APIs, the solvent may induce a change in the polymorph of the API [128]. In considering electrospinning as a downstream stage in a pharmaceutical manufacturing process, one must carefully consider the effect of the solvent, polymer and the sonication process on the API crystalline morphology.

Though direct electrospinning of an API/polymer/solvent solution for producing fibers containing crystalline API may not be as feasible as electrospinning suspensions of API crystals, extension of the study in this work (Section 5.2) would aid in applying electrospinning to prepare amorphous formulations, as understanding why an API crystallizes in the fiber can help one avoid crystallization when desired. In order to continue the study, however, a better method of determining when crystallization occurs is necessary. One approach to on-line characterization of crystallinity is *in situ* Raman. It has previously been applied in electrospinning to determine the solvent remaining in the fibers at different points in the electrospinning process [60].

Extending the study of electrospinning fibers containing crystalline API from a solution must include rigorous control and exploration of polymer concentration, API concentration, API-solvent interactions (and solubility), polymer-solvent interactions (and solubility), solvent dielectric constant, and solvent boiling point. Ideally, a polymer/API system would be used that is soluble in many solvents, and percent crystallinity in the final product would be measured for various concentrations for

each solvent. What is key is that the crystallization not be viewed merely as a standard evaporation process, but that the variation in the evaporation rate during the electrospinning process as well as the behavior of the polymer during spinning be considered.

The free surface electrospinning process may soon be ready for translation to a pharmaceutical pilot plant, such as that known as the "Red Line" at MIT. However, further development is necessary to design a method of continuously processing the non-woven mats of fibers into tablets. The mechanical properties of the electrospun mats must be understood and used to design additional equipment for this final downstream process.

Incorporation of electrospinning into a pharmaceutical manufacturing process should be feasible for many different APIs and desired product forms. This process is exciting because it can form homogeneous solid solutions for poorly water soluble APIs, but also be used to form crystalline formulations for APIs where enhanced solubility is not critical. It is easily incorporated after upstream purification steps and can be operated continuously at high production rates using free-surface electrospinning. It is a very promising addition to the toolbox of new continuous unit operations for pharmaceutical processing.

Bibliography

[1] Jörg Breitenbach. Melt extrusion: from process to drug delivery technology. *European Journal of Pharmaceutics and Biopharmaceutics*, 54(2):107–117, September 2002.

[2] Charles L. Cooney and Erin R Bell. *Melt extrusion and continuous manufacturing of pharmaceutical materials.* Thesis, Massachusetts Institute of Technology, 2011. Thesis (Ph. D.)–Massachusetts Institute of Technology, Dept. of Chemical Engineering, 2011.

[3] Jung-Hoon Chun, Won Kim, Massachusetts Institute of Technology. Dept. of Mechanical Engineering, and Massachusetts Institute of Technology. Dept. of Mechanical Engineering. *Layer bonding of solvent-cast thin films for pharmaceutical solid dosage forms.* Thesis, Massachusetts Institute of Technology, 2010. Thesis (S.M.)–Massachusetts Institute of Technology, Dept. of Mechanical Engineering, 2010.

[4] Blair Brettmann, Erin Bell, Allan Myerson, and Bernhardt Trout. Solid-state NMR characterization of high-loading solid solutions of API and excipients formed by electrospinning. *Journal of Pharmaceutical Sciences*, 101(4):1538–1545, April 2012.

[5] Gisela Buschle-Diller, Jared Cooper, Zhiwei Xie, Ye Wu, James Waldrup, and Xuehong Ren. Release of antibiotics from electrospun bicomponent fibers. *Cellulose*, 14(6):553–562, October 2007.

[6] Deng-Guang Yu, Xiao-Fei Zhang, Xia-Xia Shen, Chris Brandford-White, and Li-Min Zhu. Ultrafine ibuprofen-loaded polyvinylpyrrolidone fiber mats using electrospinning. *Polymer International*, 58(9):1010–1013, September 2009.

[7] Geert Verreck, Iksoo Chun, Joel Rosenblatt, Jef Peeters, Alex Van Dijck, Jurgen Mensch, Marc Noppe, and Marcus E. Brewster. Incorporation of drugs in an amorphous state into electrospun nanofibers composed of a water-insoluble, nonbiodegradable polymer. *Journal of Controlled Release*, 92(3):349–360, October 2003.

[8] Geert Verreck, Iksoo Chun, Jef Peeters, Joel Rosenblatt, and Marcus E Brewster. Preparation and characterization of nanofibers containing amorphous drug dispersions generated by electrostatic spinning. *Pharmaceutical Research*, 20(5):810–817, May 2003. PMID: 12751639.

[9] David Lukas, Arindam Sarkar, and Pavel Pokorny. Self-organization of jets in electrospinning from free liquid surface: A generalized approach. *Journal of Applied Physics*, 103(8):084309–084309–7, April 2008.

[10] A.L. Yarin and E. Zussman. Upward needleless electrospinning of multiple nanofibers. *Polymer*, 45(9):2977–2980, April 2004.

[11] T. Miloh, B. Spivak, and A. L Yarin. Needleless electrospinning: Electrically driven instability and multiple jetting from the free surface of a spherical liquid layer. *Journal of Applied Physics*, 106(11):114910–114910–8, December 2009.

[12] Eva Kostakova, Laszlo Meszaros, and Jan Gregr. Composite nanofibers produced by modified needleless electrospinning. *Materials Letters*, 63(28):2419–2422, November 2009.

[13] Oldrich Jirsak, Petr Sysel, Filip Sanetrnik, Jakub Hruza, and Jiri Chaloupek. Polyamic acid nanofibers produced by needleless electrospinning. *J. Nanomaterials*, 2010:49:1–49:6, January 2010.

[14] Haitao Niu, Tong Lin, and Xungai Wang. Needleless electrospinning. i. a comparison of cylinder and disk nozzles. *Journal of Applied Polymer Science*, 114(6):3524–3530, December 2009.

[15] Xin Wang, Haitao Niu, Tong Lin, and Xungai Wang. Needleless electrospinning of nanofibers with a conical wire coil. *Polymer Engineering & Science*, 49(8):1582–1586, August 2009.

[16] Bingan Lu, Yajiang Wang, Yanxia Liu, Huigao Duan, Jinyuan Zhou, Zhenxing Zhang, Youqing Wang, Xiaodong Li, Wei Wang, Wei Lan, and Erqing Xie. Superhigh-Throughput needleless electrospinning using a rotary cone as spinneret. *Small*, 6(15):1612–1616, August 2010.

[17] Keith M. Forward and Gregory C. Rutledge. Free surface electrospinning from a wire electrode. *Chemical Engineering Journal*, 183(0):492–503, February 2012.

[18] J.S. Varabhas, G.G. Chase, S Tripatanasuwan, and D.H. Reneker. Electrospun jets launched from polymeric bubbles. *Journal of Engineered Fibers and Fabrics*, 4:46–50, 2009.

[19] Santi Tungprapa, Ittipol Jangchud, and Pitt Supaphol. Release characteristics of four model drugs from drug-loaded electrospun cellulose acetate fiber mats. *Polymer*, 48(17):5030–5041, August 2007.

[20] Deng-Guang Yu, Xia-Xia Shen, Chris Branford-White, Kenneth White, Li-Min Zhu, and S W Annie Bligh. Oral fast-dissolving drug delivery membranes prepared from electrospun polyvinylpyrrolidone ultrafine fibers. *Nanotechnology*, 20(5):055104, February 2009.

[21] B C Hancock and G Zografi. Characteristics and significance of the amorphous state in pharmaceutical systems. *Journal of Pharmaceutical Sciences*, 86(1):1–12, January 1997. PMID: 9002452.

[22] Vasu Kumar Kakumanu and Arvind K Bansal. Enthalpy relaxation studies of celecoxib amorphous mixtures. *Pharmaceutical Research*, 19(12):1873–1878, December 2002. PMID: 12523668.

[23] Tamaki Miyazaki, Sumie Yoshioka, Yukio Aso, and Shigeo Kojima. Ability of polyvinylpyrrolidone and polyacrylic acid to inhibit the crystallization of amorphous acetaminophen. *Journal of Pharmaceutical Sciences*, 93(11):2710–2717, November 2004.

[24] Hajime Konno and Lynne S Taylor. Influence of different polymers on the crystallization tendency of molecularly dispersed amorphous felodipine. *Journal of Pharmaceutical Sciences*, 95(12):2692–2705, December 2006.

[25] L S Taylor and G Zografi. Spectroscopic characterization of interactions between PVP and indomethacin in amorphous molecular dispersions. *Pharmaceutical Research*, 14(12):1691–1698, December 1997. PMID: 9453055.

[26] Manfred Gordon and James S Taylor. Ideal copolymers and the second-order transitions of synthetic rubbers. i. non-crystalline copolymers. *Journal of Applied Chemistry*, 2(9):493–500, September 1952.

[27] W.Z Cai, K Schmidt-Rohr, N Egger, B Gerharz, and H.W Spiess. A solid-state n.m.r. study of microphase structure and segmental dynamics of poly(styrene-b-methylphenylsiloxane) diblock copolymers. *Polymer*, 34(2):267–276, 1993.

[28] Sonja Krause and Magdy Iskandar. Phase separation in styrene-alpha-methyl styrene block copolymers. *Polymer Science and Technology*, 10:231–243, 1977.

[29] Ann Newman, David Engers, Simon Bates, Igor Ivanisevic, Ron C Kelly, and George Zografi. Characterization of amorphous API:Polymer mixtures using x-ray powder diffraction. *Journal of Pharmaceutical Sciences*, 97(11):4840–4856, November 2008.

[30] Feng Qian, Jun Huang, Qing Zhu, Raja Haddadin, John Gawel, Robert Garmise, and Munir Hussain. Is a distinctive single tg a reliable indicator

for the homogeneity of amorphous solid dispersion? *International Journal of Pharmaceutics*, 395(1-2):232–235, August 2010.

[31] Dieter Ameye, Eveline Pringels, Paul Foreman, Jean Paul Remon, Peter Adriaensens, Liesbet Storme, and Jan Gelan. Correlation between the molecular morphology and the biocompatibility of bioadhesive carriers prepared from spray-dried starch/Carbopol® blends. *Polymer*, 46(7):2338–2345, March 2005.

[32] Jirí Spevácek, Jirí Brus, Thomas Divers, and Yves Grohens. Solid-state NMR study of biodegradable starch/polycaprolactone blends. *European Polymer Journal*, 43(5):1866–1875, May 2007.

[33] J. Straka, P. Schmidt, J. Dybal, B. Schneider, and J. Spevácek. Blends of poly(ethylene oxide)/poly(methyl methacrylate). an i.r. and n.m.r. study. *Polymer*, 36(6):1147–1155, March 1995.

[34] V. J. McBrierty, D. C. Douglass, and T. K. Kwei. Compatibility in blends of poly(methyl methacrylate) and poly(styrene-co-acrylonitrile). 2. an NMR study. *Macromolecules*, 11(6):1265–1267, November 1978.

[35] Ru-Rong Wu, Hsien-Ming Kao, J. -C. Chiang, and E. M. Woo. Solid-state NMR studies on phase behavior and motional mobility in binary blends of polystyrene and poly(cyclohexyl methacrylate). *Polymer*, 43(1):171–176, January 2002.

[36] Anshuman A. Ambike, K.R. Mahadik, and Anant Paradkar. Stability study of amorphous valdecoxib. *International Journal of Pharmaceutics*, 282(1-2):151–162, September 2004.

[37] Sing Yian Chew, Todd C Hufnagel, Chwee Teck Lim, and Kam W Leong. Mechanical properties of single electrospun drug-encapsulated nanofibres. *Nanotechnology*, 17(15):3880–3891, August 2006.

[38] Mădălina V. Natu, Hermínio C. de Sousa, and M.H. Gil. Effects of drug solubility, state and loading on controlled release in bicomponent electrospun fibers. *International Journal of Pharmaceutics*, 397(1–2):50–58, September 2010.

[39] Francis Ignatious, Linghong Sun, Chao-Pin Lee, and John Baldoni. Electrospun nanofibers in oral drug delivery. *Pharmaceutical Research*, 27(4):576–588, February 2010.

[40] M. Wang, H. Singh, T.A. Hatton, and G.C. Rutledge. Field-responsive superparamagnetic composite nanofibers by electrospinning. *Polymer*, 45(16):5505–5514, July 2004.

[41] Shahar Kedem, Judith Schmidt, Yaron Paz, and Yachin Cohen. Composite polymer nanofibers with carbon nanotubes and titanium dioxide particles. *Langmuir*, 21(12):5600–5604, June 2005.

[42] Christopher Drew, Xianyan Wang, Lynne A. Samuelson, and Jayant Kumar. The effect of viscosity and filler on electrospun fiber morphology. *Journal of Macromolecular Science, Part A*, 40(12):1415–1422, 2003.

[43] Patcharaporn Wutticharoenmongkol, Neeracha Sanchavanakit, Prasit Pavasant, and Pitt Supaphol. Preparation and characterization of novel bone scaffolds based on electrospun polycaprolactone fibers filled with nanoparticles. *Macromolecular Bioscience*, 6(1):70–77, January 2006.

[44] Yazhou Wang, Bochu Wang, Guixue Wang, Tieying Yin, and Qingsong Yu. A novel method for preparing electrospun fibers with nano-/micro-scale porous structures. *Polymer Bulletin*, 63(2):259–265, April 2009.

[45] Manish K. Tiwari, Alexander L. Yarin, and Constantine M. Megaridis. Electrospun fibrous nanocomposites as permeable, flexible strain sensors. *Journal of Applied Physics*, 103(4):044305, 2008.

[46] Shili Xiao, Mingwu Shen, Rui Guo, Shanyuan Wang, and Xiangyang Shi. Immobilization of zerovalent iron nanoparticles into electrospun polymer nanofibers: Synthesis, characterization, and potential environmental applications. *The Journal of Physical Chemistry C*, 113(42):18062–18068, October 2009.

[47] Xuelong Chen, Suying Wei, Cem Gunesoglu, Jiahua Zhu, Cara S Southworth, Luyi Sun, Amar B Karki, David P Young, and Zhanhu Guo. Electrospun magnetic fibrillar polystyrene nanocomposites reinforced with nickel nanoparticles. *Macromolecular Chemistry and Physics*, 211(16):1775–1783, August 2010.

[48] Yael Dror, Wael Salalha, Rafail L. Khalfin, Yachin Cohen, Alexander L. Yarin, and Eyal Zussman. Carbon nanotubes embedded in oriented polymer nanofibers by electrospinning. *Langmuir*, 19(17):7012–7020, 2003.

[49] Haoqing Hou, Jason J. Ge, Jun Zeng, Qing Li, Darrell H. Reneker, Andreas Greiner, and Stephen Z. D. Cheng. Electrospun polyacrylonitrile nanofibers containing a high concentration of Well-Aligned multiwall carbon nanotubes. *Chemistry of Materials*, 17(5):967–973, March 2005.

[50] W Salalha, J Kuhn, Y Dror, and E Zussman. Encapsulation of bacteria and viruses in electrospun nanofibres. *Nanotechnology*, 17(18):4675–4681, September 2006.

[51] M. Wang, J.H. Yu, A.J. Hsieh, and G.C. Rutledge. Effect of tethering chemistry of cationic surfactants on clay exfoliation, electrospinning and diameter of PMMA/clay nanocomposite fibers. *Polymer*, 51(26):6295–6302, December 2010.

[52] M. Wang, A.J. Hsieh, and G.C. Rutledge. Electrospinning of poly(MMA-co-MAA) copolymers and their layered silicate nanocomposites for improved thermal properties. *Polymer*, 46(10):3407–3418, April 2005.

[53] Jong-Min Lim, Jun Hyuk Moon, Gi-Ra Yi, Chul-Joon Heo, and Seung-Man Yang. Fabrication of One-Dimensional colloidal assemblies from electrospun nanofibers. *Langmuir*, 22(8):3445–3449, 2006.

[54] Liwen Ji and Xiangwu Zhang. Electrospun carbon nanofibers containing silicon particles as an energy-storage medium. *Carbon*, 47(14):3219–3226, November 2009.

[55] E. Hugh Stitt and David W Rooney. Switching from batch to continuous processing for fine and Intermediate-Scale chemicals manufacture. In *Novel Concepts in Catalysis and Chemical Reactors*, pages 309–330. Wiley-VCH Verlag GmbH & Co. KGaA.

[56] K Plumb. Continuous processing in the pharmaceutical industry: Changing the mind set. *Chemical Engineering Research and Design*, 83(6):730–738, June 2005.

[57] William James Morton. Method of dispersing fluids, July 1902. U.S. Classification: 264/10.

[58] Jian H Yu and Gregory C Rutledge. Electrospinning. In *Encyclopedia Of Polymer Science and Technology.* John Wiley & Sons, Inc.

[59] Gregory C. Rutledge and Sergey V. Fridrikh. Formation of fibers by electrospinning. *Advanced Drug Delivery Reviews*, 59(14):1384–1391, December 2007.

[60] J. S. Stephens, S. Frisk, S. Megelski, J. F. Rabolt, and D. Bruce Chase. "Real time" raman studies of electrospun fibers. *Applied Spectroscopy*, 55(10):1287–1290, October 2001.

[61] Moses M Hohman, Michael Shin, Gregory Rutledge, and Michael P Brenner. Electrospinning and electrically forced jets. II. applications. *Physics of Fluids*, 13(8):2221–2236, August 2001.

[62] Moses M Hohman, Michael Shin, Gregory Rutledge, and Michael P Brenner. Electrospinning and electrically forced jets. i. stability theory. *Physics of Fluids*, 13(8):2201–2220, August 2001.

[63] Sergey V. Fridrikh, Jian H. Yu, Michael P. Brenner, and Gregory C. Rutledge. Controlling the fiber diameter during electrospinning. *Physical Review Letters*, 90(14):144502, April 2003.

[64] S.A. Theron, E. Zussman, and A.L. Yarin. Experimental investigation of the governing parameters in the electrospinning of polymer solutions. *Polymer*, 45(6):2017–2030, March 2004.

[65] Arun Kumar, Ming Wei, Carol Barry, Julie Chen, and Joey Mead. Controlling fiber repulsion in multijet electrospinning for higher throughput. *Macromolecular Materials and Engineering*, 295(8):701–708, August 2010.

[66] Alessio Varesano, Riccardo A. Carletto, and Giorgio Mazzuchetti. Experimental investigations on the multi-jet electrospinning process. *Journal of Materials Processing Technology*, 209(11):5178–5185, June 2009.

[67] Chandan Bhugra and Michael J Pikal. Role of thermodynamic, molecular, and kinetic factors in crystallization from the amorphous state. *Journal of Pharmaceutical Sciences*, 97(4):1329–1349, April 2008.

[68] G L Amidon, H Lennernäs, V P Shah, and J R Crison. A theoretical basis for a biopharmaceutic drug classification: the correlation of in vitro drug product dissolution and in vivo bioavailability. *Pharmaceutical Research*, 12(3):413–420, March 1995. PMID: 7617530.

[69] Lian Yu. Amorphous pharmaceutical solids: preparation, characterization and stabilization. *Advanced Drug Delivery Reviews*, 48(1):27–42, May 2001.

[70] B. C Hancock, S. L Shamblin, and G. Zografi. Molecular mobility of amorphous pharmaceutical solids below their glass transition temperatures. *Pharmaceutical research*, 12(6):799–806.

[71] Christian Leuner and Jennifer Dressman. Improving drug solubility for oral delivery using solid dispersions. *European Journal of Pharmaceutics and Biopharmaceutics*, 50(1):47–60, July 2000.

[72] David B. Williams, C. Barry Carter, David B. Williams, and C. Barry Carter. Transmission electron microscopy. pages 3–22. Springer US, 2009.

[73] Naho Furuyama, Susumu Hasegawa, Takeshi Hamaura, Shuichi Yada, Hiroaki Nakagami, Etsuo Yonemochi, and Katsuhide Terada. Evaluation of solid dispersions on a molecular level by the raman mapping technique. *International Journal of Pharmaceutics*, 361(1–2):12–18, September 2008.

[74] Dirk Jan van Drooge, Kevin Braeckmans, Wouter L. J Hinrichs, Katrien Remaut, Stefaan C De Smedt, and Henderik W Frijlink. Characterization of the mode of incorporation of lipophilic compounds in solid dispersions at the nanoscale using fluorescence resonance energy transfer (FRET). *Macromolecular Rapid Communications*, 27(14):1149–1155, July 2006.

[75] Curtis Marcott, Michael Lo, Kevin Kjoller, Craig Prater, and Isao Noda. Spatial differentiation of Sub-Micrometer domains in a poly(hydroxyalkanoate) copolymer using instrumentation that combines atomic force microscopy (AFM) and infrared (IR) spectroscopy. *Applied Spectroscopy*, 65(10):1145–1150, October 2011.

[76] Elaine Merisko-Liversidge and Gary G. Liversidge. Nanosizing for oral and parenteral drug delivery: A perspective on formulating poorly-water soluble compounds using wet media milling technology. *Advanced Drug Delivery Reviews*, 63(6):427–440, May 2011.

[77] Zhiguo Zheng, Xingcai Zhang, Daniel Carbo, Cheryl Clark, Cherie-Ann Nathan, and Yuri Lvov. Sonication-Assisted synthesis of Polyelectrolyte-Coated curcumin nanoparticles. *Langmuir*, 26(11):7679–7681, June 2010.

[78] Miroslav Variny, Sandra Alvarez de Miguel, Barry D. Moore, and Jan Sefcik. Formation of valine microcrystals through rapid antisolvent precipitation. *Journal of Dispersion Science and Technology*, 29(4):617–620, 2008.

[79] Hong Zhao, Jie-Xin Wang, Qi-An Wang, Jian-Feng Chen, and Jimmy Yun. Controlled liquid antisolvent precipitation of hydrophobic pharmaceutical nanoparticles in a microchannel reactor. *Ind. Eng. Chem. Res.*, 46(24):8229–8235, 2007.

[80] Michal E. Matteucci, Margaret A. Hotze, Keith P. Johnston, and Robert O. Williams. Drug nanoparticles by antisolvent precipitation: Mixing energy versus surfactant stabilization. *Langmuir*, 22(21):8951–8959, 2006.

[81] Anne Zimmermann, Anna Millqvist-Fureby, Michiel Ringkjøbing Elema, Tue Hansen, Anette Müllertz, and Lars Hovgaard. Adsorption of pharmaceutical excipients onto microcrystals of siramesine hydrochloride: Effects on physicochemical properties. *European Journal of Pharmaceutics and Biopharmaceutics*, 71(1):109–116, January 2009.

[82] Norbert Rasenack, Hartwig Steckel, and Bernd W Müller. Micronization of anti-inflammatory drugs for pulmonary delivery by a controlled crystallization process. *Journal of Pharmaceutical Sciences*, 92(1):35–44, January 2003.

[83] Norbert Rasenack, Helge Hartenhauer, and Bernd W Müller. Microcrystals for dissolution rate enhancement of poorly water-soluble drugs. *International Journal of Pharmaceutics*, 254(2):137–145, March 2003.

[84] Norbert Rasenack, Hartwig Steckel, and Bernd W Müller. Preparation of microcrystals by in situ micronization. *Powder Technology*, 143–144(0):291–296, June 2004.

[85] D. Douroumis and A. Fahr. Nano- and micro-particulate formulations of poorly water-soluble drugs by using a novel optimized technique. *European Journal of Pharmaceutics and Biopharmaceutics*, 63(2):173–175, June 2006.

[86] Michal E. Matteucci, Blair K. Brettmann, True L. Rogers, Edmund J. Elder, Robert O. Williams, and Keith P. Johnston. Design of potent amorphous drug nanoparticles for rapid generation of highly supersaturated media. *Molecular Pharmaceutics*, 4(5):782–793, October 2007.

[87] Koichi Itoh, Adchara Pongpeerapat, Yuichi Tozuka, Toshio Oguchi, and Keiji Yamamoto. Nanoparticle formation of poorly Water-Soluble drugs from ternary

ground mixtures with PVP and SDS. *Chemical and Pharmaceutical Bulletin*, 51(2):171–174, 2003.

[88] Daniel C. Harris. *Quantitative Chemical Analysis*. W. H. Freeman and Co., April 2010.

[89] Melinda J. Duer. *Introduction to solid-state NMR spectroscopy*. John Wiley & Sons, 2004.

[90] Andrew E. Bennett, Chad M. Rienstra, Miche?le Auger, K. V. Lakshmi, and Robert G. Griffin. Heteronuclear decoupling in rotating solids. *The Journal of Chemical Physics*, 103(16):6951, 1995.

[91] S. Spiegel, K. Schmidt-Rohr, C. Boeffel, and H.W. Spiess. 1H spin diffusion coefficients of highly mobile polymers. *Polymer*, 34(21):4566–4569, November 1993.

[92] J. Clauss, K. Schmidt-Rohr, and H. W Spiess. Determination of domain sizes in heterogeneous polymers by solid-state NMR. *Acta Polymerica*, 44(1):1–17, February 1993.

[93] Marco Geppi, Salvatore Guccione, Giulia Mollica, Rosario Pignatello, and Carlo A. Veracini. Molecular properties of ibuprofen and its solid dispersions with eudragit RL100 studied by Solid-State nuclear magnetic resonance. *Pharmaceutical Research*, 22(9):1544–1555, August 2005.

[94] Tran N Pham, Simon A Watson, Andrew J Edwards, Manisha Chavda, Jacalyn S Clawson, Mark Strohmeier, and Frederick G Vogt. Analysis of amorphous solid dispersions using 2D Solid-State NMR and (1)H t(1) relaxation measurements. *Molecular Pharmaceutics*, August 2010. PMID: 20681586.

[95] A.B. Barnes, G. De Paëpe, P.C.A. van der Wel, K.-N. Hu, C.-G. Joo, V.S. Bajaj, M.L. Mak-Jurkauskas, J.R. Sirigiri, J. Herzfeld, R.J. Temkin, and R.G. Griffin. High-Field dynamic nuclear polarization for solid and solution biological NMR.

Applied magnetic resonance, 34(3-4):237–263, August 2008. PMID: 19194532 PMCID: 2634864.

[96] Galia T. Debelouchina, Marvin J. Bayro, Patrick C. A. van der Wel, Marc A. Caporini, Alexander B. Barnes, Melanie Rosay, Werner E. Maas, and Robert G. Griffin. Dynamic nuclear polarization-enhanced solid-state NMR spectroscopy of GNNQQNY nanocrystals and amyloid fibrils. *Phys. Chem. Chem. Phys.*, 12(22):5911–5919.

[97] Thorsten Maly, Galia T Debelouchina, Vikram S Bajaj, Kan-Nian Hu, Chan-Gyu Joo, Melody L Mak–Jurkauskas, Jagadishwar R Sirigiri, Patrick C. A van der Wel, Judith Herzfeld, Richard J Temkin, and Robert G Griffin. Dynamic nuclear polarization at high magnetic fields. *The Journal of Chemical Physics*, 128(5):052211–052211–19, February 2008.

[98] Andrew E. Bennett, Chad M. Rienstra, Janet M. Griffiths, Weiguo Zhen, Peter T. Lansbury, and Robert G. Griffin. Homonuclear radio frequency-driven recoupling in rotating solids. *The Journal of Chemical Physics*, 108(22):9463, 1998.

[99] G Van den Mooter, M Wuyts, N Blaton, R Busson, P Grobet, P Augustijns, and R Kinget. Physical stabilisation of amorphous ketoconazole in solid dispersions with polyvinylpyrrolidone k25. *European Journal of Pharmaceutical Sciences: Official Journal of the European Federation for Pharmaceutical Sciences*, 12(3):261–269, January 2001. PMID: 11113645.

[100] T Matsumoto and G Zografi. Physical properties of solid molecular dispersions of indomethacin with poly(vinylpyrrolidone) and poly(vinylpyrrolidone-co-vinyl-acetate) in relation to indomethacin crystallization. *Pharmaceutical Research*, 16(11):1722–1728, November 1999. PMID: 10571278.

[101] Feng Zhang and James W. McGinity. Properties of Sustained-Release tablets prepared by Hot-Melt extrusion. *Pharmaceutical Development and Technology*, 4(2):241–250, January 1999.

[102] Bernard Van Eerdenbrugh, Michiel Van Speybroeck, Raf Mols, Kristof Houthoofd, Johan A. Martens, Ludo Froyen, Jan Van Humbeeck, Patrick Augustijns, and Guy Van den Mooter. Itraconazole/TPGS/Aerosil®200 solid dispersions: Characterization, physical stability and in vivo performance. *European Journal of Pharmaceutical Sciences*, 38(3):270–278, October 2009.

[103] Stephen J Byard, Susan L Jackson, Andrew Smail, Michel Bauer, and David C Apperley. Studies on the crystallinity of a pharmaceutical development drug substance. *Journal of Pharmaceutical Sciences*, 94(6):1321–1335, June 2005.

[104] Shaun Fitzpatrick, James F. McCabe, Catherine R. Petts, and Steven W. Booth. Effect of moisture on polyvinylpyrrolidone in accelerated stability testing. *International Journal of Pharmaceutics*, 246(1-2):143–151, October 2002.

[105] Joseph W Lubach, Dawei Xu, Brigitte E Segmuller, and Eric J Munson. Investigation of the effects of pharmaceutical processing upon solid-state NMR relaxation times and implications to solid-state formulation stability. *Journal of Pharmaceutical Sciences*, 96(4):777–787, April 2007. PMID: 17238201.

[106] C. A Oksanan and G. Zografi. Molecular mobility in mixtures of absorbed water and solid poly(vinylpyrrolidone). *Pharmaceutical research*, 10(6):791–799.

[107] Dionysios Douroumis, Nikolaos Bouropoulos, and Alfred Fahr. Physicochemical characterization of solid dispersions of three antiepileptic drugs prepared by solvent evaporation method. *Journal of Pharmacy and Pharmacology*, 59(5):645–653, May 2007.

[108] Hongsen Peng, Shaobing Zhou, Tao Guo, Yanshan Li, Xiaohong Li, Jianxin Wang, and Jie Weng. In vitro degradation and release profiles for electrospun polymeric fibers containing paracetanol. *Colloids and Surfaces B: Biointerfaces*, 66(2):206–212, October 2008.

[109] M.E. Brewster, Geert Verreck, Iksoo Chun, Joel Rosenblatt, J. Mensch, A. Van Dijck, M. Noppe, A. Arien, M. Bruining, and Jef Peeters. The use of polymer-

based electrospun nanofibers containing amorphoous drug dispersions for the delivery of poorly water-soluble pharmaceutics. *Pharmazie*, 59(5):387–391, November 2004.

[110] E.P.S. Tan, S.Y. Ng, and C.T. Lim. Tensile testing of a single ultrafine polymeric fiber. *Biomaterials*, 26(13):1453–1456, May 2005.

[111] Won Keun Son, Ji Ho Youk, Taek Seung Lee, and Won Ho Park. The effects of solution properties and polyelectrolyte on electrospinning of ultrafine poly(ethylene oxide) fibers. *Polymer*, 45(9):2959–2966.

[112] C. T Lim, E. P. S Tan, and S. Y Ng. Effects of crystalline morphology on the tensile properties of electrospun polymer nanofibers. *Applied Physics Letters*, 92(14):141908–141908–3, April 2008.

[113] L Landau and V Levich. Dragging of a liquid by a moving plate. *Acta Physicochim URSS*, 17:42–54, 1942.

[114] B.V. Derjaguin. On the thickness of the liquid film adhering to the walls of a vessel after emptying. *Acta Physicochim URSS*, 20:349–352, 1945.

[115] D. Quere. Fluid coating on a fiber. *Annual review of fluid mechanics*, 31:347–384.

[116] Itai Cohen and Sidney R. Nagel. Scaling at the selective withdrawal transition through a tube suspended above the fluid surface. *Physical Review Letters*, 88(7):074501, February 2002.

[117] Itai Cohen, Hui Li, James L Hougland, Milan Mrksich, and Sidney R Nagel. Using selective withdrawal to coat microparticles. *Science*, 292(5515):265–267, April 2001.

[118] Michael H May and Michael V Sefton. Conformal coating of small particles and cell aggregates at a Liquid-Liquid interface. *Annals of the New York Academy of Sciences*, 875(1):126–134, June 1999.

[119] Michael Manga and H. A. Stone. Low reynolds number motion of bubbles, drops and rigid spheres through fluid–fluid interfaces. *Journal of Fluid Mechanics*, 287:279–298, 1995.

[120] A. S Geller, S. H Lee, and L. G Leal. The creeping motion of a spherical particle normal to a deformable interface. *Journal of Fluid Mechanics*, 169:27–69.

[121] S.H Lee and L.G Leal. The motion of a sphere in the presence of a deformable interface: II. a numerical study of the translation of a sphere normal to an interface. *Journal of Colloid and Interface Science*, 87(1):81–106, May 1982.

[122] Jong-Min Lim, Gi-Ra Yi, Jun Hyuk Moon, Chul-Joon Heo, and Seung-Man Yang. Superhydrophobic films of electrospun fibers with Multiple-Scale surface morphology. *Langmuir*, 23(15):7981–7989, 2007.

[123] Marco B Pranzo, Dyanne Cruickshank, Massimo Coruzzi, Mino R Caira, and Ruggero Bettini. Enantiotropically related albendazole polymorphs. *Journal of Pharmaceutical Sciences*, 99(9):3731–3742, September 2010.

[124] Jie Lu, Xiu-Juan Wang, Xia Yang, and Chi-Bun Ching. Polymorphism and crystallization of famotidine. *Crystal Growth & Design*, 7(9):1590–1598, 2007.

[125] Patrick J Marsac, Tonglei Li, and Lynne S Taylor. Estimation of drug-polymer miscibility and solubility in amorphous solid dispersions using experimentally determined interaction parameters. *Pharmaceutical Research*, 26(1):139–151, January 2009. PMID: 18779927.

[126] Galia T. Debelouchina, Geoffrey W. Platt, Marvin J. Bayro, Sheena E. Radford, and Robert G. Griffin. Magic angle spinning NMR analysis of ?2-Microglobulin amyloid fibrils in two distinct morphologies. *J. Am. Chem. Soc.*, 132(30):10414–10423, 2010.

[127] Chad M. Rienstra, Mary E. Hatcher, Leonard J. Mueller, Sun, Stephen W. Fesik, and Robert G. Griffin. Efficient multispin homonuclear Double-

Quantum recoupling for Magic-Angle spinning NMR: 13C-13C correlation spectroscopy of U-13C-Erythromycin a. *Journal of the American Chemical Society*, 120(41):10602–10612, October 1998.

[128] Geoff G.Z Zhang, Devalina Law, Eric A Schmitt, and Yihong Qiu. Phase transformation considerations during process development and manufacture of solid oral dosage forms. *Advanced Drug Delivery Reviews*, 56(3):371–390, February 2004.